3D bioprinting of alginate and calcium phosphate cement (CPC) scaffolds for drug delivery and tissue regeneration

by

Yan Wu

Submitted in accordance with the requirements for the degree of Doctor of Philosophy

University of Sussex

May 2022

I hereby declare that this thesis has not been and will not be, submitted in whole or in part to another University for the award of any other degree.

Signature:..... .....

Table of Content

List of Figures

List of tables

Acknowledgements

Grateful for all the unconditional love from my parents, my grandmom, my empathetic friends, my dog and my counsellors.

Thank you to my supervisors Prof. Ali Nokhodchi, Prof. Mohammed Maniruzzaman and academic peers who helped me through this journey.

I am grateful for Dr. Lisa Woodbine for all her kind help/training and collaboration on cell/tissue culture studies. I miss every single second working with her at the Genome Damage and Stability Centre (GDSC).

I thank Dr.Lamia Heikal, Prof. Gordon Ferns, Prof. Pietro Ghezzi for their expertise and assistance throughout the collaborative work on Real-Time qPCR ,ELISA and statistic analylsis for EPO loaded scaffolds.

Publications and poster presentation

Publications

• Wu, Yan, Lisa Woodbine, Antony M. Carr, Amit R. Pillai, Ali Nokhodchi, and Mohammed Maniruzzaman. "3D printed calcium phosphate cement (CPC) scaffolds for anti-cancer drug delivery." Pharmaceutics 12, no. 11 (2020): 1077.

• Wu, Yan, Lamia Heikal, Gordon Ferns, Pietro Ghezzi, Ali Nokhodchi, and Mohammed Maniruzzaman. "3D bioprinting of novel biocompatible scaffolds for endothelial cell repair." Polymers 11, no. 12 (2019): 1924.

Poster presentation

Academy of Pharmaceutical Science conference, London, UK,11-13th Sep 2019

“3D printed calcium phosphate cement (CPC) scaffolds for anti-cancer drug delivery”

Abstract

3D bioprinting is manufactural biotechnology which was used to create a drug delivery system with advanced functions and personalised tissue regeneration. In this study, 3D scaffolds were bio-printed using different bio-ink formulations including pure alginate, alginate-methylcellulose (MC), polylactic acid (PLA) with polyethylene glycol (PEG), and calcium phosphate cement (CPC). The properties of biomaterials were analysed by viscometer and texture analyser. Confocal microscopy, scanning electron microscopy (SEM) and X-Ray powder diffraction (XRD) were applied for surface evaluation of the samples. *In vitro* cell studies were used for testing cell viability and anti-cancer function of 3D bio-printed scaffolds. The mathematical models between the concentration of pure alginate (C) and viscosity (V) in different pH have been explored, which were $V=0.0019C^{4.9061}$ at pH=1.2, $V=73.097e^{0.1788C}$ at pH=6.6 and $V=0.4059C^{2.7997}$ at pH=7.2 respectively. Among all the 3D bio-printed alginate-MC scaffolds, the scaffold made from alginate-MC with a ratio of 1:1 showed a positive effect on cancer cells and inhibited the growth of cancer cells within 4 days, indicating its effective function in anti-cancer drug delivery system. Besides, 3D bio-printed PLA/PEG scaffolds loaded with growth factor erythropoietin (EPO) were proved to be valid for assisting cell repair. And 5-Fluorouracil (5-FU) coated CPC scaffolds showed effective controlled-release drug delivery and anti-cancer function within 4 days. Those 3D bio-printed novel scaffolds illustrated their outstanding potential for future clinical use in both drug delivery and tissue engineering field. Finally, the change of cell behaviour was observed visually by culturing scaffolds with 1BR, HEK293T-GFP and U2OS-GFP cell lines for 28

days. The quantitative analysis showed that the size and structure of scaffolds were two important factors affecting the behaviour of cells and 3D CPC scaffolds in size S (diameter ~9.4mm) is the most suitable one culturing with 1BR cells. The whole thesis explored 3D bio-printed scaffolds in three perspectives, formulations, scaffolds and *in vitro* functions, which contributed to understanding bio-inks/scaffolds' physical-chemical properties, clinical functions and cell-scaffold interactions.

Chapter 1 A review on 3D bioprinting for novel drug delivery systems and tissue regeneration.

1.1 Introduction

3D printing, also known as an addictive manufactory (AM), was born in 1984 when Charles Hull invented stereolithography (SLA)[1]. It was a fascinating innovation for solving the problem of building items in a certain shape which is hard to be achieved by the traditional manufacturing method. Three-dimensional bioprinting (3D bio-printing) is a subclass of AM for printing bio-active 3D tissues and organs layer by layer using cell-loaded bio-materials[2-4]. The fabrication of biomaterials can be fast achieved in any computer-designed structure automatically in 3D bio-printing process.

The start of a novel field 3D bio-printing was marked when the first scaffold for the human ladder was printed in 2001. And 2002 witnessed the birth of the first commercialized extrusion-based bioprinter “3D-Bioplotter”. Afterwards, the 3D fabrication technology without scaffolds was presented in 2004. Till 2019, scientists from Tel Aviv University bio-printed cardioid structure, which push 3D bioprinting technology towards its final goal, printing human organs, for the first time[5].

Even though 3D bio-printing shares the same idea of printing layer by layer as original 3D printing, its unique application of biomaterial in printing/manufactory opens a door of tissue engineering. And its terminal goal is to print personalized human tissue and organs, which solve the global organ shortage circumstance in the future. So far, bio-printing technique has been applied in different areas, such

as human tissue regeneration and implantation, drug delivery, cancer studies and surgery practice [2,6].

Recently, there are plenty of research achievements on 3D bio-printing for medical use. Parka and his colleagues printed an organ-on-a-chip which can add complex stimuli with *in vitro* tissue models to make it closer to living human tissues[7]. 3D hexagonal liver lobule-like in vitro tissue was made by Ma and his colleagues using a laser-assisted bioprinting system[8]. A liver model with sandwiched structures composed of endothelial cell layer and liver cancer cell layer was produced by inkjet bioprinting technology[9]. Kang's group fabricated muscle fibre-like bundle structures with PCL pillars applying micro-extrusion bioprinting system[10]. 3D aligned-muscle constructs with PCL-geometrical constraints were also created by the same technique [11]. What's more, a hybrid 3D cell printing system combined with extrusion and ink-jet modules was used for making a 3D skin model composed of a fibroblast-populated 3D dermal layer with a transwell system and keratinocytes of the epidermal layer[12].

Due to the differences in individuals' bodies, there is an increasing tendency of the importance of personalized medicine nowadays, and 3D bioprinting technology provides the opportunity of fitting the needs of it, including building biocompatible implants, tissue regeneration using different patient's own cells and the creation of novel drug delivery systems. It even can be applied in the food industry such as chocolate printing and artificial meat though this review will focus on the applications of 3D bio-printing in medical use in recent 10 years.

In recent three years, there is a rapidly increasing research interest in 3D bio-printing for tissue engineering in terms of new fabrication biomaterials and

different creatively designed scaffolds. According to this experimental research, it is promising that the medical applications of 3D bio-printing can be more effective in the near future. Also, patient-specific tissue models, organ-on-a-chip can be possibly be developed by using 3D bio-printing and hopefully applied in the actual clinic personalised treatment one day[7].

Some cutting-edge research found that conformational changes can be required for the materials designed for tissues engineering, while materials fabricated 3D bio-printing cannot meet the need[13]. Ashammakhi and his colleagues define four-dimensional printing (4D bio-printing) as “3D printing of cell-laden materials in which the printed structures would be able to respond to an external stimulus or internal cell forces”. It is a new technique which is able to include time-dependence into 3D printed tissue constructs. And there are other potential applications of 4D bio-printing besides tissue engineering, such as bio-actuators, biosensors and biorobots[14]. It can become a new development opportunity and a research hotspot for bio-printing techniques in tissue engineering soon.

Along with the development of 3D bioprinting technology, the business market also keeps growing. According to Global 3D Bioprinting Market Size & Trends Report, the global 3D bioprinting market size was valued at USD 1.4 billion in 2020. And it is predicted that the market size will grow at 15.8% rate annually between 2021 and 2028. The players in the 3D bioprinting market are mainly in North America, Europe and Asia. While North America dominated the largest scale of market share 32.4% in 2020. As we can see from the Figure 1.1, the commercial applications of 3D bioprinting relevant technology cover medical and dental use, biosensors, consumer/personal product testing, bio-inks and manufacturing food/animal products. And bioprinting for medical use takes the

biggest market share globally in 2020, which may be due to the increasing old population and the urgent demands of organ implantation[15].

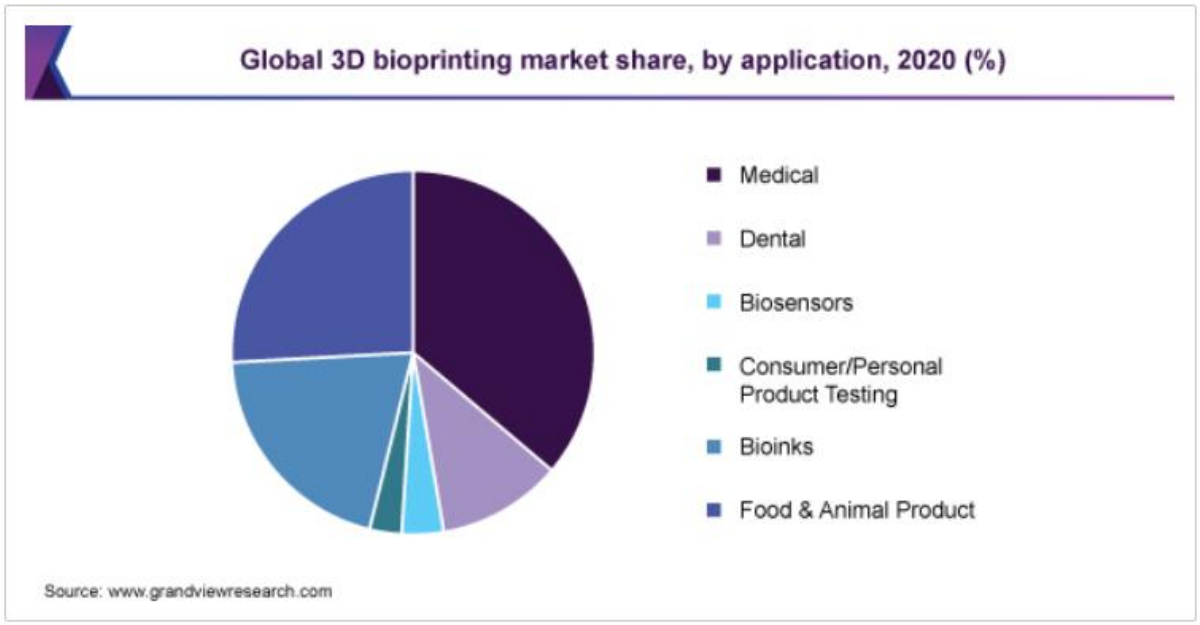

Figure 1.1 Global 3D bioprinting market share by application[15]

In this chapter, the basic concepts of 3D bioprinting technology will be covered, which includes the currently used bio-inks, the printing process, 3D bio-scaffolds and other printing outcomes, the applications of 3D bioprinting in drug delivery systems and tissue regeneration areas. And last but not the least, the current research gaps and limitations of this area will be discussed as the final part.

1.2 Bio-inks

Bio-inks, made of biocompatible and printable materials, are widely used in 3D bio-printing. Bio-inks can be mixed with cells prior to the printing process or be cultured with cells after they are printed in a specific computer-designed

structure[16]. Ideally, they are supposed to have appropriate mechanical, proper rheological properties, degradability, cost-effectiveness, having the ability to maintain their structure for a predictable period and non-toxicity[17-18]. In this section, the bio-inks which has been formulated and used in the following studies for 3D bio-printing will be introduced.

1.2.1 Polymer-based bio-inks

Polymer-based bio-inks take a lot of seats in the bio-ink field so far because of their low cost, easy accessibility and high biodegradability. Alginate, collagen, hyaluronic acid and gelatine are four types of polymers which are popularly used for making bio-inks. Other ingredients, such as polylactic acid (PLA), polyethylene glycol (PEG), starch and chitosan, are also tested and chosen to be the base of bio-inks in the previous research[19]. What's more, synthetic polymers, polycaprolactone, polyamide, polydimethylsiloxane, as well as these thermoplastic ones including acrylonitrile butadiene styrene and polylactic acid are all studied before. PLGA and PVC were also applied for medical use. Especially, Polyetheretherketone (PEEK) was used in producing bone regenerative materials for orthopedic applications[20].

Alginate, as one of the most popular bio-ink ingredients, was originally extracted from brown seaweed, which made alginate purely natural ingredients with low or no toxicity. Its chemical structure illustrates in Figure 1.2. However, due to the small amount of active binding sites are contained, purely applying natural bio-inks like alginate for bioprinting can lead to low bio-functionality and cell adhesion. So, they are usually formulated with chemical conjugation of synthetic and natural

polymers to enhance cellular responses and improve performance in 3D bioprinting process[7]. Besides, bio-inks containing alginate are required to be cross-linked after being printed as 3D shapes. Sodium carbonate, which has a chemical structure as shown in Figure 1.3, is normally used as the cross-linking solution for linking polymers as chains.

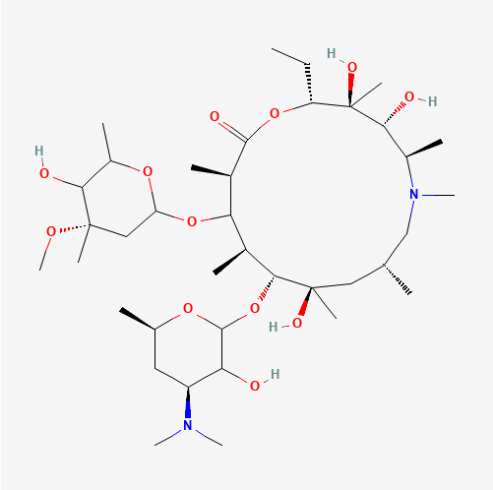

Figure 1.2 Alginic acid sodium salt (from brown algae, viscosity of 2% solution at 25℃)[21]

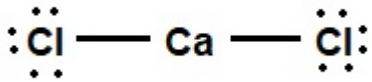

Figure 1.3 Lewis structure of Calcium chloride ($CaCl_2$)

1.2.2 Calcium phosphate cement (CPC)

Calcium phosphate is a common ingredient which can be found in several living organisms, such as bone and teeth. Its chemical structure illustrates in Figure 1.4.

Due to its unique physical-chemical properties, such as being set at room temperature (23 ± 1 °C), it has become one of the novel popular bio-inks for bone regeneration. Calcium phosphate ceramics were applied to the additive powder printing at the very beginning[22]. And it has been proved by previous studies that oil-based CPC is the proper material for 3D bio-printing in mild conditions at room temperature (23 ± 1 °C)[23].

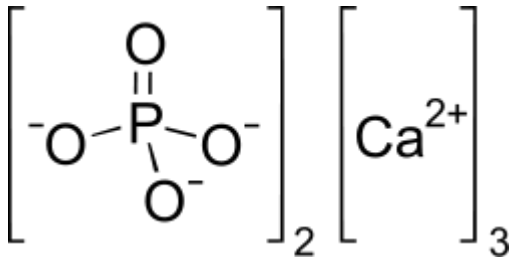

Figure 1.4 Chemical structure of Calcium Phosphate

1.3 3D bio-printing

3D bio-printing, as state-of-art printing technology, is designed to fabricate biological living tissues by patterning cells. The highlight of bio-printing is the variability of scaffold designs and its unique printing process with living cells[24]. The process of 3D bio-printing and different types of bio-printers will be introduced, followed by the summary of printing outcomes and the review of its recent applications in drug delivery and tissue regeneration.

1.3.1 3D bioprinters and printing process

There are several different 3D bio-printing techniques, they can be categorized as Ink-jet bioprinting systems (which is also known as droplet-based printing

techniques), Laser-assisted bioprinting systems and extrusion-based bioprinting systems[25,2].

Because the tiny droplets (1–100 picoliters) are applied as building blocks in inkjet bioprinting systems[26]. it offers a relatively high resolution than extrusion bioprinting. Ink-jet bio-printing shares the same principle as traditional ink-jet 3D printing. It can generate the droplet by an electrical, heating or mechanical pulse followed by the fabrication stage according to the computer-designed shapes. In most cases, low viscosity bio-inks are chosen to apply in this printing system[7].

Laser-induced forward transfer and laser-guided direct writing are two kinds of laser-assisted bioprinting systems. The droplet is deposited and formed by using laser, which is similar to the droplet-based techniques. While stereolithography and digital light projection, other two kinds of laser-assisted bioprinting systems, are applied to build the 3D constructs from a bulk medium with laser[27]. The resolution and printing speed of laser-assisted bioprinting systems are generally very high.

In an extrusion-based bioprinting system, the bio-ink is extruded through a syringe to a predesigned structure under the drive of mechanical or pneumatic pressure[28]. The technology can print with a very high density of cells, while it has very limited resolution. High viscosity bio-ink can be used in the system for keeping a good definition, but higher cell apoptotic activity will also be led to during the printing process[29].

These 3D bio-printing techniques have a common printing process, which is usually divided into three stages: pre-processing, processing and post-processing. It illustrates in Figure 1.5 below.

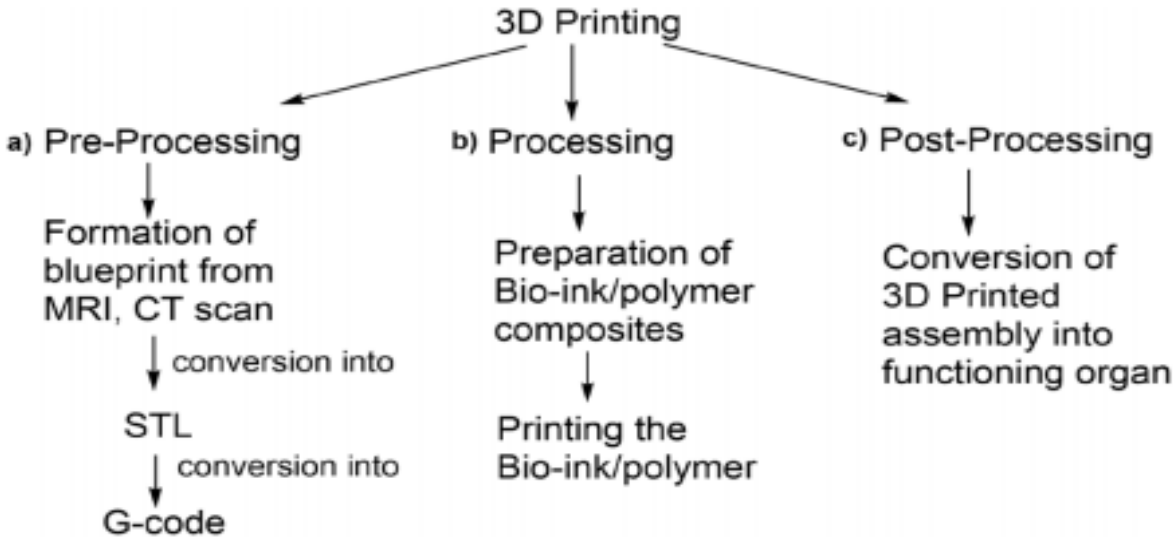

Figure 1.5. The basic process of 3D bio-printing[20]

And the currently available commercial 3D bio-printers are listed in Table 1.1 below.

Table 1.1 commercial 3D bio-printers[30]

Bioprinter and manufacturer	Fabrication technique	Specified resolution	Recommended materials
3Dn300TE, NScrypt	Extrusion-based	Line widths 20–100 μm	Not specified (viscosity range: 0.001–1000 Pa s)
3D-Bioplotter®, Envisiontec[a]	Extrusion-based	Minimum strand diameter 100 μm	Hydrogels, ceramic, metal pastes, thermoplasts
Bioscaffolder®, Gesim[a]	Extrusion-based	Not specified	Hydrogels, biopolymers (collagen, alginate) bone, cement paste, biocompatible silicones and metling polymers (CPL, PLA)
Biobot 1, Biobots[a]	Extrusion-based	Layer resolution 100 μm	Hydrogels, biopolymers (viscosity range: 100–10^4 Pa s, see table 3 for more details)
Inkredible+, Cellink[a]	Extrusion-based	Layer resolution 50–100 μm	Hydrogels (see table 3)
Biofactory®, RegenHU[a]	Extrusion-based Inkjet	Not specified	Bioink, Osteoink (see table 3 for more details)
Revolution, Ourobotics	Extrusion-based	Not specified	Collagen, gelatin, alginates, chitosan
Bio3D Explorers, Bio3D technologies[a]	Extrusion-based	Not specified	Not specified
CellJet Cell Printer, Digilab		Droplet size 20 nl–4μl	Water-based, hydrogels, alginate, polyethylene glycol
BioAssemblyBot, advanced solutions	Extrusion-based	Not specified	Not specified
Regenova, Cyfuse	Spheroid assembly	Related to spheroid diameter	Cells only (scaffold/biomaterial-free approach)
NovoGen MMX, Organovo[b]	Inkjet	20 μm	Cellular hydrogels
Dimatix Materials Printer, Fujifilm	Inkjet	20 μm	Water-based, solvent, acidic or basic fluids
Poietis[b]	LIFT	20 μm	Not specified

[a]Light curing system. [b]Not for sale, but utilized for bioprinting human tissue.

1.3.2 Applications of 3D bioprinting

In order to regenerate functional tissues, it is necessary to produce scaffolds to provide mechanical stability and promote cell ingrowth, especially for bone tissues. 3D bio-printing technology can be applied to meet the requirements of clinical regenerative tissues, such as specific shapes and sizes. The process of applying the technique in the clinic shows in Figure 1.6[6]. It was reported that homogeneously distributed cell-laden scaffolds can minimize the risk of rejection and increase the speed of integration with the host tissue in vivo[31, 32]. Current 3D bio-printed scaffolds for bone and their studies *in vitro, in vivo* and in situ are introduced in this section.

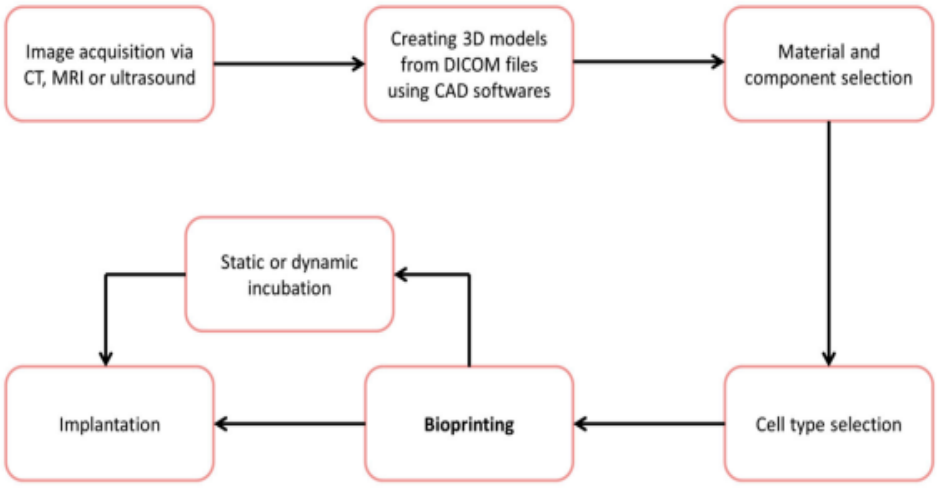

Figure 1.6 3D bioprinting process applied in the clinic[6]

Generating 3D bio-printed scaffolds for providing a pathway to the cells to form the functional tissues has become a popular technique in tissue regeneration for bone. The scaffolds are prepared by using biomaterials to make sure its

necessary characteristics, including biodegradability, high surface to volume ratio, biocompatibility, and sufficient mechanical properties[20].

Its high biocompatibility, automation capability, the function of preventing homogeneity issues during the cell seeding stage and personalized customization make it a suitable technique for tissue engineering, especially for bone regeneration. Cells, biological molecules and biomaterials can work together as bio-ink with a 3D bio-printer for producing allogeneic and autologous tissue implants or a bionic model for testing drugs and surgery plactice[6,14].

Tissue engineering is a technique that fabricates tissues or organs to reintroduce, heal and reconstruct the body when physical damage happened[32]. Producing tissues or organs which are highly similar to the original parts in terms of chemical composition as well as biological and mechanical properties is the main goal of tissue engineering[34].

In recent years, bone tissue engineering has become one of the most attractive research directions. The fabrication of appropriate bone replacement material is the key element for bone tissue regeneration. The functions of the bone matrix include simulating the bones' shape and providing the support for re-grow of natural bone cells. Due to the various characteristics of bones, such as mechanical strength unique shape, porosity and osteoconductivity, the high function of biomaterials and fabrication techniques are indispensable for bone tissue engineering[35-37].

Especially, 3D bio-printing has outstanding advantages for the regeneration or replacement of bone. The bio-printed bone implants can have personalised

shapes, high similarity compared to the original body parts and minimized immunological rejection because of containing the patients' own cells.

One of the tricky parts of bone replacement is the various shapes within every individual patient. Some parts of human bones have special shapes, and they are quite hard to be made by any other manufactory technology. Also, everyone is different in terms of the environment of the oral cavity. It is not possible that the "standard" shape of the artificial tooth can fit every patient. Unfit replacement materials can cause a lot of pain from the beginning of surgery to a long period of time, even the whole life of patients. 3D bio-printed materials are one of the best solutions to this situation. Any shape can be designed and achieved easily in the printing process, which means the material can be designed to meet every patient's need.

The strength of skeletal and teeth are quite hard to be replaced by other materials. These biomaterials which are the most similar to the original human skeletal are used in bio-printing, such as alginate. It will make sure that patients recover from surgery in the quickest way and come back to normal life with full and brilliant body functions. 3D bio-printed material will give patients a normal life without any worries or low self-esteem.

The immunogenetic reactions can be reduced to a minimum because of using patients' own cells in replacement material by 3D bio-printing. Compared to the traditional treatments, one of the highlights of 3D bio-printing is that the individual's cell will be used during the process of the manufactory. As a result, there is much less possibility that immunogenetic reactions will happen when the body finds the implanted material. It is really promising that the implanted material,

which was printed by bio-printer can be accepted by patients' body quickly. Also, the choice of printing material can minimize the side effects for the human body and prevent the second harm to the patients after surgery.

1.4 The key research gaps in the field

As the summary in previous paragraphs, plenty of achievements and progress have been achieved in the past 10 years in the field of 3D bio-printing, especially its applications in pharmaceutics and tissue regeneration. However, there are still lots of vital research gaps which are yet to be explored.

1.4.1 Gaps of bio-printing materials and technology

So far, even though there have been loads of novel bio-inks tested and analysed by using different experimental methods, there still are more physic-chemical properties information of bio-inks remaining unknown or unclear. 3D bio-printing, as a young scientific area, our steps of understanding the technology are still at the early-on stage. Plenty of questions is awaited to be solved, such as the factors which affect the bio-inks' printing properties, and the effect of bioprinting parameters on the printing outcomes. The wider and fast application of 3D bio-printing may be achieved after those mysteries have been explored.

What's more, the method of finding new or potential bio-inks in 3D bio-printing still remains as testing from scratch. Every research group all over the world starts in their own way to try different potential materials as bio-inks, which caused the waste of time and cost on the way to printable and useful bio-ink formulations. The Lack of effective methodology and direction for finding or choosing appropriate bio-inks and printing parameters for different pharmaceutical applications/areas of tissue regeneration has become one of the main reasons

for the low speed of creating new potential bio-inks for specific applications. In my opinion, big data analysis and predictive analysis can be effective tools to organise currently available information on bio-ink properties and even to build a model for fast material/formulation choosing. Potentially, it is a solution of accelerating the development of 3D bio-printing industry in the near future as well. While this combinational application of technologies has not been paid attention to or tried yet.

Although 3D bio-printing techniques developed extremely fast these years, there is still some space for the improvement of 3D bio-printing techniques and tissue engineering.

The shortage of ideal printing materials is one of the main barriers to the improvement of bio-printing. The ideal printing material not only needs to have appropriate physical properties for extrusion but also can provide a biocompatible environment for loading living cells in tissue engineering. These current biomaterials for regenerative medicine, such as alginate, collagen and fibrin gel are not developed for bioprinting originally, so the biological and physical conditions are barely satisfied specifically meeting the bioprinting needs[7,38-39]. Ideal bio-inks for bio-printing are still waiting to be formulated and tested in future research.

The printing resolution and post-printing viability are the two major limitations of bioprinting technology. It is reported that the currently available bioprinters with a micro-resolution are still insufficient for imitating the structure and functions of the real tissue. There are still some unknown factors which could affect the viability of bio-printed tissue. Modelling can be applied in more research in the future in

order to analyse the effect of parameters on the post-printing viability and even optimize filament integrity during bioprinting extrusion. In a word, the ability to improve resolution and viability are the main factors which can lead to the future development of 3D bio-printing technology[2].

Also, there are still some research gaps waiting for filling in this area because it is still a raising technique. For example, Osaki and his colleagues found that perfusable microvascular networks lake for most of the current solid organs which were made by tissue engineering[40]. The structure has the functions of replicating endocrine signalling, imitating blood tissue or organ barrier and constructing tissues of macroscopic scale. While the need is ignored by researchers so far[41]. What's more, the co-culturing technology should be advanced for the culture of liver, nerve and heart cells soon. In addition, it is necessary to focus on researching the effects of the scaffold design parameters on cell metabolic activities and understanding the interaction between multiple types of cells.

1.4.2 Gaps in applications

Moreover, there are also some gaps remaining during the applications of 3D bio-printing. The efficacy of scaffolds made of different bio-ink formulations as novel drug delivery systems has yet to be studied by dissolution test etc, especially for anti-cancer drug delivery. And the way of 3D bio-printed materials affects or interact with cells and change the cells' behaviour, the safety and toxicity of 3D bio-printed material in the short or long term, are still unknown or unclear, which are waiting to be analysed in vitro cell culture studies.

Besides, the reinfection after bio-printed implants is still one of the commonest reasons of regenerative tissue failure currently, which is an essential and urgent problem requiring to be solved. The potential solution relays on the creation of novel bio-ink formulations containing anti-cancer or anti-bacterial ingredients, or the successful coating of 3D bio-printed scaffolds. The new effective bio-ink formulations and mechanical properties of scaffolds are still yet to be analysed. Solving those unknowns will be milestones on the road towards the 3D bio-printing of personalised regenerative tissues or organs which can be successfully used in clinical surgery in the future.

Apart from the technology limitations and challenges, there are also translational barriers and some ethical issues which need to be overcome.

It is increasingly difficult to get grants and funding for doing clinical trials for new bio-printed products. Also, the spending time and cost for meeting complex regulations lead to the barriers to the translation between the technique and clinical applications. These financial problems and challenges faced by the research pioneers hinder the development of technology seriously[42].

In the near future, it is said that the ethical issues that 3D bio-printing tissue engineering may associate could be the uncertain long-term risk of implanted cells, the difficulty of wider and fair popularization of the technology because of the high cost and the possible abuse of the technology caused by the lack of regulation and governance etc[43-45].

1.5 Conclusion

In a word, this chapter has presented the relevant background information of 3D bioprinting field in general which is needed for one to understand 3D bioprinting in the aspect of biomaterial, printing mechanism, bio-scaffolds and the current clinical applications of both drug delivery and tissue regeneration. In addition, it is followed by an analysis of the key research gaps and future perspectives in the biomaterials and applications of 3D bioprinting technology so far. In summary, 3D bio-printing technology for biomedical use is advancing rapidly in the past 10 years. Although there is still space to be improved continually, printing fully functional personalized human organs, which is known as the final goal of 3D bio-printing, is promising to achieve in the near future.

1.6 The aims and objectives

The aim of this overall study is to analysis and upgrade the current 3D bioprinting material and bio-fabrication technology for advanced applications in creating novel drug delivery systems and tissue regeneration. The objectives are:

(1) To create different bio-inks and scaffolds with anti-cancer functions. (2) To compare the physical-chemical properties of different bio-inks and the mechanical properties of scaffolds. (3) To evaluate the therapeutic functions of CPC and polymer-based bio-inks and scaffolds, such as analyzing coated CPC scaffolds as an anti-cancer drug delivery system and investigating the properties and cell repair function of EPO loaded PLA/PEG scaffolds. (4) To study the cell behaviour diversity when culturing with scaffolds in different structures and sizes.

Thus, the research has essential meanings as it contributes to the current understanding of biomaterials for bioprinting. The research not only provides more information on the properties of novel biomaterials but also gives insight into the applications on the bio-printed scaffolds, such as anti-cancer drug-loaded scaffolds as effective drug delivery systems and EPO-loaded scaffolds for clinical cell repair use. Those analysis data is valuable for further exploration on formulating the appropriate bioinks for 3D bioprinting in the applications of drug delivery and tissue regeneration. At the same time, those scaffolds are a successful attempt for promising clinical use with effective in vitro trial results.

Chapter 2 explored the effect of pH value and alginate concentration on the physic-chemical properties (viscosity, syringability and dipping) of pure alginate bio-inks while Chapter 3 investigates the physic-chemical properties of alginate-based bio-ink formulations and the drug delivery properties of 5-FU loaded scaffolds through cell culture studies. Chapter 4 looked at novel EPO-loaded PLA/PEG scaffolds for cell repair while Chapter 5 looked at the properties and anti-cancer drug delivery function of 5-FU coated CPC scaffolds. Then, chapter 6 gave insight of how the 1BR, U2OS HEK293T-GFP and HeLa-GFP cell lines changes behaviour when they were cultured with scaffolds in different structures and sizes in both the short and long term. Finally, Chapter 7 provides a summary of all the findings throughout the thesis and proposes further future investigations.

1.7 The novelty of the thesis

- Scaffolds bioprinted using a specific alginate-based bioink (alginate-methylcellulose 1:1) were confirmed *in vitro* effectively delivering a model anti-cancer drug, 5-fluorouracil (5-FU).
- 3D bioprinted scaffolds made with novel Polylactic acid (PLA) and polyethylene glycol (PEG) formulations were proved to have cell repair functions.
- Anti-cancer drug 5-fluorouracil (5-FU) coated calcium phosphate scaffolds were confirmed *in vitro* to be an effective and novel drug delivery system for anti-cancer therapy.

Chapter 2 The pre-bioprinting analysis on the physical-chemical of pure alginate bioinks

2.1 Introduction

Among many novel bio-inks for bio-printing, alginate is still the most frequently used and natural non-toxic material[46]. Alginate will keep playing an important role as one of the necessary and popular ingredients in bio-ink formulations due to its high biocompatibility, biodegradability and low-cost[47].

Viscosity is a measure of the resistance for fluid to flow at a given rate[48]. The pH value and the concentration are two important factors impacting the viscosity of pure alginate bio-inks[47]. Those two factors can cause a huge change in bio-ink properties and the final bio-printing outcomes. Syringability is to measure how capable the fluid can be dispensed from a syringe. While this area has not been investigated in detail yet. This research gap can cause the waste of time and material for trying different bio-ink formulations and slowing down the process of novel formulation development and effectiveness of the whole bio-printing process.

Phosphate-buffered saline (PBS) is a water-based salt solution widely used in biological research[49]. PBS with pH values of 1.2, 6.6 and 7.2 were chosen as examples of strong acidic, weak acidic and weak alkaline environments, respectively, in this chapter for bio-inks. Excel is a commonly used data analysing tool for developing mathematic models[50], which are useful for predicting the properties of alginate bio-inks in the early ink making process and increasing the

effectiveness of choosing suitable alginate bio-ink formulations for following bio-printing.

This chapter aims to find the effect of alginate concentration on the physical-chemical properties of alginate bio-inks in different pH environments. Viscosity, dipping properties and syringability of every bio-ink formulation were tested for comparison. The data was analysed visually and statistically for building a more specific and predictable mathematic model.

2.2 Material and methods

2.2.1 Materials

Alginate acid, sodium salt (viscosity of 2% solution at 25℃) was purchased from Acros organics, Thermo Fisher Scientific, USA; phosphate buffer (PBS, pH=1.2, 6.6 and 7.2) were purchased from Sigma-Aldrich, Merck, Germany.

2.2.2 Methods

2.2.2.1 The preparation of bio-inks

PBS solution in three different pH values (1.2, 6.6 and 7.2) were used to make alginate bio-inks in the concentration of 10, 15, 20, 25, 30, 35, 40 g/L. The composition of formulations was indicated in Table 2.1. For every formulation, alginate was weighed accurately and dispersed uniformly in PBS under rapid agitation via a magnetic stirrer until the mixture was homogeneous.

Table 2.1. Composition of pure alginate bio-ink formulations

Concentration of bio-inks (g/L)	Alginate (g)	PBS (mL) (pH=1.2/6.6/7.2)
10	3	300
15	4.5	300
20	6	300
25	7.5	300
30	9	300
35	10.5	300
40	12	300

2.2.2.2 Viscosity test for bio-inks

Viscosity measurements of all bio-inks were undertaken using Brookfield DV2T viscometer (Brookfield, USA). In order to measure the viscosity of all the formulations under the same experimental conditions, the test was conducted at a speed of 6 RPM for 5 s. The test module of the viscometer was set as a single point average (average data for 1 second at the end of the step). Spindles numbers LV-1 to 4 were used for bio-inks depending on their viscosity range, the specific spindle used for every bio-ink was illustrated in Tables 2.2 to 2.4.

2.2.2.3 Dipping test for bio-inks

The dipping test was conducted by texture analyzer (Stable Micro Systems, Surrey, UK) with a ½'' diameter cylinder probe (Batch NO. 15522). The test

method was set as ‘Return to Start’ and the mode was compression. The test speed was 2 mm/Sec. The data was analyzed by Exponent software.

2.2.2.4 Syringability test for bio-inks

Syringability was evaluated by texture analyser (Stable Micro System, Surry, UK) with a 5 ml stringers probe. The test speed was set up at 5 mm/Sec. The test method was set as ‘Return to Start’ and the mode was compression. The target mode was set to a distance of 40 mm. The data was analyzed by Exponent software.

2.2.2.5 Data analysis

The data analysis was conducted using the Excel software for researching the relations between the pure alginate bio-ink formulations and their physical-chemical properties.

2.3 Results and discussion

2.3.1 Viscosity test for alginate bio-inks

2.3.1.1 Visually comparison

The viscosity of alginate bio-inks was shown in Tables 2.2 to 2.4. The viscosity of bio-inks in pH=1.2, 6.6 and 7.2 all have a positive correlation with the concentration of alginate. For bio-inks in PBS pH=1.2 (Table 2.2), the viscosity goes up nearly 20 times when the concentration increased from 10 g/L to 15 g/L. There is also a big increase in viscosity between 15 g/L and 20 g/L alginate bio-inks. The results showed that the viscosity of 30 g/L alginate bio-ink is around 7 times higher than when 25 g/L bio-ink was used. In terms of the alginate bio-inks in PBS pH=6.6 (Table 2.3), the viscosity increases the fastest while the

concentration of alginate changes from 25 g/L to 30 g/L, which is a similar trend compared to the alginates in pH=1.2. Surprisingly, the viscosity of 40 g/L alginate bio-inks in pH=1.2 and pH=6.6 is nearly 10 times of the 40 g/L alginate bio-inks in pH=7.2 (Table 2.4). The pH value of PBS plays a vital impact on the viscosity of alginate bio-inks when its pH was changed from acid to weak alkaline. The trend of the fastest viscosity changes between 25 g/L and 30 g/L alginate bio-inks belonged to PBS pH =7.2 compared to the other two environments, pH=1.2 and 6.6.

Table 2.2 The viscosity of alginate bio-inks in PBS pH= 1.2

Formulations (g/L)	Spindle number	Speed (RPM)	Time (s)	Viscosity (cP)
10	LV-1(61)	6	5	109
15	LV-2(62)	6	5	1885
20	LV-1(61)	6	5	6504
25	LV-3(63)	6	5	6540
30	LV-4(64)	6	5	43200
35	LV-4(64)	6	5	83300
40	LV-4(64)	6	5	118800

Table 2.3 The viscosity of alginate bio-inks in PBS pH= 6.6

Formulations (g/L)	Spindle number	Speed (RPM)	Time (s)	Viscosity(cP)
10	LV-1(61)	6	5	465
15	LV-2(62)	6	5	1065
20	LV-2(62)	6	5	2755
25	LV-3(63)	6	5	4580
30	LV-4(64)	6	5	18200
35	LV-4(64)	6	5	42600
40	LV-4(64)	6	5	89000

Table 2.4 The viscosity of alginate bio-inks in PBS pH= 7.2

Formulations (g/L)	Spindle number	Speed (RPM)	Time (s)	Viscosity(cP)
10	LV-1(61)	6	5	256
15	LV-1(61)	6	5	796
20	LV-1(61)	6	5	1782
25	LV-3(63)	6	5	2700
30	LV-3(63)	6	5	7300

35	LV-3(63)	6	5	9860
40	LV-3(63)	6	5	10060

2.3.1.2 Statistical analysis and mathematic model.

Figure 2.1 illustrates how the two factors, alginate concentration and pH value of PBS affect the viscosity of alginate bio-inks. As we can see, for those bio-inks which have the same pH value, there is index-based growth of viscosity when the concentration of alginate increases from 10 g/L to 40 g/L. Though the viscosity of those bio-inks in pH=7.2 increased at a significantly ($p < 0.05$) slower speed compared to bio-inks in pH=1.2 and 6.6. It is due to the high impact caused by the changing of pH value from acid to alkaline, even though pH 7.2 is such a weak alkaline environment. In a word, the concentration of alginate and pH value are two important factors for the viscosity of alginate bio-inks. The index-based fictions relevant to those two factors are useful for calculating and predicting the bio-inks viscosity, which can be a guide for choosing suitable alginate bio-ink formulations used in bio-printing. This indicates that by changing the concentration of alginate and also the pH of the medium any viscosity was achievable for alginate bio-inks and the viscosity of the polymeric bio-ink can be modulated easily.

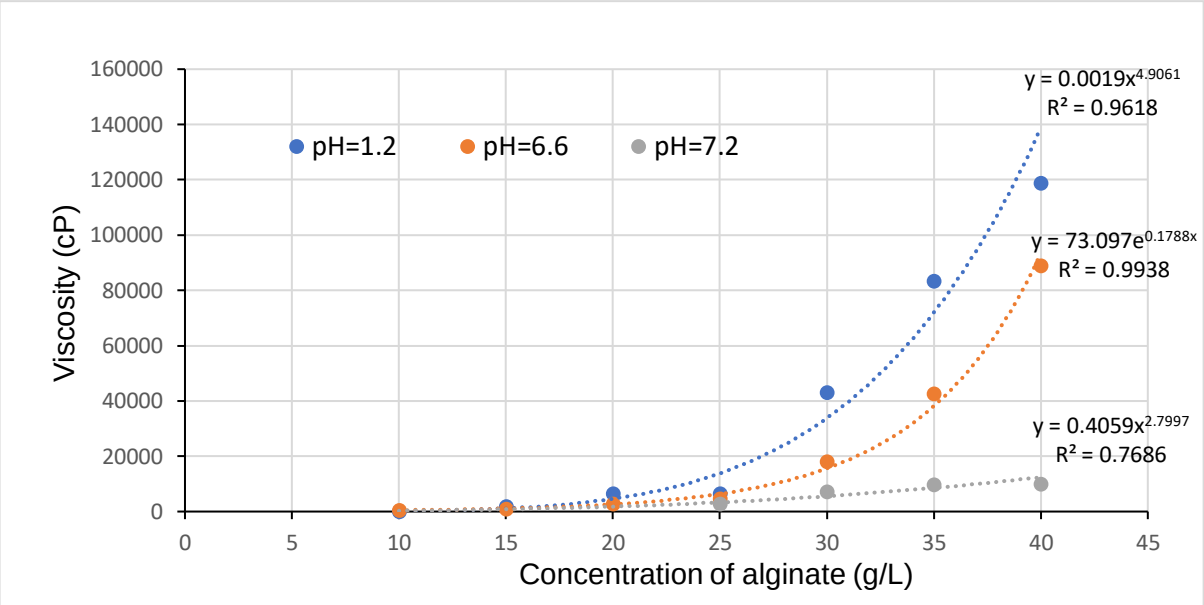

Figure 2.1 The effect of alginate concentration and pH value on the viscosity of alginate bio-inks.

2.3.2 Dipping test for alginate bio-inks

The dipping test results for alginate bio-inks in three different pH values are shown in Figures 2.2-2.4. Every sample was distinguished and tabled with a different color in those figures. In three pH environments, bio-inks share the same trend that the higher concentration of the alginate bio-inks requires more force to dip in. Bio-ink containing 40 g/L alginates in pH=1.2 (Figure 2.2) need the maximum force to dip in when compared to all the other bio-inks in pH=6.6 and 7.2 (Figure 2.3-2.4), which may be because it has the highest viscosity within all bio-inks. Interestingly, for bio-inks in pH=1.2 and 6.6, the force required for 25 g/L and 30 g/L has big differences (Figures 2.2-2.3) while it shows no significance ($p > 0.05$) for bio-inks in those two specific concentrations when was pH=7.2 (Figure 2.4). This could be due to the impact of pH value being more vital in an acidic environment compared to an alkaline environment.

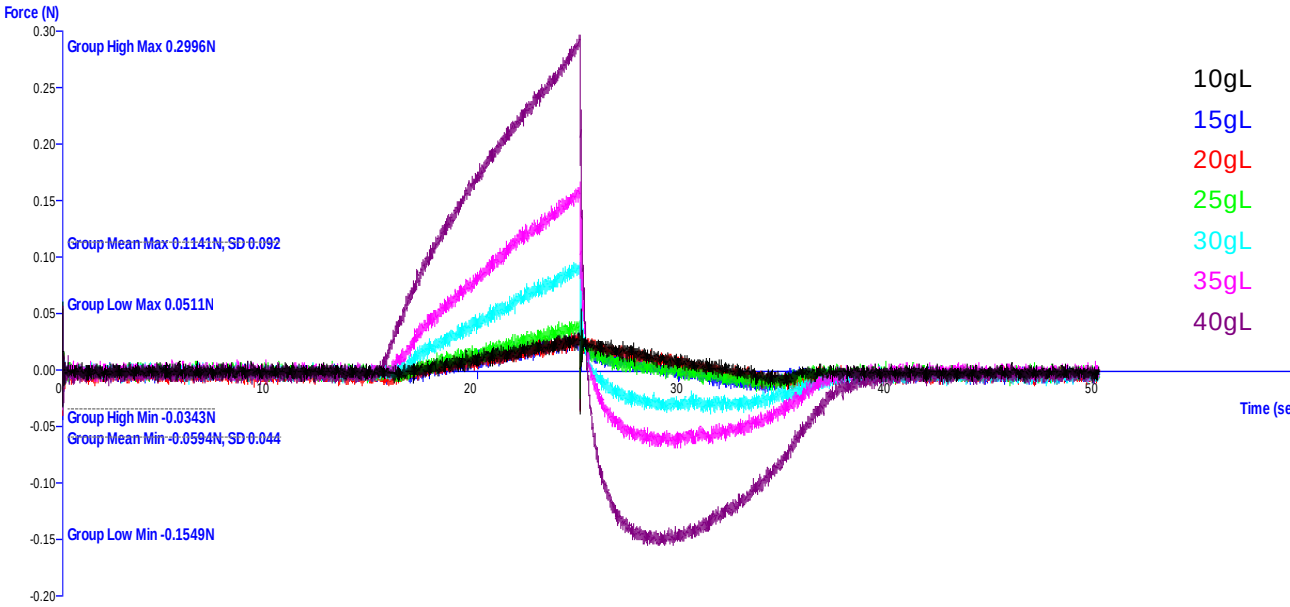

Figure 2.2 Dipping test of alginate bio-inks with PBS pH=1.2.

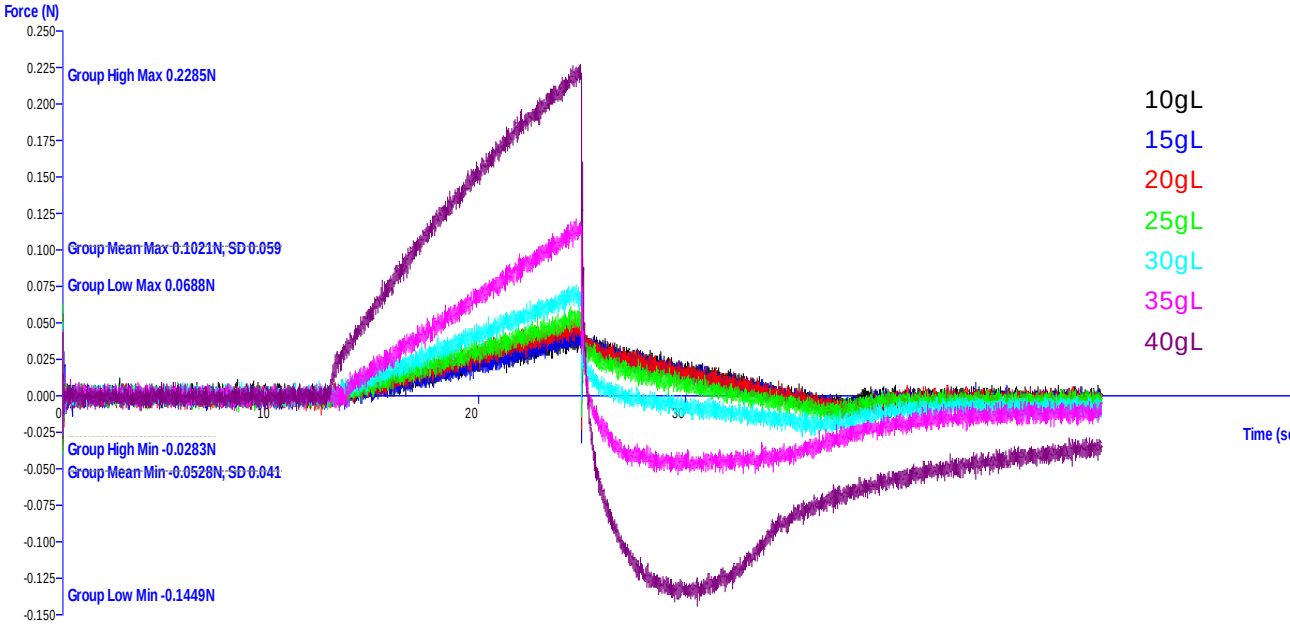

Figure 2.3 Dipping test of alginate bio-inks with PBS pH=6.6.

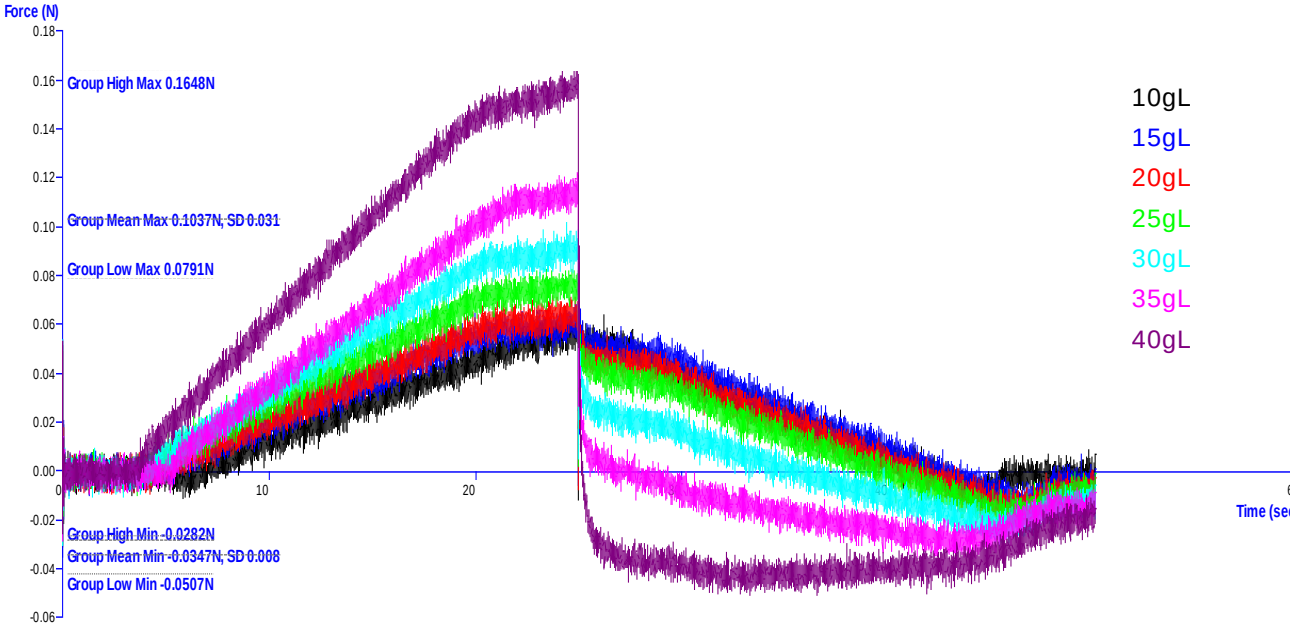

Figure 2.4 Dipping test of alginate bio-inks with PBS pH=7.2.

2.3.3 Syringability test for alginate bio-inks

The results of syringability test for alginate bio-inks in three pH values are illustrated in Figures 2.5 to 2.7. Similar to the trend in the previous dipping test results, the force required for each bio-ink formulation increases with the concentration. However, the bio-inks in pH=7.2 (Figure 2.7) need more force for extrusion compared to those formulations in pH=1.2 and 6.6 (Figure 2.5 and 2.6). This unique syringability parameter may be due to the rheology of bio-inks in pH=7.2 which was affected by the weak alkaline environment compared to acidic ones. The rheology profile may be another factor impacting pure alginate bio-ink during extrusion through syringes with needles, which requires further analysis.

It was interesting to note that bio-ink containing 15 g/L alginate needed more force to be extruded than the sample containing 20 g/L in pH=1.2 (Figure 2.5).

This was unexpected and no reason was explored for the strange behaviour of bio-ink containing 15 g/l of alginate.

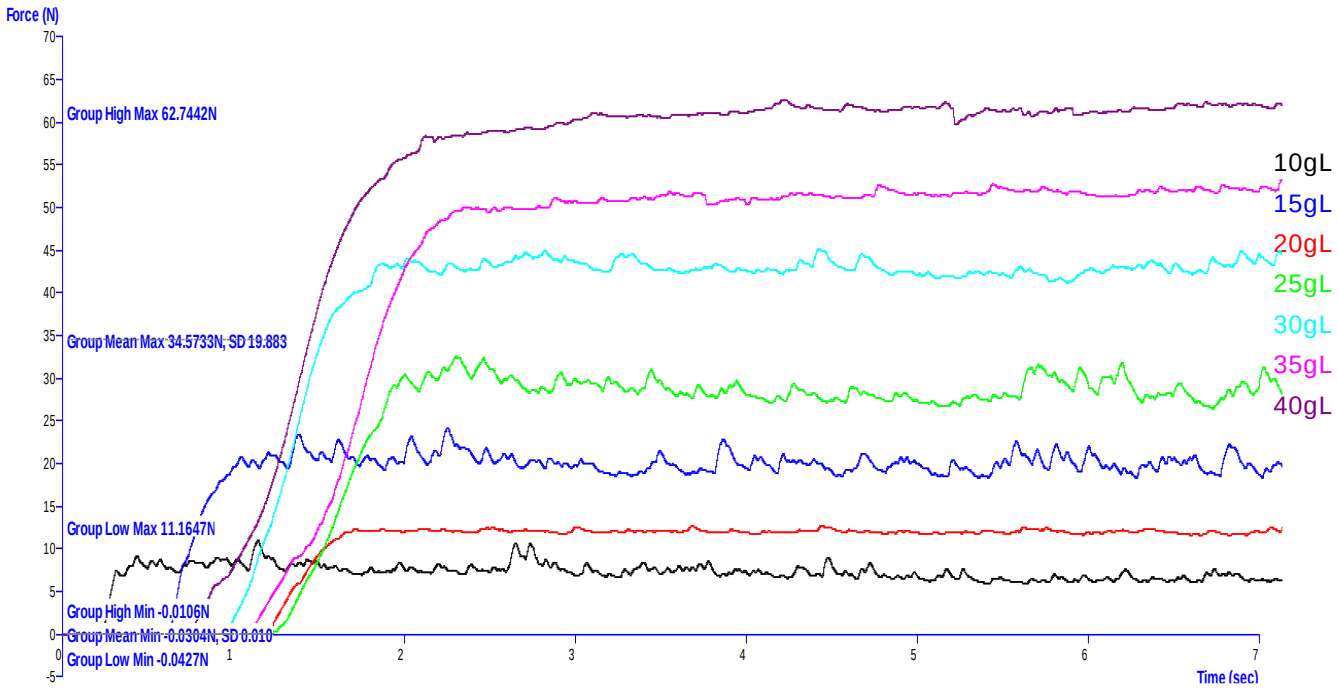

Figure 2.5 Syringability test of alginate bio-inks with PBS pH=1.2.

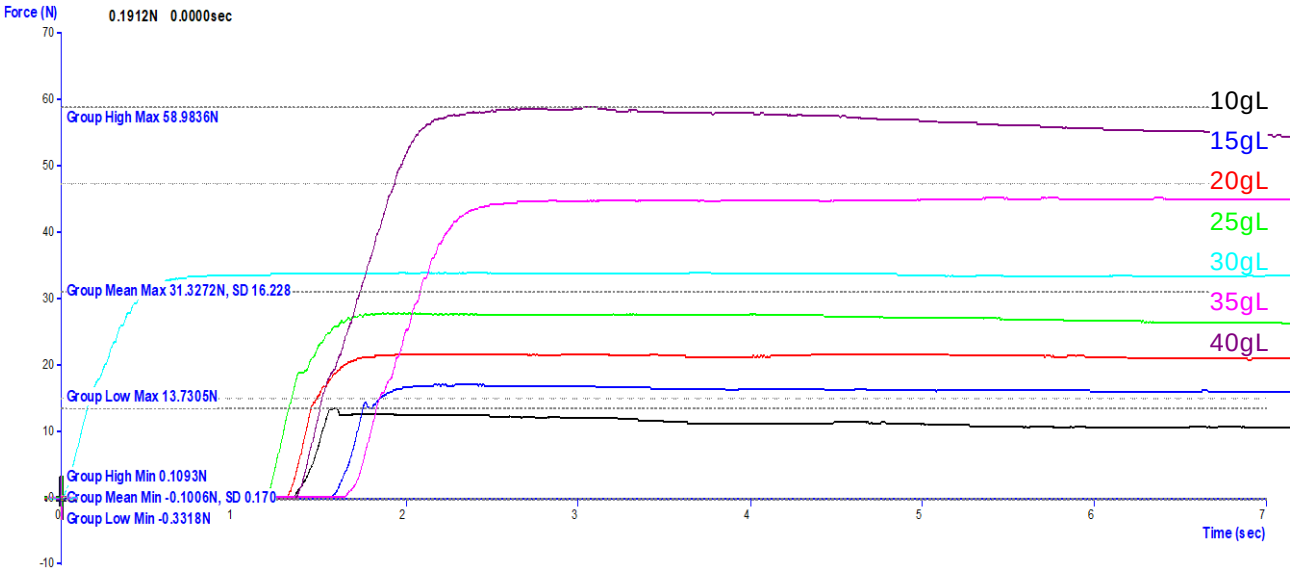

Figure 2.6 Syringability test of alginate bio-inks with PBS pH=6.6.

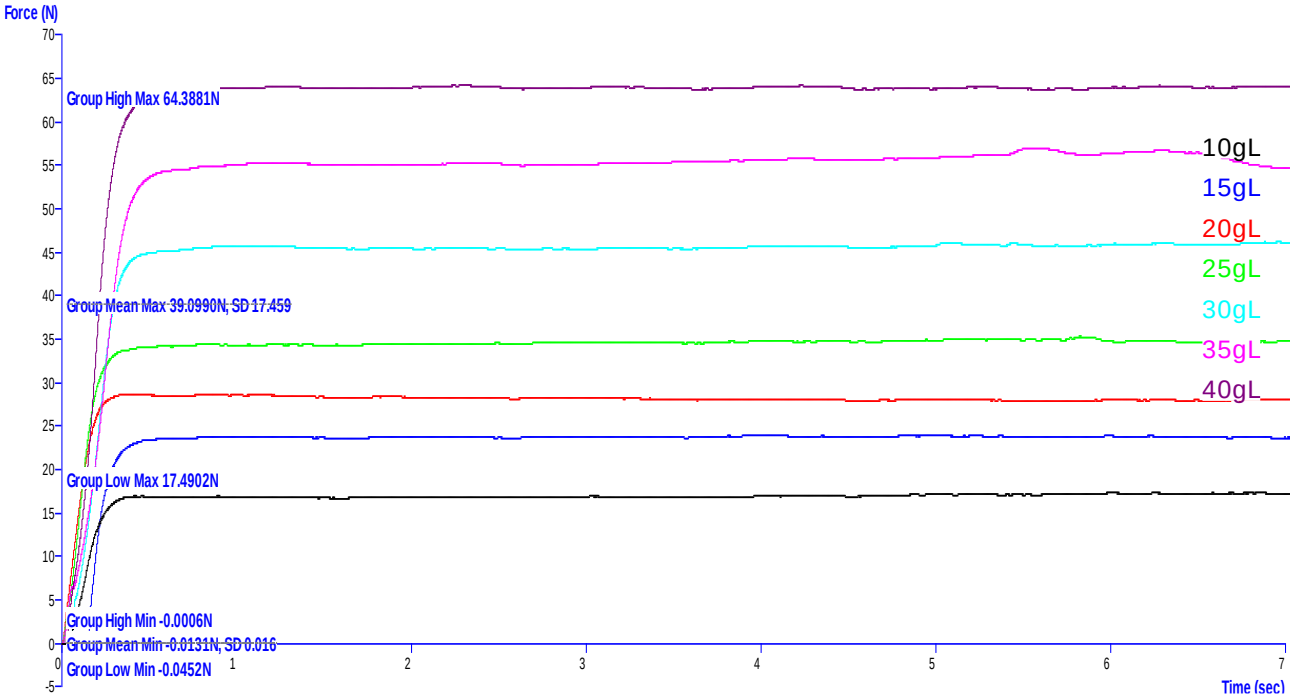

Figure 2.7 Syringability test of alginate bio-inks with PBS pH=7.2.

2.4 Conclusion

In conclusion, this chapter analysed how the concentration and pH value affect the viscosity, dipping and syringability of alginate bio-inks. The mathematic models of the changing physical-chemical properties for alginate bio-inks were found, the relationship between the concentration of alginate (C) and viscosity (V) is $V=0.0019C^{4.9061}$ at pH=1.2, $V=73.097e^{0.1788C}$ at pH=6.6 and $V=0.4059C^{2.7997}$ at pH=7.2 perspectively. The model can be helpful and in increasing the effectiveness of the formulation development and designing suitable alginate-based bio-inks during the pre 3D bio-printing stage.

Chapter 3 3D bioprinting of novel alginate-based scaffolds as an anti-cancer drug delivery system

3.1 Introduction

3D bio-printing, as cutting-edge printing technology, is designed to fabricate biological living tissues by patterning cells. The highlight of bio-printing is the variability of scaffold designs and its unique printing process with living cells[51]. Bio-printing technique has been applied in different areas, such as human tissue regeneration and implantation, drug delivery, cancer studies and surgery practice[52-53]. Recently, there are plenty of research achievements on 3D bio-printing for medical use. Park and his colleagues have printed an organ-on-a-chip which can add complex stimuli with in vitro tissue models to make it closer to living human tissues[54]. 3D hexagonal liver lobule like in vitro tissue has been made by Ma and his colleagues using a laser-assisted bioprinting system[55]. A liver model with a sandwiched structure composed of an endothelial cell layer and liver cancer cell layer was produced by ink-jet bioprinting technology[56]. Kang's group fabricated muscle fiber-like bundle structures with PCL pillars applying a microextrusion bioprinting system[57]. 3D aligned-muscle constructs with PCL-geometrical constraints were also created by the same technique[58]. A hybrid 3D cell printing system combined with extrusion and ink-jet modules were used for making a 3D skin model composed of a fibroblast-populated 3D dermal layer with a transwell system and keratinocytes of the epidermal layer[59]. Although the technology is advanced at high speed, it is still limited by the currently

available bio-printing materials and bio-inks and the most ideal materials for bio-printing is still yet to be discovered.

Alginate is one of the most popular natural bio-inks applied in 3D bio-printing. The natural bio-inks, such as collagen, gelatin and fibrin has brilliant biological features to provide biochemical and physical stimuli[60]. However, due to containing a small amount of active binding sites, natural bio-inks such as alginate can lead to low biofunctionality and cell adhesion. As a result, they are usually combined with the chemical conjugation of synthetic and natural polymers to enhance cellular responses. $CaCl_2$ and trisodium citrate (TSC) solutions can be used as crosslinkers for enhancing the stackability of alginate-based scaffolds[61]. Due to the weak bonding ability of alginate, methylcellulose (MC), a popular polymer, is commonly added to increase the polymer concentration and the viscosity of the bio-ink[62]. Nanoclays are particles of layered mineral silicates in a nano-scale. It is the potential to be used for multiple functions, such as drug delivery carriers, gas absorbents and rheological modifiers[63].

The aim of this chapter is to print 5-fluorouracil (5-FU) loaded 3D alginate-based scaffolds as a novel anti-cancer drug delivery system. For this purpose, the properties of different formulations of alginate-MC bio-inks, including their viscosity, syringability, cross-linking function and microscopic morphology, were evaluated for finding the most suitable bio-ink. For comparison purposes, the alginate-based bio-inks contained nanoclay were evaluated in this research. The Alginate-MC 1:1 and 2:1 w/w (formulations 2 and 7) bio-ink was chosen for

loading 5-Fluorouracil (5-FU) and was 3D bio-printed as scaffolds. And the efficiency of killings cancer cells was tested by in vitro cell culture.

3.2 Materials and methods

3.2.1 Materials

Nano-clays (hydrophilic bentonite), algainte, methylcellulose(MC), deionised water, phosphate buffer (PBS, pH=7.4) were all purchased from Sigma-Aldrich, Merck, Germany. Viscometer (Brookfield DV2T), LV spindles 61-64 was used to measure the viscosity. Calcium chloride hexahydrate (CaCl2, 98+%, for analysis, purchased from Acros Organic, Thermo Fisher Scientific, USA). SE3D mini bio-printer was used to print scaffolds. Cell lines (HeLa and HEK293T) all stably express GFP constructs (generated at GDSC, Sussex, UK) were maintained in DMEM supplemented with 10% FCS, penicillin/streptomycin and L-Glutamine at 37℃ and 5% CO2. Those solutions for cell culture are purchased from Fisher Scientific, Thermo Fisher Scientific, USA.

3.2.2 Methods

3.2.2.1 Preparation of bio-ink formulations with methylcellulose (MC)

The composition of formulations was indicated in Table 3.1. For every formulation, alginate was weighed accurately and dispersed uniformly under rapid agitation via a magnetic stirrer in deionised water before methylcellulose (MC) or nano-clays were added to the alginate solution. It usually took 2 hours for bio-inks to swell if the formulation contained MC. Nano-clays were the final ingredients to be added and stirred until the mixture was homogeneous.

Table 3.1. Composition of bio-ink formulations with MC

Formulation Code	Nano-clays (g)	Alginate (g)	MC (g)	Deionised water (mL)
F1	0	1.2	0	40
F2	0	1.2	1.2	40
F3	1.2	1.2	1.2	40
F4	0	1.2	2.4	40
F5	1.2	1.2	2.4	40
F6	0	2.4	0	40
F7	0	2.4	1.2	40
F8	1.2	2.4	1.2	40
F9	0	2.4	2.4	40

3.2.2.2 Viscosity test for bio-ink formulations

Viscosity measurements of all bio-inks were undertaken using Brookfield DV2T viscometer (Brookfield, USA). In order to measure the viscosity of all the formulations under the same experimental conditions, the test was conducted at a speed of 2 RPM for 5 s. The test module of the viscometer was set as a single point average (average data for 1 second at the end of the step).

3.2.2.3 Syringability assessment for bio-ink formulations

Syringability was evaluated by texture analyser (Stable Micro System, Surry, UK) with a 5 ml stringers probe. The test speed was set up at 5 mm/Sec. The test method was set as 'Return to Start' and the mode was compression. The target mode was set to a distance of 40 mm. The data was analyzed by Exponent software.

3.2.2.4 Dipping assessment for bio-ink formulations

The dipping test was conducted by texture analyzer (Stable Micro Systems, Surrey, UK) with a ½'' diameter cylinder probe (Batch NO. 15522). The test method was set as 'Return to Start' and the mode was compression. The test speed was 2 mm/Sec. The data was analyzed by Exponent software.

3.2.2.5 The cross-linking of scaffolds

Once the constructs are fabricated on a Petri dish via the 3D bio-printer (SE3D), 0.5 M CaCl2 was added to this construct and immersed the scaffolds for 10 minutes in the solution until the scaffold structure is fully settled.

3.2.2.6 Microscopy assessment for bio-inks

Images of bio-inks were taken (at 10x magnification) using Floid® Cell Imaging Station (Thermo Fisher Scientific, Waltham, MA, USA). The intensity of lighting was chosen as 30% for all bio-inks.

3.2.2.7 3D bio-printing of drug-loaded alginate-MC

Different amounts of 5-FU powder were fully dissolved in DI water at 80 ºC to obtain 1%, 2%, 5%, 10% 5-FU solution. They were mixed homogeneously with

alginate-MC bio-ink formulations No.2 and NO.7 for 3D bio-printing after cooled down to room temperature (23 ± 1 °C).

3.2.2.8 Cell study of drug-loaded alginate-MC scaffolds

The obtained scaffolds were sterilised by UV light for 1 hour (for sterilisation) and transferred to 12 well plates. Cells were plated at a density of 0.4x105. After 1 day and 4 day culture, the scaffolds were transferred to a new 12 well plates and washed three times with PBS pH=7.4. And then cells in every well were count perspectively. Final Images were taken 4 days post-seeding at 4x magnification using Floid® Cell Imaging Station (Thermo Fisher Scientific, Waltham, MA, USA).

3.3 Results and discussion

3.3.1 Microscopy assessment for bio-inks

All bio-ink formulations (F1 to F9) were assessed under a microscope (Figure 3.1). Compared F1, F2 and F4, the increased percentage of MC in the bio-ink leads to more white dots under the microscope. It can be observed that formulations F3, F5 and F8, appear to be greyer under the white light of the microscope. It is due to the suspension of hydrophilic bentonite, which is known as nanoclay in those formulations. The micromorphology can be changed when the nanoclay is involved. And in terms of the F9, the polymer concentration is too high and covers the whole view under microscopy.

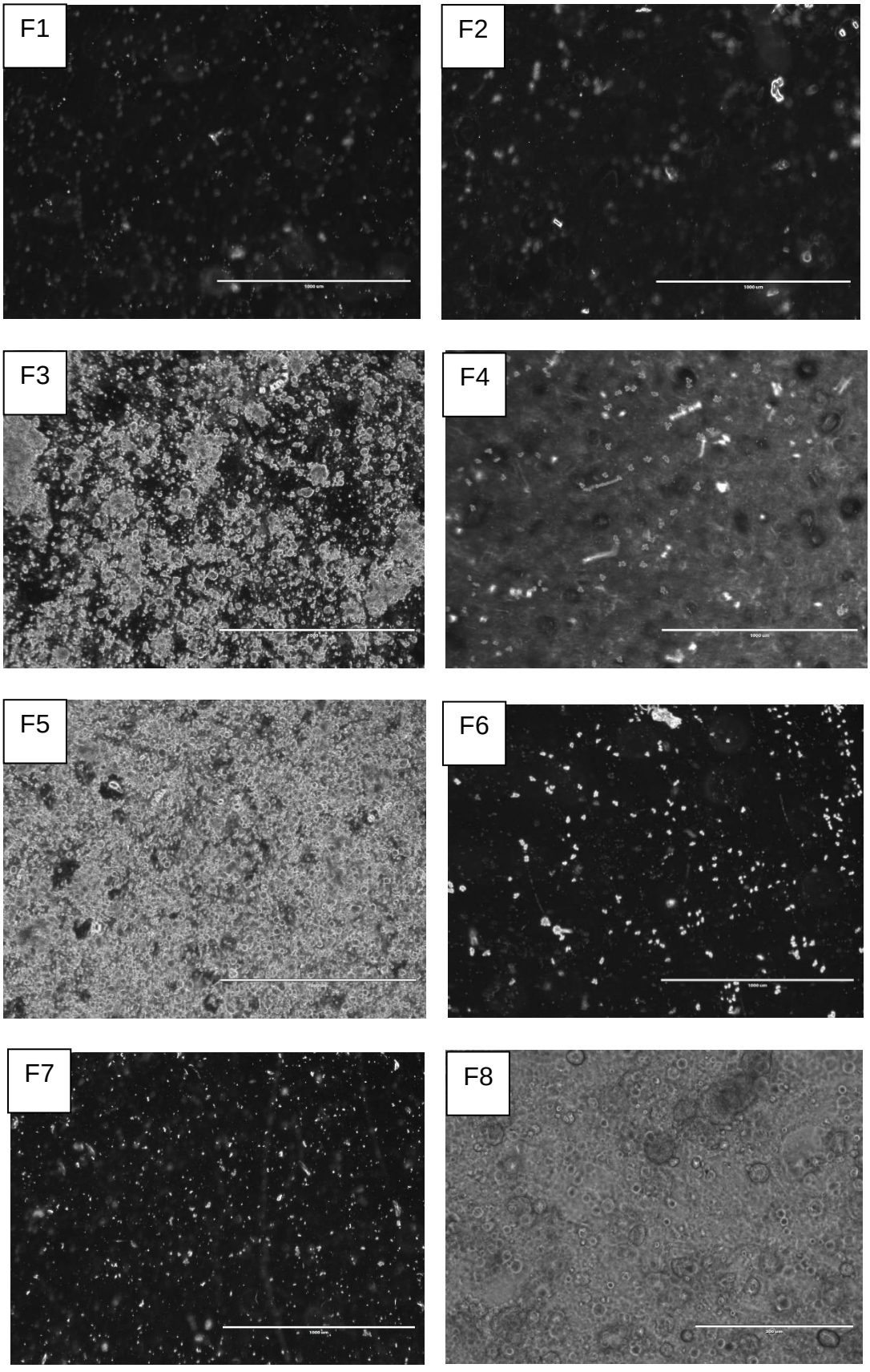
F1
F2
F3
F4
F5
F6
F7
F8

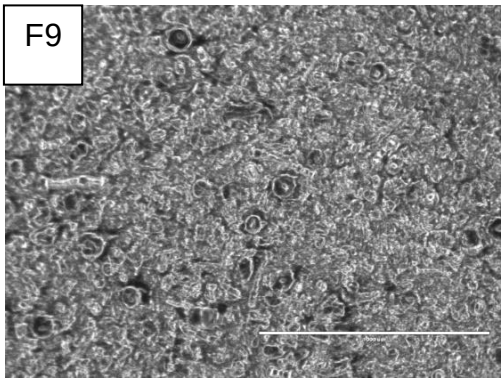

Figure 3.1. Microscopy assessment for bio-ink formulations 1-9.

3.3.2 Viscosity test for bio-ink formulations

The viscosity of formulations 1-9 is shown in Table 3.2. The table shows that different formulations have different viscosity. The value of viscosity depends on the type of materials used in the preparation of bio-ink. F1 showed the lowest viscosity and F9 showed the highest viscosity. Bio-ink with various viscosity was prepared to investigate the syringability of bio-ink formulations. It seems the presence of nanoclays in the solution has less impact on the viscosity of the solutions compared to alginate or MC. For example, in Formulation F8, there is 1.2 g nanoclay, when it is replaced by an extra 1.2 g of MC the viscosity increased from 209200 to 227400 cP. This is also true when the viscosity of F3 is compared with F4. This indicates that the presence of clay can tune the viscosity of the solution to reach the desired viscosity needed for the syrnigability or bio-printing. Comparing the viscosity of the formulations F4 (the amount of MC doubled compared to alginate) and F7 (the amount of alginate doubled compared to MC) indicates that the presence of more alginate in the formulation can have a remarkable effect on the increase in the viscosity of the formulation compared to when the amount of MC is more than the amount of alginate in the formulation.

Table 3.2. The viscosity of various bio-ink formulations

Formulation Code	Spindle	Speed (RPM)	Torque (%)	Time (s)	Viscosity(cP)
F1	LV-3(63)	2	22	5	13200
F2	LV-4(64)	2	60.2	5	180600
F3	LV-4(64)	2	63.3	5	189900
F4	LV-4(64)	2	56.7	5	170100
F5	LV-4(64)	2	57.1	5	171300
F6	LV-4(64)	2	47.2	5	141600
F7	LV-4(64)	2	68.8	5	206400
F8	LV-4(64)	2	69.9	5	209200
F9	LV-4(64)	2	75.8	5	227400

3.3.3 Dipping test for bio-inks formulations

The result of the dipping test for bio-inks formulations 1 to 5 is shown in Figure 3.2, and for the formulation 6 to 9 is shown in Figure 3.3. The maximum force required during dipping goes up along with the increase of alginate concentration. The main reason for the differences in parameters for formulations could be due to changes in the viscosity of the bio-inks. Surprisingly, the formulation that has the maximum viscosity did not require the highest intensity of force to dip in. As a result, the concentration of polymers contained in formulations is another

parameter causing to have different dipping properties. Comparing Figure 3.2 and Figure 3.3 showed that, the maximum force required for dipping increases by nearly 5 times when the concentration of alginate is doubled in formulations 6 to 9.

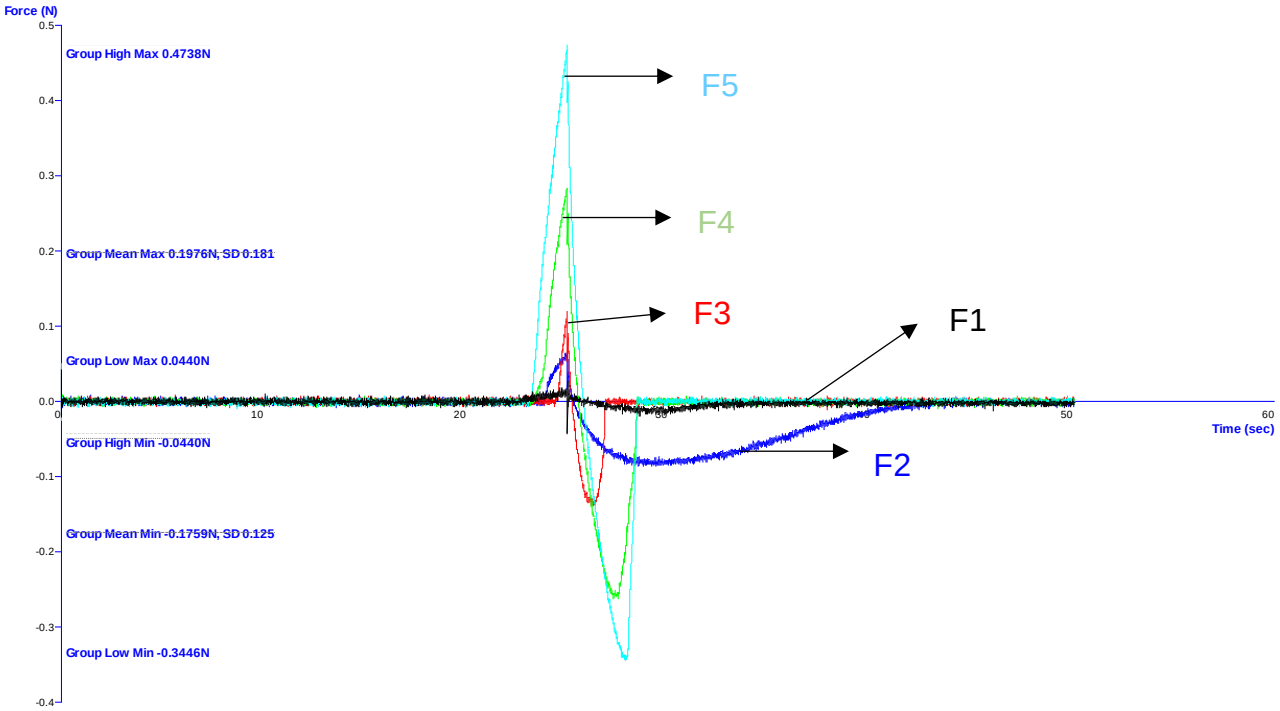

Figure 3.2. Dipping test for bio-inks formulation 1 to 5.

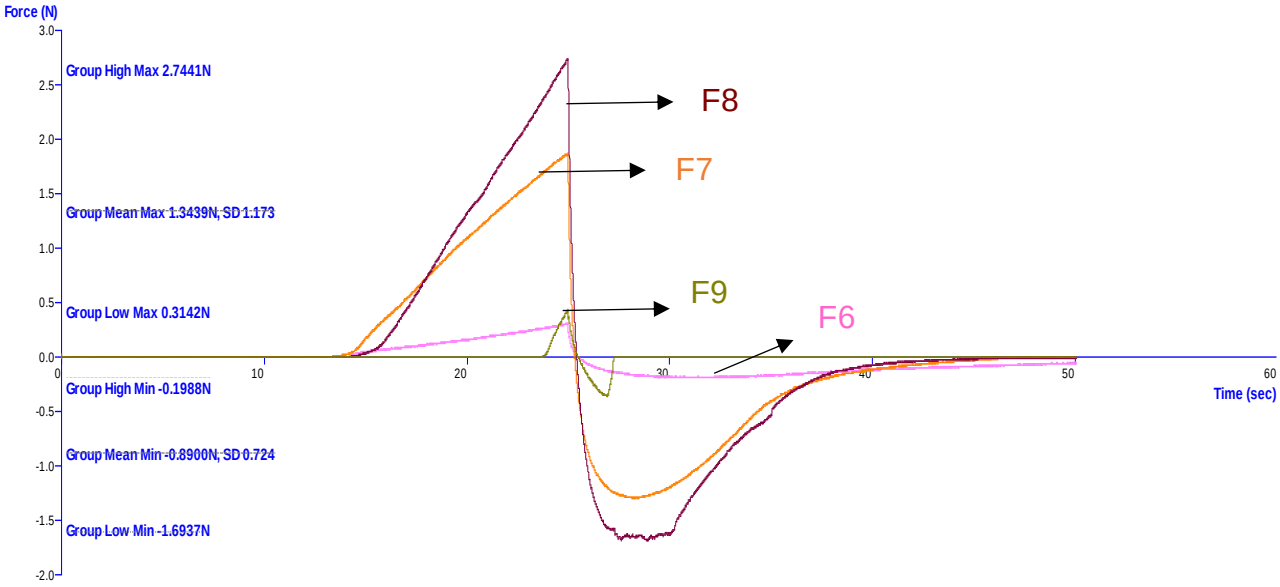

Figure 3.3. Dipping test for bio-inks formulations 6 to 9.

3.3.4 Syringability assessment for bio-ink formulations

The result of syringability test for bio-ink formulations 1 to 7 is shown in Figure 3.4. Formulations 8 and 9 failed the test, as they had very high viscosity with poor syringability. As expected, formulation 7, which has the highest polymer concentration and viscosity, is the hardest to extrude through the needle. Compared to the changing concentration of alginate in bio-inks, the increase in the concentration of MC and nanoclay can remarkably increase the maximum force required to extrude the bio-ink through the syringe hence reducing the easiness of extrusion.

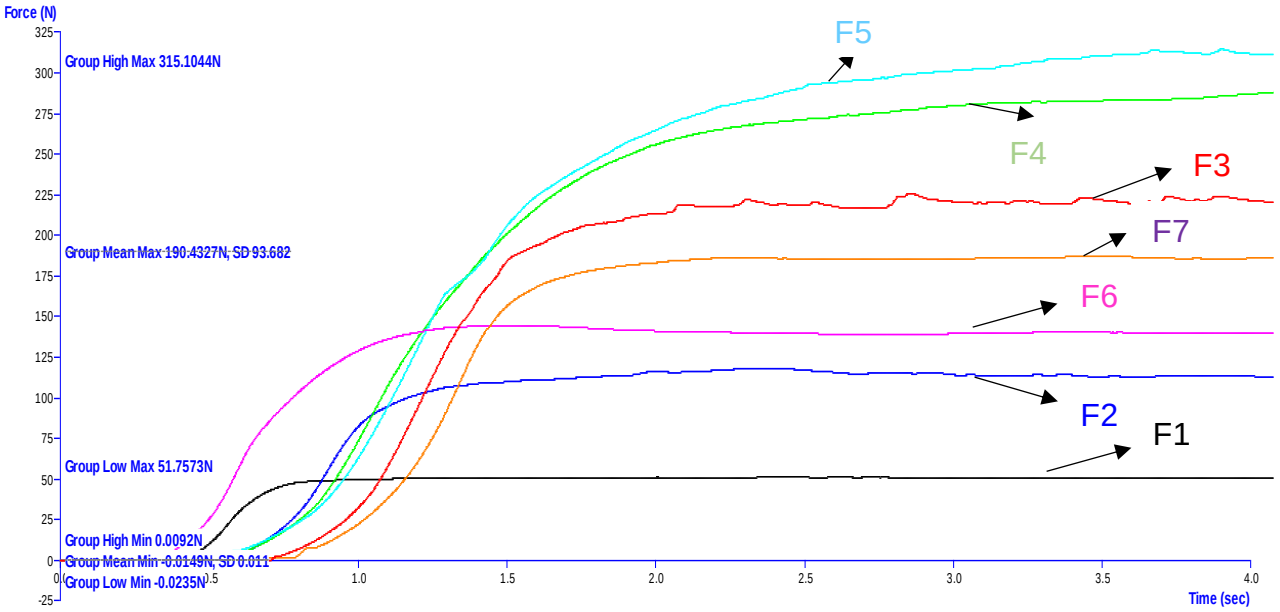

Figure 3.4. The syringability assessment of bio-ink formulations 1-7.

3.3.5. 3D bio-printing of drug-loaded alginate-MC

To assess the bioprinting of the scaffolds, 1% to 10% v/v 5-FU solutions are loaded into the alginate:MC 1:1 and 2:1 bio-inks. These scaffolds were printed in the same square shown in Figure 3.5. It is obvious from the figure, depending on the type of formulations the quality of the printed scaffold varied. The difference in the quality of the scaffold could be due to the changes in the viscosity of the bio-ink. It was observed that when the drug was loaded the viscosity of the bio-inks changed. The changes in the viscosity made some of the holes got smaller (Figure 3.5). It is obvious from the figure when the concentration of the drug increased some of the holes start disappearing. This was the case, particularly for alginate:MC (2:1) where the concentration of alginate is high. This indicates that the ratio of 1:1 alginate:MC could be more suitable for bioprinting the scaffolds.

Formulation	Formulation 2 (Alginate MC 1:1)	Formulation 7 (Alginate MC 2:1)
1% 5-FU solution loaded	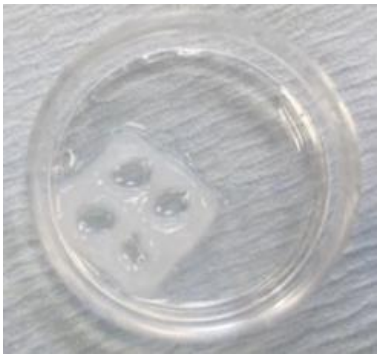	
2% 5-FU solution loaded		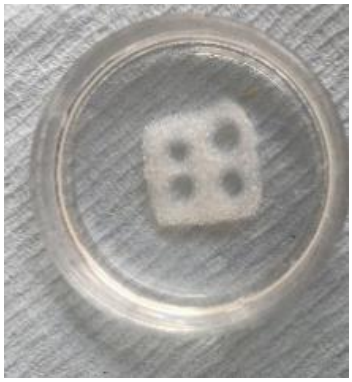
5% 5-FU solution loaded		
10% 5-FU solution loaded	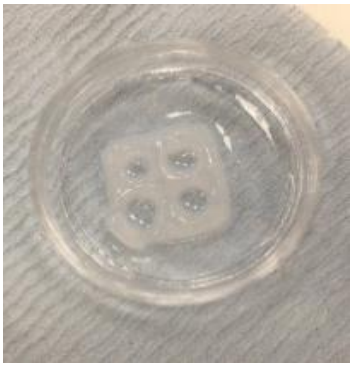	

20% 5-FU solution loaded

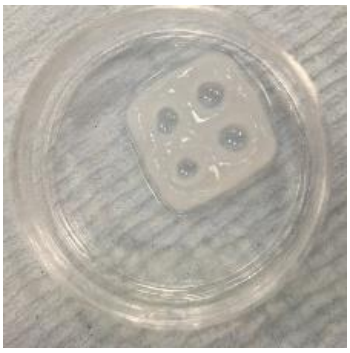

Figure 3.5. Bioprinting of various scaffolds of alginate-MC loaded with varying 5-FU.

3.3.6 Cell study of drug-loaded alginate-MC scaffolds

The results of cell culture with 5-FU loaded alginate-MC scaffold were shown in Figure 3.6. The smaller number of HEK293T and HeLa cells after 4-day culture with 5-FU loaded scaffolds under the fluorescent light of microscopy compared to the cell-only group. Figure 3.7 showed that all the scaffolds had similar inhibited effects on both HEK293T and HeLa cell counts. During the 4 days culture, these drug-loaded scaffolds inhibited the growth of HEK293T and HeLa cancer cells constantly. When cultured with scaffolds without 5-FU, the cell number of HEK293T and HeLa increased at the same speed as the cell-only group during the first-day culture. While it decreased fast afterward, which may be due to the polymer within blank scaffolds providing an environment disliked by the cells in the long term.

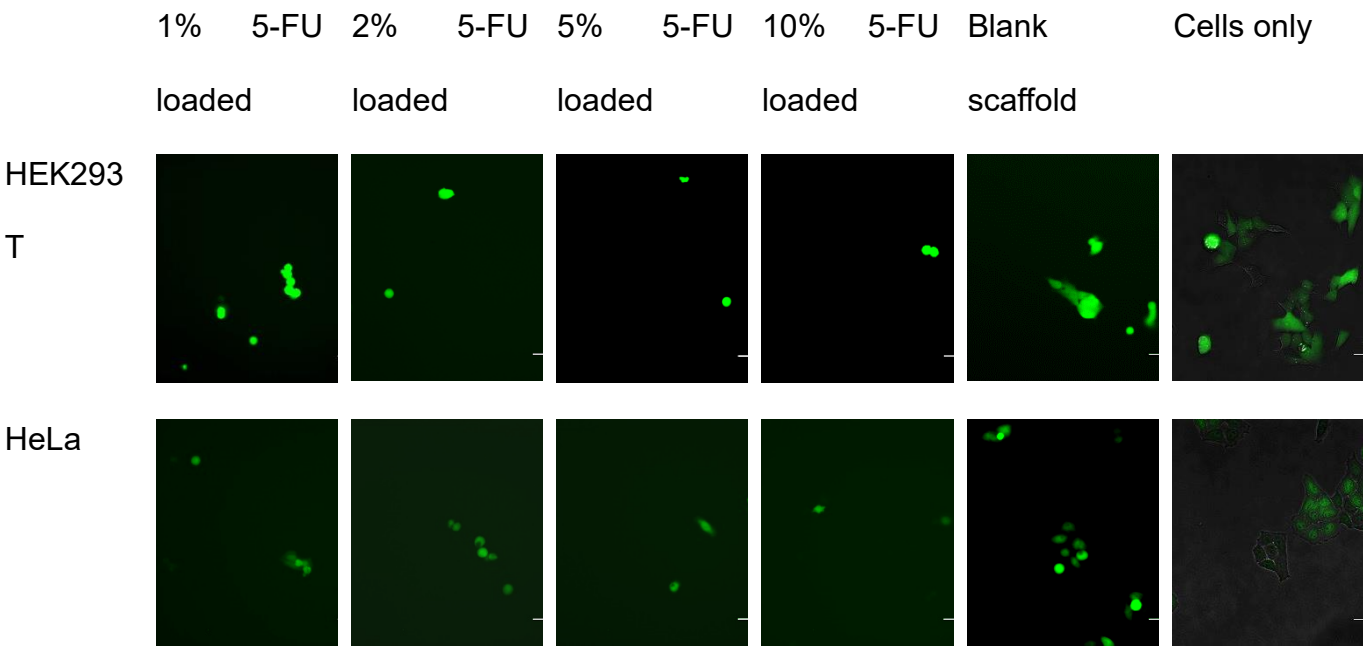

Figure 3.6 Microscopy figures of cancer cells cultured with scaffolds after 4 days

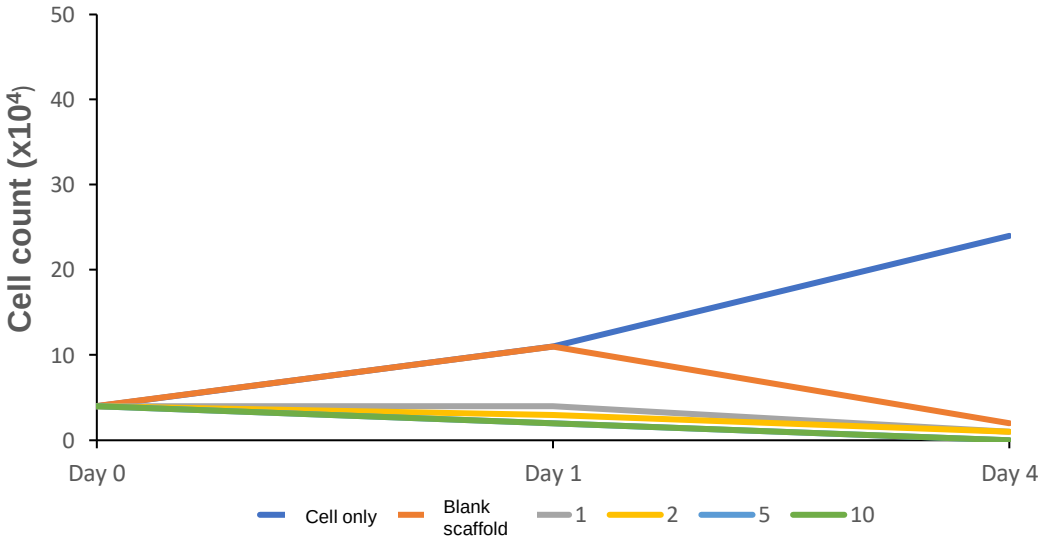

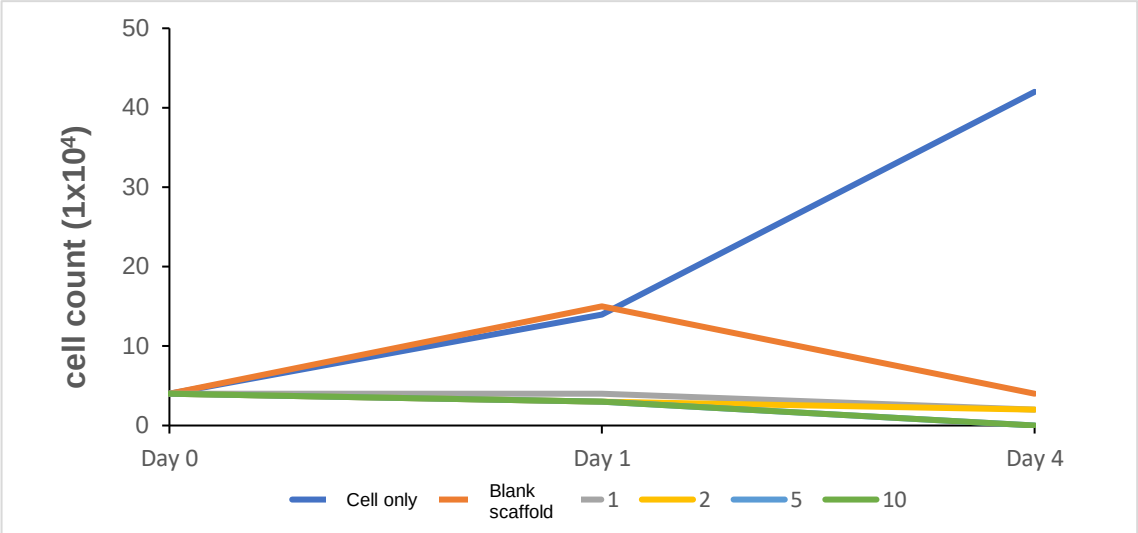

Figure 3.7 *In vitro* cell culture assessment of alginate-MC scaffolds loaded with (1) 1%, (2) 2%, (5) 5%, (10) 10% 5-FU solutions with GFP labelled HEK293T (the upper) and HeLa (below) cancer cells.

3.4 Conclusion

In this research, the mechanical properties of 9 alginate-based bio-ink formulations were evaluated through microscopy, viscosity, syringability and dipping test. The results showed that bio-ink formulations 2 (alginate:MC, 1:1) and 7 (alginate:MC, 2:1) are suitable formulations to make scaffolds via bio-printing and load 5-FU. The cell culture study of 5-FU loaded bio-ink formulation 2 (alginate-MC 1:1) scaffolds shows the positive cancer cell killing and inhibiting results, which confirm that the scaffolds can be efficient drug delivery systems for cancer treatment.

Chapter 4 3D bioprinting of novel biocompatible scaffolds for endothelial cell repair

4.1 Introduction

Three-dimensional bioprinting (3DP), which has emerged as an innovative additive manufacturing technology[64-66], is revolutionizing the field of tissue engineering and thus the future of medicine and medical implants. Similarly, novel biocompatible bio-inks (with or without a drug) is also equally transforming tissue engineering applications and can be used to fabricate complex geometries of personalized medical devices, e.g., scaffolds, providing novel platforms beyond the current state of the art. There is an opportunity for technological innovation in the fabrication of novel scaffolds or biomaterials using 3DP that requires a convergence of expertise in biomaterial, pharmaceutical, and vascular biological fields.

A major challenge for tissue engineering has been to mimic the micro and macro environment of human tissues via a widely used method to generate cell-seeded scaffolds both in anatomically complex geometries and intra-cellular architectures with controlled cell distribution. Studies have revealed that the critical characteristic of a biomaterial, as well as the control of the inner micro- and macro-scale features of the engineered tissue, is considered a key quality parameter to fabricate complex anatomical, patient-specific structures with high shape fidelity in tissue engineering applications[67-68]. In response to this currently unmet need, advances in additive manufacturing and thus 3DP have inspired scientists to employ this innovative technology for biomaterial and tissue engineering strategies[69,70]. Bioprinting, in particular, has gained attention for its

ability to control and deposit sequential layers of biomaterials, allowing the tailoring of a specific geometry to an object and permitting the placement of cells and biological molecules[71-72]. As a result, 3DP offers numerous possibilities for the future of tissue engineering and organ regeneration. Bioprinting can be combined with Computer-Aided Design (CAD) technology using patients' medical images to allow the biofabrication of biomimetic-shaped 3D structures unique to the target tissue or organ in a personalized manner. Because of the challenges encountered when bioprinting, considerable improvements need to be made in order to bioprint complex constructs or cell-laden 3D tissue constructs by means of developing suitable biomaterials and bio-ink formulations with optimum properties such as viscosity for successful 3D (bio)printing[73-74]. 3D bioprinted scaffolds built for individual patients are favoured over customization of mass-produced products when meeting the specific needs of each patient. The benefits of its clinical application include easy adaptation and fixation, reduced surgical time, and favorable aesthetic results.

Coronary heart disease (CHD) is initiated when the cell lining of arteries (the endothelium) is injured. Endothelial regrowth appears to be an important process limiting CHD. When cells are injured, they activate an inflammatory reaction which induces the expression of the innate repair receptor (IRR), which activates tissue protection and repair[75]. Despite the early and strong expression of IRR within injured tissues, local production of tissue-protective cytokines (TPCs) such as erythropoietin (EPO) is delayed, transient and relatively weak[76]. This provides an opportunity to intervene with exogenous TPCs that act as innate repair activators, targeting the fundamental processes of tissue injury at a level that controls both the self-damaging and the regenerative components, representing

a promising therapeutic approach[77]. EPO has been shown to be tissue-protective in models of ischaemic, traumatic and inflammatory injury[78]. Hypoxia enhances the reparative response of ECs to EPO[79-80]. This is likely to be mediated by hypoxia-inducible factor (HIF)-1. Dimethyloxalylglycine (DMOG) is a HIF-1α inducer and mimics conditions similar to hypoxia[81-85].

The use of biomaterials such as biocompatible or biodegradable copolymer (e.g., polylactic acid, pluronic F127[86]), is a common strategy for reducing the risk of thrombosis and restenosis. Blood compatibility remains a major issue and several surface modifications have been used to mitigate this problem. We aimed to use a novel bio-therapeutic material, with intrinsic tissue-protective activity, to fabricate a novel scaffold by means of an optimized 3D bio-printing technology that can promote EC repair and may offer a promising alternative therapy to existing biomaterials such as polylactic acid (PLA) and pluronic F127. Among other biomaterials, both polylactic acid (PLA) and pluronic F127 biopolymers have been used as a suitable polymeric carrier for the development of bio-inks because of its superior biocompatibility and printing fidelity[87]. We also wished to apply this 3DP technology to prevent restenosis, based on triggering the endogenous repair mechanisms of the endothelial cells of the artery wall.

4.2. Materials and Methods

4.2.1. Materials

Polylactic acid (PLA) MW 60,000, polyethylene glycol (PEG) MW 400 were purchased from Sigma Aldrich (Dorset, UK). Pluronic F127-based biomaterials were purchased from SE3D (Santa Clara, CA, USA). Dimethyloxalylglycine

(DMOG) was purchased from Sigma Aldrich (Dorset, UK) and Erythropoietin (EPO) was purchased from Araim Pharmaceuticals (New York, NY, USA). All materials required for cell culture assessment and analytical studies were purchased from Sigma Aldrich (Dorset, UK) unless otherwise stated. All solvents and chemicals were of analytical grade and used as received.

4.2.2. Preparation of Bioinks Containing EPO and DMOG

The biomaterial matrix was prepared from a mixture of poly (lactic acid) (PLA) and Polyethylene glycol 400 (PEG) and Pluronic F127 in different concentrations as shown in Table 4.1. Briefly, PLA was prepared as a 15% solution by dissolving the PLA pellets in chloroform. PEG was then dissolved in the PLA solution. PLA: PEG matrix was prepared in the following concentrations: 7:0, 6:1 and 5:2 *w*/*w* ratios. A wide range of inks was developed and only the best four (for PLA/PEG only 5:2 *w*/*w* ratio was selected) were used for this part of the study (Table 4.1). Model drugs, i.e., EPO and/or DMOG, were loaded on the biomaterial matrix (bio-ink) to reach a final concentration of 20%–30% (*w*/*w*).

Table 4.1. Formulation compositions of printing inks containing PEO and DMOG (*w*/*w* ratio).

Formulations	Pluronic F127	PLA/PEG mixture	EPO(2µg/mL)/ DMOG	Peak Positive Force (N)	Viscosity (cP)	Injectability
1	4	0	1	56.604	7.4×10^3	Pass
2	0	49	1	55.253	10.0×10^3	Pass
3	1	0	0	56.585	6.0×10^3	Pass
4	0	49	0	55.038	12.0×10^3	Pass

4.2.3. Rheology Measurement of the Inks

Once optimized, the ink formulations were subject to a rheology measurement study. The viscosity of the inks was measured both at constant and increasing shear rates using a plate rheometer (RheoStress® RS 1, Karlsruhe, Germany) with a plate–plate distance of 0.052 mm. The viscosity of the pastes was determined by applying a constant shear rate of 10 s^{-1} for 500 s. After an initial amplitude sweep test to detect the viscoelastic region, oscillatory frequency sweep tests (f = 0.01–10 s^{-1}; 1.0 Hz) were performed at 25 °C on all ink formulations as shown in Table 4.1.

4.2.4. Extrudability/Injectability of the Inks Developed for Bioprinting

Injectability of the bio-ink formulations is an important factor to consider in order to ensure the required dose is delivered effectively and more precisely, and with ease. In general terms, the force which is applied to a syringe plunger during the injection of a formulation via a needle is classified in three ways: stiction, overcoming the resistance force of the syringe plunger; plateau force, energy that accumulates as the formulation glides through the needle under a constant force and finally end constraint force. These three types of forces were recorded manually and were classified as ‘pass’ or ‘fail’, based on whether they did or didn′t expel the formulation steadily out of the syringe, respectively. Based on the preliminary observation and the analysis, only those 4 formulations (Table 4.1) were used for 3D bioprinting. It was measured using was evaluated by texture analyser (Stable Micro System, Surry, UK).

4.2.5. 3D Bioprinting of Scaffolds

An optimized 3D bioprinting platform (Figure 4.1) was used to fabricate all macro-porous scaffolds with a diameter of 10 mm. The thickness of all developed scaffolds was set at ~1–3 mm as a default in order to avoid any possible effect of the varying thickness of the scaffolds on the actual release of the drug. The adopted printing process was later applied for the printing of different scaffolds with various geometries and intricacies of the constructs. The print resolution was set at 100 µm and the construct was directly printed (via r3bEL mini bioprinter, SE3D, Santa Clara, CA, USA) in a petri dish placed on the print bed in ambient temperature (23 ± 1 °C). The various developed viscous printing inks were drawn into a 22-gauge printing syringe with an internal diameter of ~640 µm from which the inks were extruded at a speed of ~100 mm/min to print the constructs. Computer-Aided Design (CAD) was utilized to develop the design of the scaffolds with the required geometry (rectangular pores). Once the fabrication process was optimized, all printed scaffolds were immediately removed from the print bed and the petri dish was stored at 37 °C in an incubator for 24 h to cure the 3D printed scaffolds prior to utilizing it for further analysis.

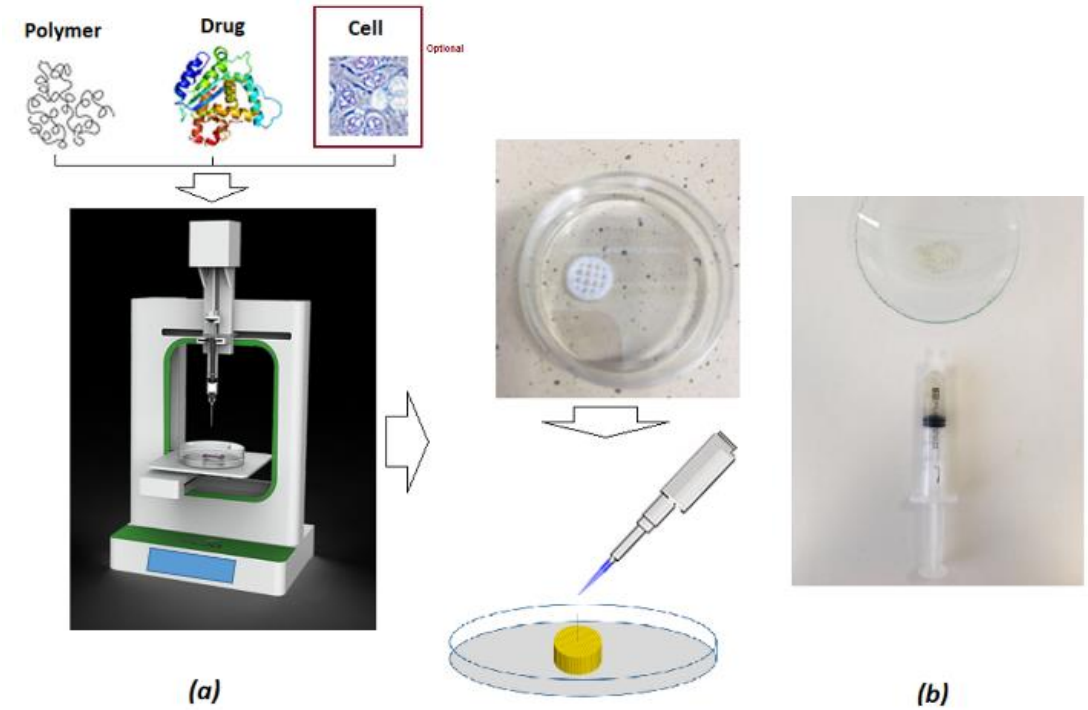

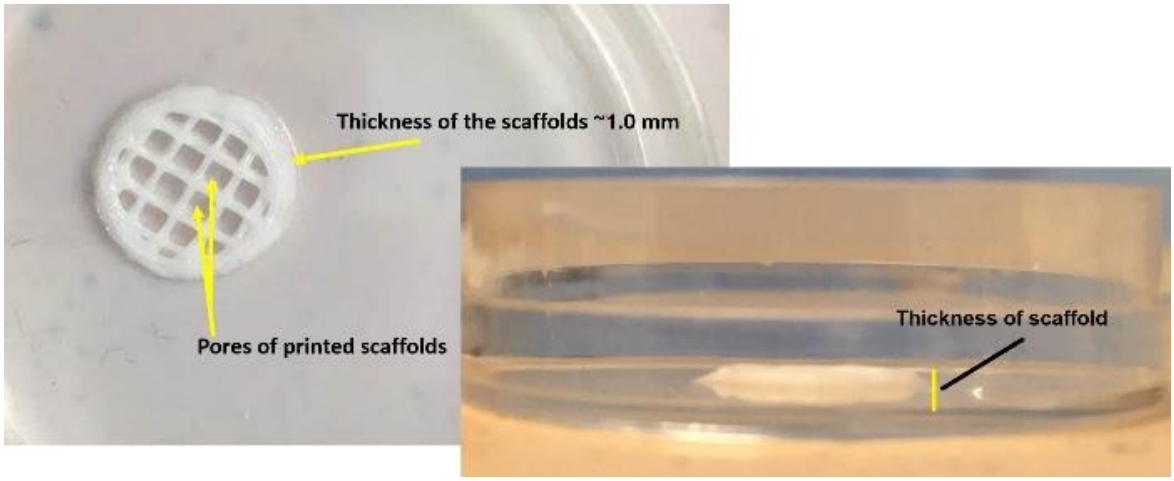

Figure 4.1. Schematic diagram of (**a**) the optimized 3D bioprinting process, (**b**) the extrudable bio-ink, and (**c**) the printed scaffold with 3D texture.

4.2.6. Surface Morphology of the Inks and Scaffolds

The surface morphology of the fabricated scaffolds was studied using a scanning electron microscope (Jeol JMS 820, Freising, Germany). The samples were placed on a double-sided carbon tape and sputter-coated with gold using a sputter coater (Edwards S-150 sputter coater, Edwards High Vacuum Co. International, Sanborn, NY, USA). After the samples were sputter-coated, they were placed into the SEM where the surface structure was then observed and recorded at various magnifications using the SEM operating at 3 kV. An optical microscope (Celestron Tetraview, Torrance, California, United States) was also utilized to investigate the surface of the viscous inks as well as scaffolds to visualize the texture of the ink formulations prior to the 3D printing and the surface of the developed scaffolds to determine the distribution of the deposited substances on the surface of the scaffolds. 20x objective lense was used and the figure of bioinks were captured using the 5MP CMOS built-in digital camera.

4.2.7. Mechanical Properties of the Scaffolds Developed

Uniaxial compressive tests were applied to scaffolds and Young′s modulus and compressive strength were obtained from the data. For the purpose of this study, the scaffold strips (3–5 mm in length) were attached to a 75-mm-diameter adhesive rig probe with a double-sided adhesive tape on a TA.HD.plus Texture Analyser (Stable Micro Systems, Surrey, UK) fitted with a 5-kg load cell in compression mode. The probe, lined with the scaffolds, was lowered towards the surface at a pretest speed of 0.5 mm/s, test speed of 0.5 mm/s and post speed of 1.00 mm/s. The maximum force required to penetrate the scaffolds was

determined. The mechanical analysis was conducted at room temperature (23 ± 1 °C) (23 ± 1 °C) and run in triplicate (n = 3).

4.2.8. Thermal Analysis

The solid-state of the drugs was analyzed via differential scanning calorimetry (DSC) (DCS 4000, Perkin Elmer, Waltham, MA, USA). The study was performed on the chosen bio-ink formulations, which were utilized for the development of the scaffolds. The crystallinity of the substances used in the formulations was examined using data presented in each of the DSC traces. Samples weighing between 3 and 6 mg were sealed in an aluminium pan and placed in the DSC machine with a scanning rate of 10 °C/min (from 25 to 265 °C) under nitrogen atmosphere.

4.2.9. Drug Release Study from the Scaffold

The scaffolds were placed into PBS (500 µL, pH=7.4). The PBS containing the released drug was removed at different time intervals (5, 15, 30 min, 1, 2, 4, 24 and 48 h) and replaced with fresh PBS each time. The aliquots removed were kept at −20 °C until further analysis. Rat aortic endothelial cells (RAECs) were seeded into 24-well plates and cultured until approximately 80% confluency in 21% O_2. 100 µL of the aliquots with the released drug at different time intervals was added on RAECs and left for 2 h. As DMOG is a HIF-1α inducer, its release from the scaffold into PBS solution was quantitatively measured indirectly using a bioassay for measuring HIF-1α. In another set of experiments, DMOG was measured indirectly by measuring the gene expression of VEGF using real-time

qPCR. EPO released from the scaffold in PBS solution was also quantitatively measured directly using an ELISA kit for EPO.

4.2.10. Real-Time qPCR

Treated cells were lysed using TRIzol (Invitrogen/ Life Technologies, Dartford, UK) and RNA was extracted and purified as described previously[88]. RNA quality and concentration were determined using a NanoDrop ND-1000 (NanoDrop Technologies). Reverse transcription and real-time quantitative PCR (qPCR) for VEGF and β2-microglobulin (a housekeeping gene), were carried out on RNA samples using Taqman gene expression assays (Applied Biosystems/Life Technologies, Dartford, UK) as previously reported[89]. For gene expression quantification, the comparative threshold cycle (ΔΔCt) method was used following Applied Biosystems/Life Technologies′ guidelines. Results were normalized to β2-microglobulin expression and expressed as arbitrary units using one of the untreated samples as a calibrator as specified in the figure legend.

4.2.11. HIF-1α Enzyme-Linked Immunosorbent Assay (ELISA)

HIF-1α was measured using a commercial ELISA kit (R&D systems/ Biotechne, UK) following the manufacturers′ instructions. Endothelial cells were lysed in 80 µL lysis buffer (25 mmol/L Tris HCl pH 7.6, 0.1% SDS, 1% deoxycholate, 1% NP40, 0.5 mol/L EDTA, 40 mmol/L EGTA and protease inhibitors). Lysates were then centrifuged at 11,000× *g* for 15 min at 4 °C and the supernatant was collected. Protein concentrations were quantified using a BCA reagent kit (Pierce Biotechnology, Rockford, IL, USA) Results are expressed as pg/mg protein.

4.2.12. Statistical Analysis

All values were evaluated by one-way analysis of variance followed by Bonferroni's multiple comparison tests (GraphPad Prism 7). Significant differences were assumed at $p < 0.05$.

4.3. Results and Discussion

4.3.1. Bioink Formulation and Assessment: 3D Printing

All bioprinting inks, as shown in Table 4.1, were prepared by blending the optimized amount of either F127 or PLA/PEG mixed with the drugs. Viscosities of the different bio-ink compositions or drug-loaded formulations were compared with those without the drugs. As can be seen from Table 4.1, the addition of the drug solutions to the actual ink formulations resulted in slightly lower viscosity. Blank formulations without the drugs showed quite high viscosity values of 74 and 120 Pa·s for F127 and PLA/PEG systems, respectively. Upon loading the drug into the formulations, the viscosity seemed to be reduced to 60 and 100 Pa·s for the F127 and PLA/PEG formulations, respectively. This could be attributed to the low-viscosity solution of the drug affecting the original viscosity of the blank polymeric pastes. Nonetheless, the slight observed reduction in the viscosity values did not significantly ($p > 0.05$) affect the actual printing process. None of the ink formulations were autoclaved prior to the actual printing, as in our previous screening study it had been found that autoclaving did not significantly ($p > 0.05$) alter the viscosity. Therefore, all scaffolds were fabricated by using the ink formulations as received without prior autoclaving. Moreover, all compositions

showed shear thinning effects at increasing shear rates, enabling extrusion through nozzles, evidenced by the inks (Figure 4.1).

All ink formulations exhibited satisfactory plotting behavior during the actual bioprinting process, as only optimized formulations were used for the purpose of this study. All optimized formulations as shown in Table 4.1 allowed plotting via the 3D printing process with high shape fidelity. Those ink formulations with drugs were extrudable at lower pressures compared to the blank, because the addition of the drug solutions slightly affected the printing fidelity.

As expected, the F127, as well as PLA/PEG blend, was also able to generate scaffolds with excellent shape fidelity with moderate mechanical pressure in the system for extrusion. This is because of the texture and homogenous composition of the bio-ink formulations, where drug particles are miscible with the polymeric carrier (Figure 4.2). The particles of the drug on the carrier polymeric matrices in the bio-inks were homogeneously distributed throughout the matrices. The average size of the particles in the developed viscous ink formulations was below 10 microns, which is adequate for extrusion through a 22-gauge needle during the 3D printing process (Figure 4.2). The rationale of the optical microscopic images was to show the dispersion of the particles (of each of the components) in the ink formulations. As can be seen in Figure 4.2, all ink formulations showed sub-micron particles dispersed throughout the tested specimen. The overall findings from these images suggest that all particles were distributed and dispersed throughout the formulations.

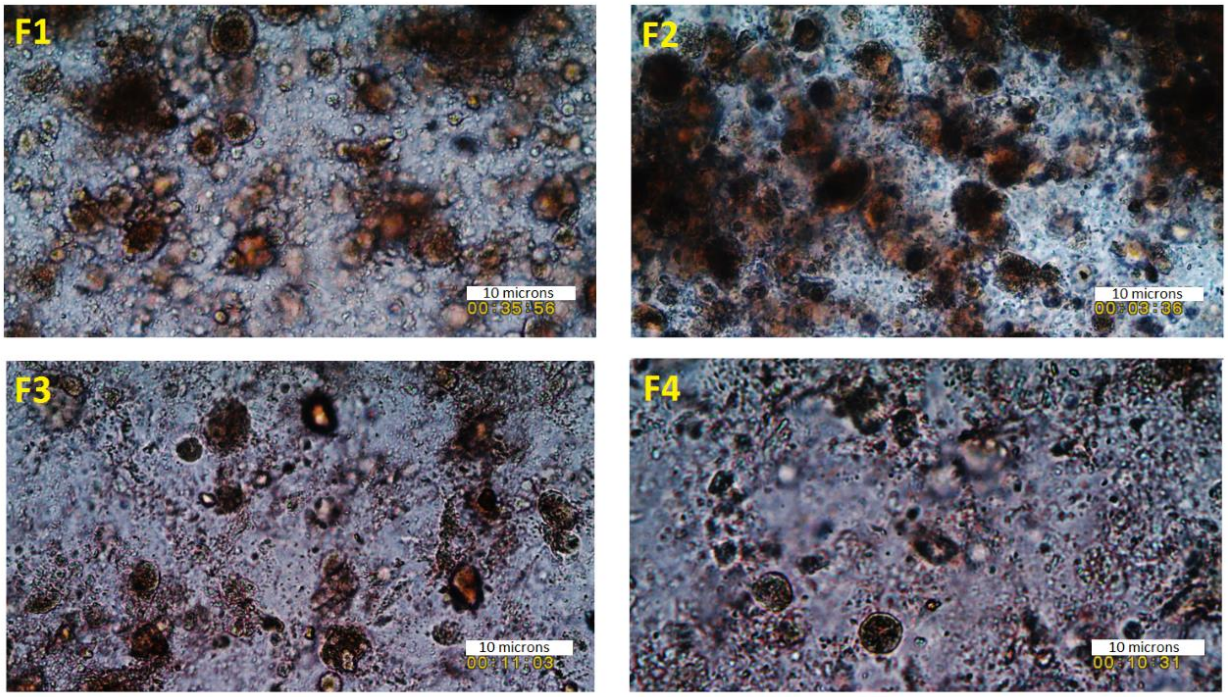

Figure 4.2. The texture and morphology of the semi-solid bioinks under an optical microscope (Celestron Tetraview, Torrance, California, United States) of formulations F1 (F127:drug 4:1), F2 (PLA/PEG:drug 49:1), F3 (F127:drug 1:0), and F4 (PLA/PEG: drug 49:0) (scale 10 microns).

Moreover, the pastes were found to have viscoelastic behavior and were tested at an amplitude in the viscoelastic region, determined by the temperature and frequency sweep tests. Figure 4.3 shows the oscillatory frequency and temperature sweep tests of the developed formulations with both F127 and PLA/PEG compositions in comparison with the blank polymeric bio-ink (F127 and PLA/PEG alone without the drugs EPO or DMOG). The storage modulus G′ indicates the elastic modulus, gelled component, while the loss modulus G″ describes the viscous modulus, a non-gelled component of the bio-ink formulations. The F127 bio-ink formulations showed a higher storage modulus compared to that of the loss modus over a broad range of temperature and

frequencies (as well as angular velocities). For F127 formulations, the G′ increased up to 10 KPa whereas the G″ value decreased 10-fold. Interestingly, the storage modulus G′ showed a plateau kind of elastic behavior after it reached the highest value above 25 °C attributed to the phase transition of the thermosensitive polymer. The property has also been investiaged and observed in other thermosensitive polymers such as Poly-N-isopropylacrylamide (PNIPAAm)[90]. A further increase in the temperature did not have any impact on the increase in the G′ values of the F127 formulations. In contrast, a slightly different phenomenon was observed in the frequency sweep tests with the F127 formulations where the G′ seemed to have decreased with the increase in the frequency whereas G″ showed an increased profile with the increase in the frequency during the test. Quite similar viscoelastic profiles were also observed in the PLA/PEG systems except for the plateau elastic points. At this crossover point, the bioinks seemed to have lost their viscous properties and behaved like an elastic solid, evidenced by the higher shear modulus. Plotting of all developed bioinks as shown in Table 4.1 was successfully performed without any stabilizing liquid by extrusion using a dosing needle with an inner diameter of ~640 µm. After the optimization of the printing process, all circular (10 mm diameter) constructs were successfully developed with high accuracy in dimensions. These scaffolds were suitable for cell culture with the potential for clinical applications (Figure 4.1).

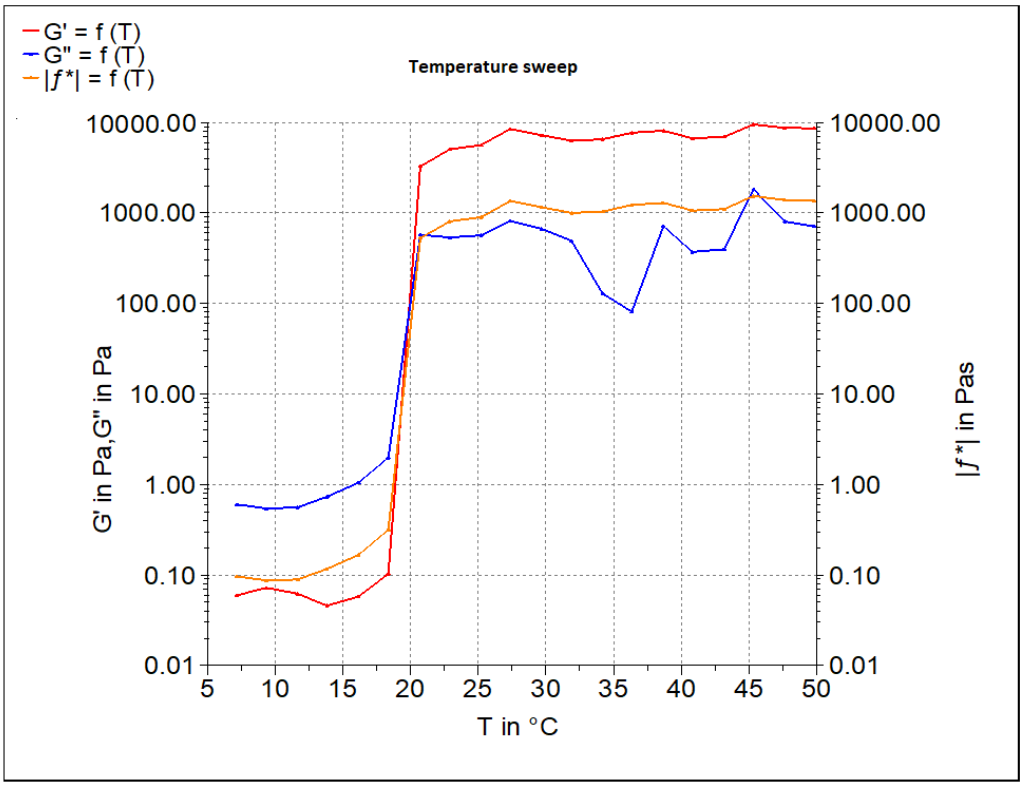

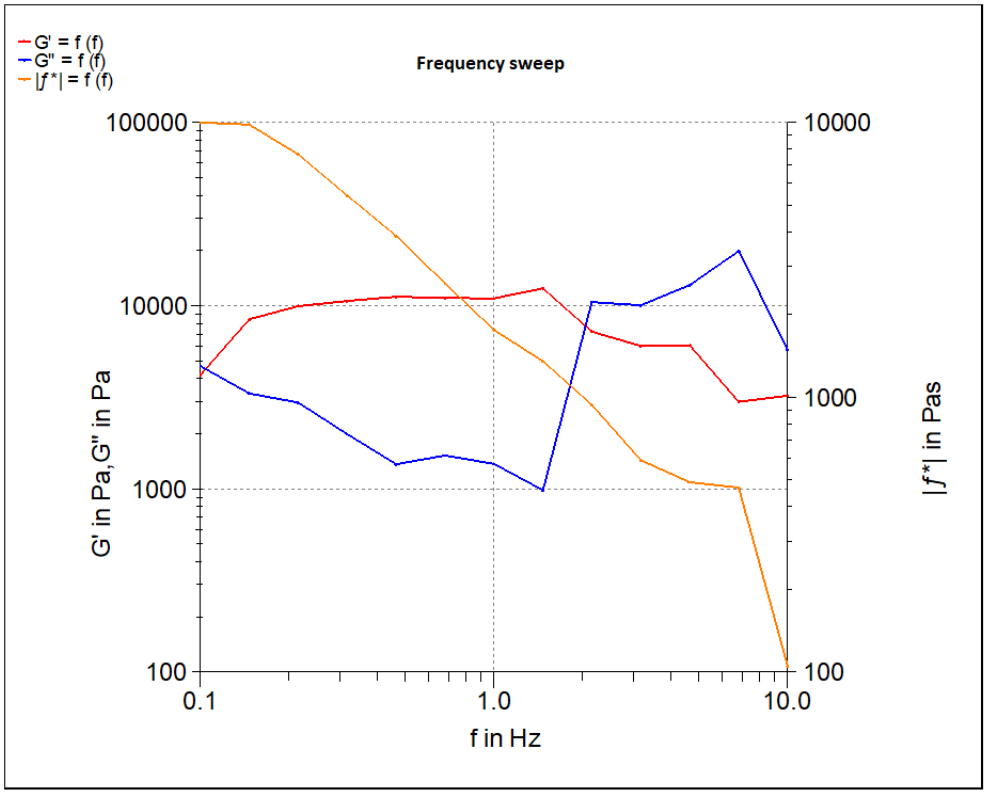

Figure 4.3. Rheology data of the bio-ink formulations represented by storage modulus (G′) and loss modulus (G″) both in temperature (test run at 5–50 °C) and frequency sweeps (test run at 25 °C) for formulation F127/EPO 4:1.

4.3.2. Surface Morphology and Characterization of Scaffolds

SEM examined the surface morphology of the developed scaffolds. The results showed a relatively smooth surface for all scaffolds prepared. SEM analysis of both the F127 and PLA/PEG-based scaffolds revealed differences in the microstructure between the outer surface and the inner structure of the strands. Figure 4.4 shows a view of the observed surfaces which are smooth surfaces. The surface morphology was unaltered over the period of cell culture analysis. There are some small particles that seemed to have been adsorbed onto the surface of the scaffolds matrices which could be attributed to the loose particles deposited during the or post-printing process. The lateral view of sliced scaffolds as shown in Figure 4.4a displayed uneven strand structures with rough areas. The rough surfaces appeared to be porous, and more micro-particles clumped together to form large agglomerates, while the smooth surfaces exhibited a dense and compact texture. A further analysis conducted via confocal microscopy revealed a homogenous particle distribution on the surface of the 3D printed scaffolds. The advanced analysis of the confocal microscopy was performed mainly in order to determine the distribution of the drug and the overall homogeneity of the scaffolds. As can be seen in Figure 4.4b, most of the phases showed a similar set of textures due to the homogeneous distribution of the combined substances represented by the fluorescent dye coating of the scaffolds. It is expected that owing to the similarity of the deposition mechanism of the drug into the scaffolds during the actual printing, this homogeneous distribution would be analogous to the drugs.

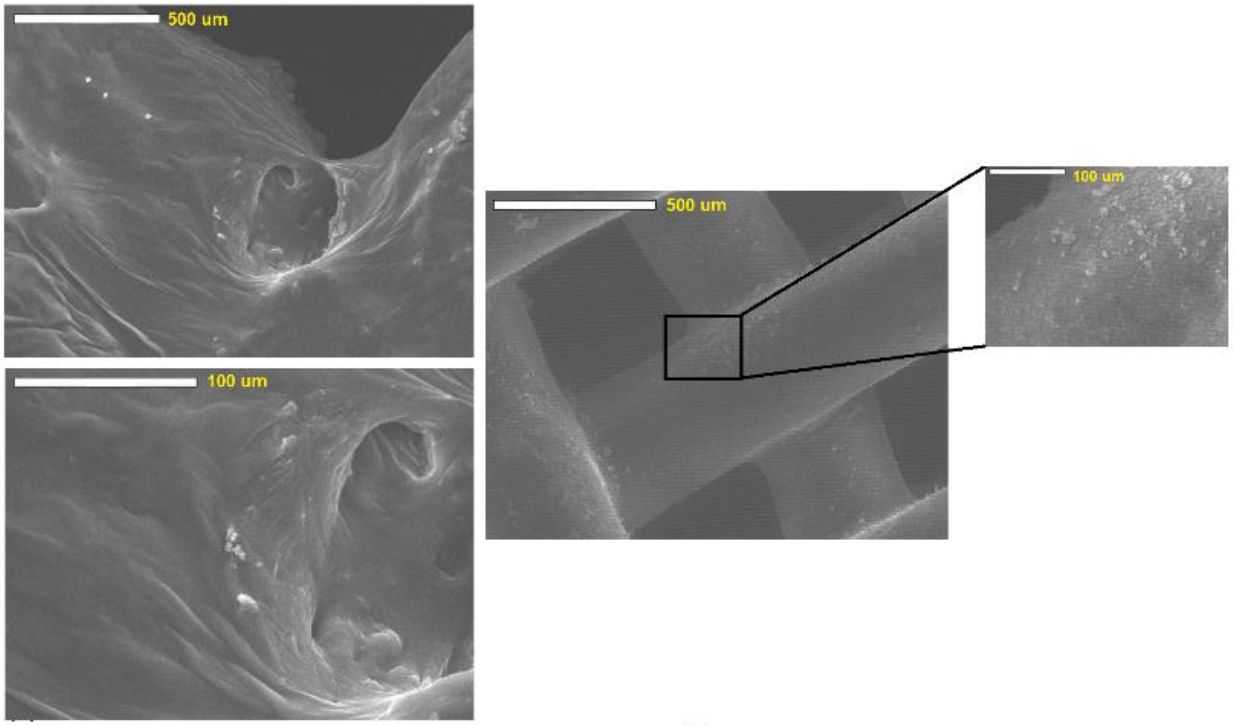

(a)

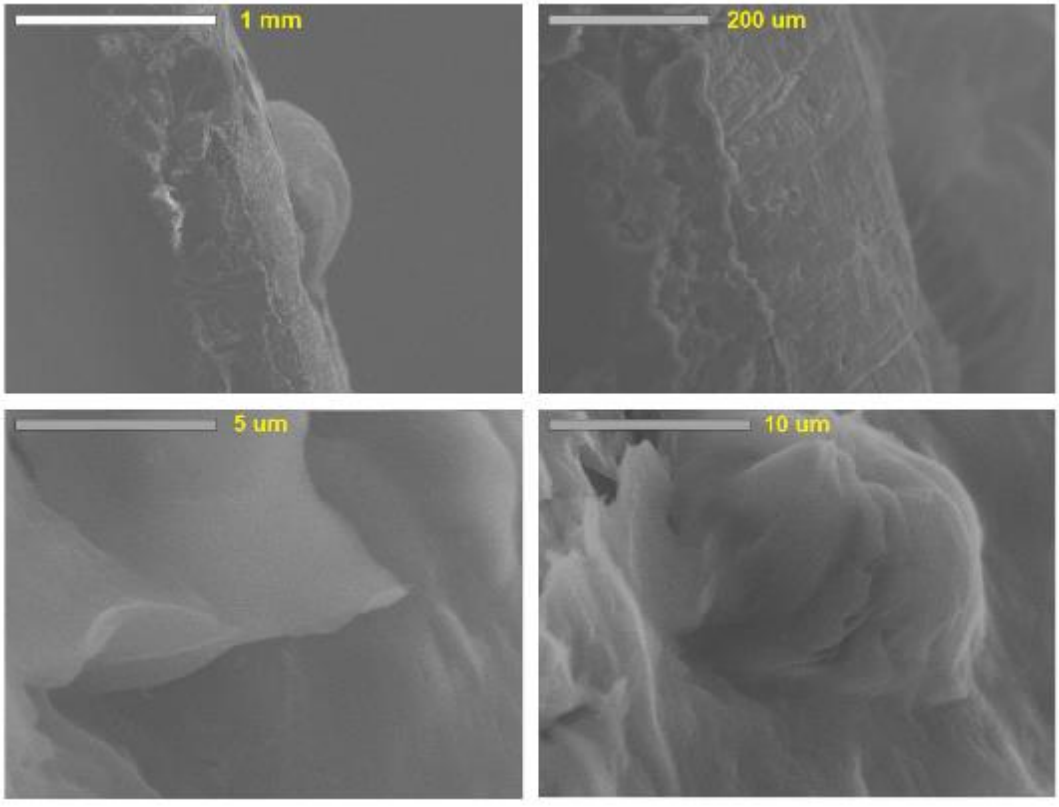

(b)

Figure 4.4. SEM images of (**a**) bio-printed, and (**b**) cross-section of PLA/PEG/EPO-based scaffolds.

4.3.3. Mechanical and Thermal Analysis

The mechanical analysis revealed that all the developed formulations showed robust properties. As can be seen in Figure 4.5, the profiles of Force and % strain of all the ink formulations showed a strength of about 55–60 N for all of the bio-inks. It appears that the addition of the drug solutions to the formulations did not have any negative impact on the force values. In contrast, the addition of drug solutions resulted in a significant ($p<0.05$) decrease in the % strain values. The blank polymeric ink formulations showed a relatively high % strain between 80–110 whereas the actual drug loaded formulations showed only between 55%–60%. This could be attributed to the inclusion of a low-viscosity aqueous solution in which the drug was dissolved in the actual formulation during the printing process. Interestingly, the presence of pluronic F127 in the formulations exhibited an additional peak force at about 30% strain when pluronic F127 was used alone or at 28% strain when used with the drug solution. This could potentially be attributed to the thermoresponsive nature of the polymer, as pluronic F127 viscous solution has a phase transition temperature around the ambient (>25 °C). Therefore, during the texture analysis testing, pluronic F127 might have undergone a phase transition and had become more robust at 28%–30% strain. After this critical point, as expected the strain profiles were seen increasing throughout the rest of the testing period. Nonetheless, the reduction in the % stain did not have any significant ($p>0.05$) effect on the printability and characterization of the resulting scaffolds.

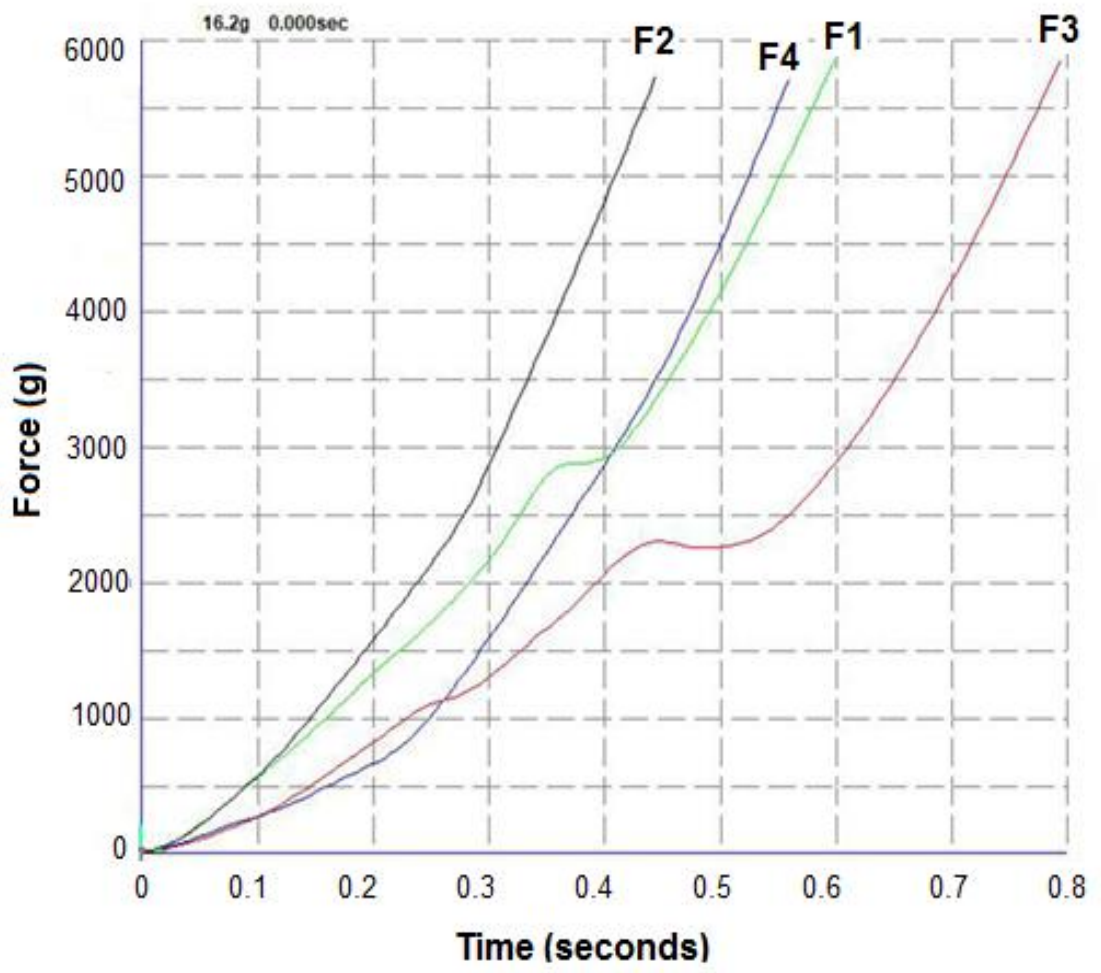

Figure 4.5. Force and travel time (as a function of strain) profiles of the bioink formulations: F1 (F127:drug 4:1), F2 (PLA/PEG:drug 49:1), F3 (F127:drug 1:0), and F4 (PLA/PEG: drug 49:0) prior to the 3D printing applications (n = 3) of porous scaffolds.

The solid-state of the drug-loaded scaffolds, as well as blank scaffolds, were studied using a differential scanning calorimetry (DSC) analysis. DSC is a sensitive and effective method to measure how the enthalpy and properties changes of materials change along with temperature and time[91]. The blank F127 exhibited a sharp thermal transition at 61.2 °C (ΔH = 135.18 J/g), which is attributed to it melting, whereas the PLA/PEG blank system showed two

endothermic transitions, one at 61.65 °C (ΔH = 42.69 J/g) and 168.45 °C (ΔH = 17.56 J/g) due to the melting of PEG and PLA, respectively (Figure 4.6). The presence of two distinct endotherms in the PLA/PEG system simply indicates the co-existence of two different crystalline phases coming from each of the polymers. The glass transition temperature of PLA was not visible, possibly owing to the enthalpy relaxation or overlapping with the melting endotherm of the low melting point PEG. For the nature of this study, no further investigation was made on this thermal event and enthalpy relaxation phenomenon. The scaffolds showed similar kinds of thermal events, where the peak intensity seemed to have been reduced. This could be attributed to the presence of the drug solution in the scaffolds. The drug solution exhibited some plasticization effects reflected by a slight reduction in the temperature and the intensity of the respective peaks at which the thermal event had occurred[92]. As a result, the F127-based drug-loaded scaffold exhibited a melting endotherm at a slightly lower temperature at 60.78 °C with the heat of fusion value of 126.21 J/g. The PLA/PEG scaffolds showed two low intensity endothermal transitions at 63.89 °C (ΔH = 41.38 J/g) and 169.16 °C (ΔH = 25.12 J/g), respectively.

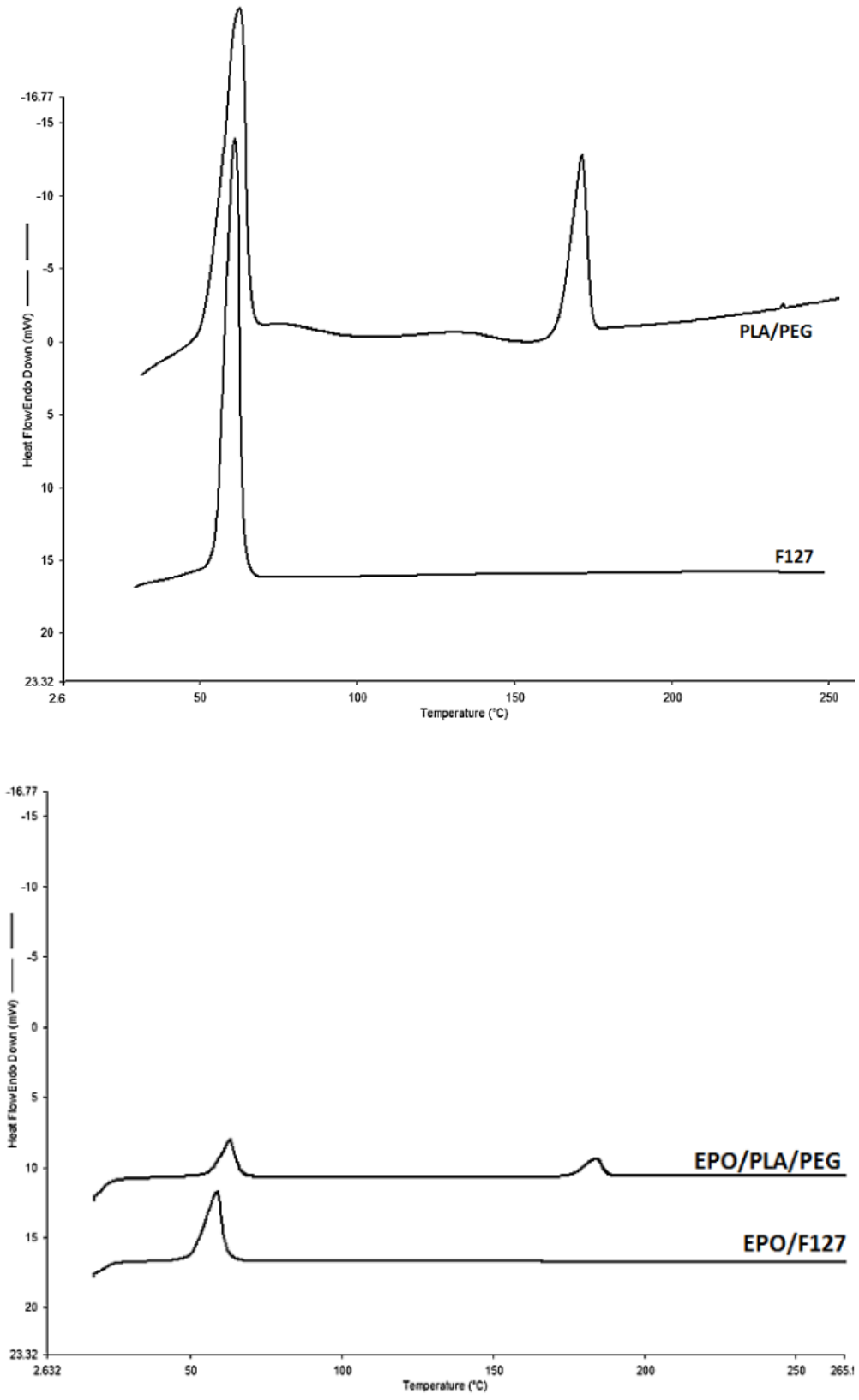

Figure 4.6. DSC thermal transitions of the blank polymeric formulations and the scaffolds.

4.3.4. Drug Release and Its Biological Activity

The *in vitro* release of both EPO and DMOG was measured over 48 h. The concentration of DMOG was quantitatively measured indirectly by measuring HIF-1α released after adding aliquots containing the released drugs at different time intervals on rat aortic endothelial cells (RAECs) for 2 h. The concentration of EPO released was also quantitatively measured directly using an ELISA kit without adding on RAECs. The presence of PEG in the formulation helped trigger the release of the drugs from the scaffold matrices. To assess the effect of PEG in the formulations, three different kinds of PEG concentrations were used for the analysis of DMOG release from the scaffolds (Figure 4.7a,b). As can be seen in Figure 4.7a, the release was faster as PEG concentration increased, and PLA concentration decreased in the biomaterial matrix prepared. For comparison purposes, when PLA alone was used, DMOG concentration reached 4% after 48 h which was as expected owing to the release retarding nature of the polylactide polymer. Interestingly, the presence of PEG in the formulations increased the release of the drug, to a certain extent, and approximately 8% DMOG release was observed when PEG concentration was 20% (*w*/*w*). This release pattern indicates that these scaffolds can potentially be used for biodegradable medical implants where a slow release for a prolonged period is desired. Similarly, the in vitro release of EPO from both the F127 and PLA/PEG matrices showed slow release of the drug over 48 h. As can be seen in Figure 4.7c, only about 9 ng/mL of EPO was released after 48 h in F127-based formulation whereas a little bit of faster release was observed for PLA/PEG formulation. As can be seen in Figure 4.7c, about 8 ng/mL of EPO was released in only 2 h. Nonetheless, both PLA/PEG and F127 formulations showed similar kinds of release patterns.

Though the presence of PEG in the formulations would be expected to help propagate the release, this has not been evident in this study. The slower release from the F127 formulations could be attributed to the possible strong entrapment of the drug within the scaffolds. For the full analysis, a longer period of study needs to be fully executed. However, since the aim of this study was to assess the suitability of the emerging bioprinting and its potential applications in endothelial cell repair no further formulation optimization was undertaken.

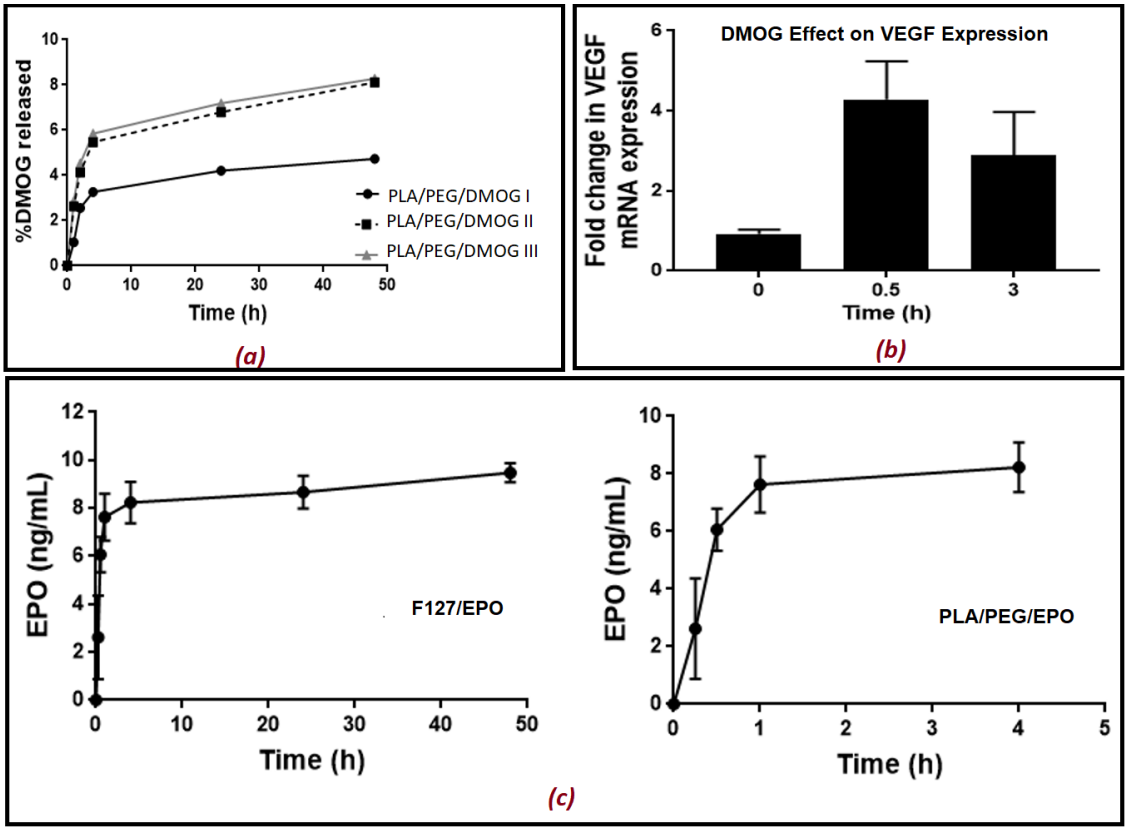

Figure 4.7. The release of HIF-1α inducer; (**a**) DMOG from 3D printed scaffolds in phosphate-buffered saline solution (PBS, pH=7.4) at room temperature (23 ± 1 °C). DMOG was used at a concentration of 30% in all the matrices prepared. (The biomaterial mixture contained PLA/PEG in the ratio 70:0, 60:10 and 50:20), (**b**) Fold change in VEGF gene expression in cell lysates after treating rat aortic endothelial cells with different samples of DMOG released at different time points

(0, 0.5 and 3 h), and VEGF gene expression VEGF mRNA levels were measured as arbitrary units versus the untreated samples. (**c**) release of EPO from the 3D printed scaffolds. Data are the mean ± SEM of 6 samples. $P < 0.01$.

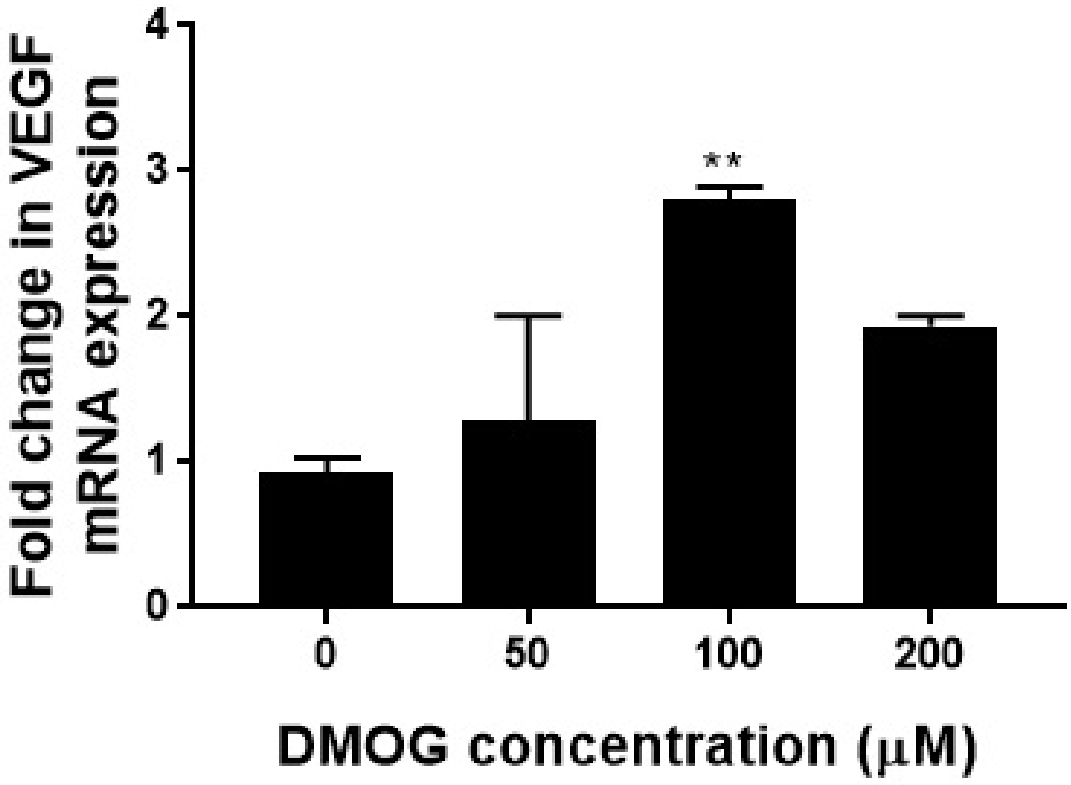

Figure 4.8. Fold change in VEGF gene expression in cell lysates after treating rat aortic endothelial cells with standard DMOG solution added in a concentration of 100 μM.

Moreover, a further investigation was conducted to study if DMOG released from the scaffolds was enough to cause a significant ($p<0.05$) increase in HIF-1α levels when incubated with RAECs for 2 h and resulted in transcriptional activation of HIF-1α target genes (VEGF). The results presented in Figure 4.7b indicated that 30 min was the optimum time for the release of DMOG from the scaffold causing an increase in the expression of the VEGF gene by 3–4 fold. This was like the

effect of standard DMOG solution added in a concentration of 100 µM (Figure 4.8). After 3 h, the DMOG released still caused a significant ($p<0.05$) increase in VEGF gene expression compared to untreated cells. Moreover, it was reported elsewhere that the optimum bioactive concentration of DMOG is 100 uM[93]. In conclusion, it can be claimed that our optimized bioprinted scaffolds showed controlled release of both EPO and DMOG when used individually. As EPO′s erythropoietic effects may increase the risk of thrombosis when EPO is administered to non-anaemic patients alone, a synergistic release of both EPO and DMOG from the same scaffold would provide an excellent alternative beyond the current state of the art. It has been reported that the hypoxia enhances the reparative response of ECs to EPO and its analogues which would likely be mediated by hypoxia inducible factor (HIF)-1α such as DMOG[94]. It can therefore be claimed that the endothelial repair would occur using a combination of EPO (the prototypic TPC) and DMOG (a HIF-1α inducer) without promoting neo-intimal growth. The foregoing will be explored in follow-on studies.

4.4. Conclusions

The optimized bio-ink formulations represent an intriguing alternative for 3D bioprinting materials when loaded with drugs. In this paper, we successfully exploited the use of emerging 3D bioprinting techniques for the development and optimization of novel bio-inks of biomaterials like F127 and PLA. As a result, a novel composite bio-ink from PLA/PEG has been synthesized and characterized. All developed bio-inks exhibited excellent printability and bio-ink properties indicated by printing/plotting fidelity. Moreover, the 3D printed constructs showed the homogenous distribution of the drugs in the scaffolds without compromising

the mechanical and thermal properties of the scaffolds. Further experiments are ongoing to confirm the final interaction between the components used in the formulations and further optimise it for the higher release of the drugs from the scaffolds. Moreover, the bio-functional benefits of the materials used in the formulations were evidenced by the sustained release of the model drugs and VEGF. The current studies demonstrate the exciting potential of our developed semi-solid formulations as a robust, and reliable bio-ink for 3D printing in biomedical applications.

Chapter 5 3D Printed Calcium Phosphate Cement (CPC) Scaffolds for Anti-Cancer Drug Delivery

5.1 Introduction

Three-dimensional bioprinting (3D bioprinting) is a subclass of additive manufacturing (AM) for printing bioactive 3D tissues and organs layer by layer using cell compatible or cell loaded bio-materials[95-97]. The fabrication of 3D constructs can be fast achieved in any computer-designed structure automatically in the 3D bioprinting process. Recently, there are many research achievements in the 3D bioprinting sphere such as the research published by Parka and his colleagues where they printed an organ-on-a-chip which can add complex stimuli in vitro tissue models to better recapitulate living human tissues[98]. Another key milestone in the realm of 3D bioprinting comes from Kang et al. who fabricated muscle fiber-like bundle structures with poly(ε-caprolactone) (PCL) pillars applying a micro-extrusion bioprinting system[99]. Further expanding on the research conducted by Kang et al., 3D aligned-muscle constructs with PCL-geometrical constraints were also created by the same technique[100]. The synergistic application of a hybrid 3D cell printing system combined with extrusion and ink-jet modules were also used for making a 3D skin model composed of a fibroblast-populated 3D dermal layer using a transwell system as well as with keratinocytes of the epidermal layer[101]. There are several different 3D bioprinting techniques which can be categorized as ink-jet bioprinting systems (which is also known as droplet-based printing techniques), laser-assisted bioprinting systems and extrusion-based bioprinting systems[102-103]. Amongst those techniques, an

extrusion-based bioprinting system has been utilized for the printing of bone grafts because of its cost-effectiveness as well as fast plotting.

Calcium phosphate cement (CPC) has appeared as an emerging bone-filling material to promote bone formation and growth which has been demonstrated in various orthopedic and dental applications (e.g., maxillary bone augmentations)[104]. CPCs have several advantages over other bone-filling materials such as setting at body temperature and being mostly injectable as well as malleable. CPCs are generally composed of one or several Ca-P phases (e.g., tetracalcium phosphate, dicalcium phosphate anhydrous) present in powder form. When CPC is mixed with an aqueous solution, it forms a solid structure (set cement) with superior biocompatibility and bioactivity compared to other synthetic bone-filling materials (e.g., polymers). There are various studies reported on the enhancement of biological performance such as biocompatibility, osteoconductivity, osteoinductivity, biodegradability, and interactions with cells of CPCs[105]. A recent study authored by Kilian et al. 2020, investigated the development of a pasty CPC alongside another alginate-based bioi-nk for the fabrication of 3D printed construct with high shape fidelity to reconstruct osteochondral tissue layers. The study concluded that the presence of a mineralized zone in the fabricated constructs potentially interfered with chondrogenesis and was found to support chondrogenic ECM production[106]. Similarly, Ahlfeld et al., 2020, investigated a two-fold study in which a novel plasma-based bio-ink was combined with a printable self-setting CPC to fabricate bone-like tissue constructs. The authors concluded that their developed novel bio-ink was a promising platform for tissue engineering applications supplemented with the combination of CPC for enhanced bioprinted bone-like

constructs[107]. Trombetta et al. 2020, reported 3D printing of bioresorbable CPC scaffolds for sustained antimicrobial drug release and investigated its efficacy of femoral implant-associated osteomyelitis in vivo. The results indicated that 3D printed CPC scaffolds loaded with antimicrobial agents showed better bone growth in a single-stage modification as opposed to traditional two-stage modifications[108]. However, most of the reported studies have either focused on the use of CPC or materials optimization. But none or very few of them have investigated the potential use of 3D printed CPC scaffolds for anti-cancer drug delivery and tissue engineering for bone cancer treatment.

5-fluorouracil (5-FU) a widely used anti-cancer drug (pKa = 8.02, logp = −0.89) with a half-life of 8 to 20 min[109] was chosen as a model drug in this experiment because of its popularity and low cost. Due to poor solubility of 5-FU in deionized water (less than 1 mg/mL at 19 °C[110]), Soluplus® (polyvinyl caprolactam-polyvinyl acetate-polyethylene glycol graft copolymer (PCL-PVAc-PEG)) and polyethylene glycol (PEG) were added to 5-FU solutions as solubility enhancers and their chemical structures are shown in Figure 5.1. Soluplus® (Figure 5.1a) is an innovative commercial excipient for improving the bioavailability and solubility of the active ingredients[111]. It has been widely used in the extrusion process because of its high flowability and excellent extrudability[112]. PEG (Figure 5.1b) is a polyether compound which is commonly utilized in the pharmaceutical industry, and it was chosen to be a good excipient for 5-FU formulations because of its hydrophilic nature.

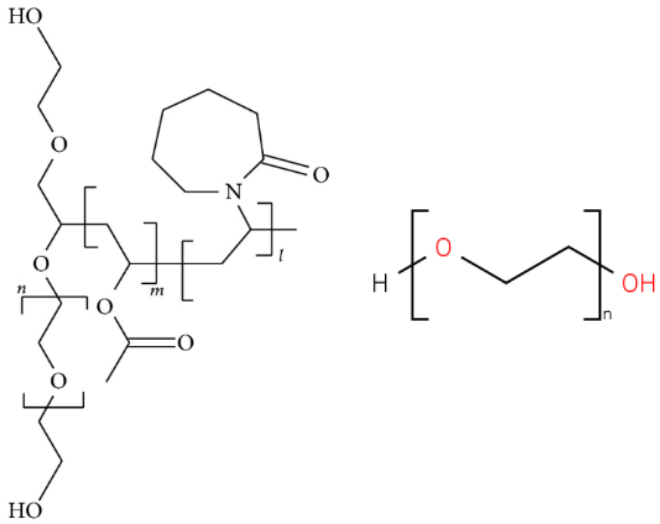

(**a**) (**b**)

Figure 5.1. Chemical structure of the excipients (**a**) Soluplus® and (**b**) polyethylene glycol (PEG).

One of the main applications of bone grafts is filling the gap in bone after the surgical removal of bone cancer tumors. While it is common that patients with bone cancer face the risk of relapse and recurrence after bone removal surgery. It commonly occurs due to the presence of non-union fractures which is a result of the inefficiency of bone healing in certain scenarios. Especially due to the large gaps left after tumor resection[113]. Tumor recurrence after placement of bone filling biomaterials remains one of the major causes of biomaterials failure in dental and orthopedic applications[114]. A local release of an anti-cancer agent from a bone implant that can provide a controlled release of the agent in surrounding cancerous tissue could be an innovative area of research for preventing recurrence after the placement of dental/orthopedic biomaterials. In situ delivery of an anti-cancer agent could potentially provide adequate therapeutic dosage while minimizing the side effects of the anti-cancer agent in the nearby uninfected

tissues. Currently, there is no available bone graft material for clinical use with anti-cancer properties that can reduce the risk of bone cancer resurgence and/or prevent the spread of cancer to other organs. A bone graft material that possesses tunable anti-cancer properties has numerous advantages over the current graft materials used in the clinic[115].

This research aims to develop a novel anti-cancer drug-coated calcium phosphate cement (CPC) scaffold to potentially decrease the relapse and resurgence of bone cancer after surgery. To the best of our knowledge, there is no anti-cancer drug-coated CPC scaffold currently available for commercial use. There has been some previous work about drug-coated 3D printed scaffolds in other matrices, such as silk fibroin, alginate, Pluronic F127, and polymeric matrices[116-118]. Owing to the superior advantages of CPCs such as rapidly setting at body temperature, we believe 3D printed CPC scaffold can be an advantageous and more suitable material for the anti-cancer drug delivery systems. This can also lead to numerous potential applications of these emerging materials in drug delivery and tissue engineering applications. For this purpose, 3D bioprinted CPC scaffolds were coated with different 5-FU formulations to be utilized as an anti-cancer drug delivery system. The coating ingredients were tested by differential scanning calorimetry (DSC). Surface analysis and texture analysis were conducted for these coated scaffolds to investigate the mechanical properties of the scaffolds before and after coating. The efficiency of the scaffold was tested by investigating its ability to kill the cancer cells *in vitro*.

5.2 Materials and Methods

5.2.1 Materials

CPC scaffolds with interconnected pores (diameter 5mm, thickness 2 mm) were printed by a semi-solid extrusion 3D printer (Innotere, Radebeul, Germany) using calcium phosphate semi-solid paste (α-tricalcium phosphate and calcium-deficient hydroxyapatite). All 3D printed scaffolds were subjected to coating using a polymeric solution of a model anti-cancer drug 5-Fluorouracil (5-FU, Acros Organics™, 99%, Fair Lawn, New Jersey, United States). Soluplus® (BASF Ltd., London, UK) and polyethylene glycol (PEG 6000, Acros Organics™, Ludwigshafen, Germany) were used. We used 0.9% NaCl solution as the dissolution medium in the dissolution test. Cancer and transformed cell lines, HeLa and HEK293T, stably expressing GFP constructs were generated at the GDSC, University of Sussex, Brighton, UK. Cell lines were maintained in DMEM supplemented with 10% FCS, penicillin/streptomycin and L-Glutamine at 37 °C and 5% CO2. PBS (pH = 7.4, Fisher Scientific, Loughborough, UK) was used for washing.

5.2.2. Methods

5.2.2.1. The Preparation of 5-FU Coating Formulations

Formulations containing 5-FU were prepared by adding 5-FU powder into DI water under stirring at 80 °C until it was fully dissolved. The ingredients of formulations F1 to F3 are illustrated in Table 5.1. Soluplus® and PEG 6000 were added to 5-FU aqueous solution for the formulations 2 and 3 at the same temperature and dissolved fully under stirring conditions.

Table 5.1. Coating formulation compositions of 5-fluorouracil (5-FU).

Formulation Code	5-FU (g)	DI Water (ml)	Soluplus (g)	PEG 6000 (g)
F1	0.5	20	0	0
F2	0.5	20	0.50	0
F3	0.5	20	0.25	0.25

5.2.2.2. 3D Printing of the Scaffolds

All tested scaffolds were obtained from Innotere (Radebeul, Germany) and 3D printed using a commercial semi-solid extrusion-based 3D printer with a layer height of ~100 microns. 3D expansion was facilitated by alternating orthogonal layers. All scaffolds were cylindrical shaped with a diameter of 5 mm, height 2 mm, and the strand distance was kept at 0.59 mm. Directly after completing the printing process, the cement setting was performed by storing the scaffolds in water solution for a prolonged period at 50 °C. The infill density of the printed scaffolds was kept at 50%.

5.2.2.3. Drug Coating for 3D Bio-Scaffolds

3D bio-scaffolds were coated with 5-FU solution by Caleva mini coater/drier 2 (Caleva Process Solutions Ltd, Dorset, UK). Each scaffold was coated with 10 mL drug solutions for 40 min using the formulation composition listed in Table 5.1. The coating temperature was set as 40 °C, the pumping speed and the agitator frequency were 3.1 rpm and 15.5 Hz respectively.

5.2.2.4. Scanning Electron Microscopy (SEM)

The surface and cross-section of the coated and uncoated blank bio-scaffolds were evaluated by using SEM (JEOL Ltd. JSM-820, Tokyo, Japan), which produced a 15-kV acceleration voltage. The entire surface and each region (apical, middle, and coronal) of each canal were examined at magnifications ranging from ×20 to ×1000. The micrographs depicting a magnification of ×200 were chosen for the morphological characterization.

5.2.2.5. Confocal Microscopy Analysis for 3D Bio-Scaffolds

Confocal microscopy Leica SP8 (Leica Microsystems Ltd., Milton Keynes, UK) was also applied for surface analysis. The wavelength was chosen as 458 nm. The microscope frame is Leica DMi6000 and 20×/0.75 objective was chosen. Live experiment support which heated live chamber (37 °C) and 5% CO_2 (humidified) was on throughout the analysis. LAS X (Leica Microsystems (UK) Ltd, Milton Keynes, UK) was used as the acquisition software.

5.2.2.6. Differential Scanning Calorimetry (DSC)

DSC was used to investigate the thermal behavior of coating materials containing 5-FU. The DSC traces of formulations F1 to F3 (the solutions were dried before performing DSC) plus individual materials were conducted using DSC 4000 with aluminum DSC pans (PerkinElmer, Waltham, MA, USA). In order to convert the solutions to powder form to do the DSC experiment, coating solutions of formulations F1 to F3 were heated to 80 °C and the temperature was kept for around 20 min (this time was enough to get dry powder). Then, the dried sample was ground into powder using mortar and pestle. A certain amount of formulation

powders (5 mg) was placed into the DSC pan and sealed with a lid. Each sample was analyzed from 30 to 400 °C at a scanning rate of 10 °C/min under nitrogen gas. Indium was used to calibrate the DSC for both melting and enthalpy.

5.2.2.7. X-Ray Powder Diffraction (XRD)

Siemens D500 X-ray Powder Diffraction (XRD) system (KS Analytical Systems, Aubrey, Texas, USA) was used to assess the solid-state of the coated scaffolds. XRD test was done at 5–50 theta, the increment was set as 0.1. The data was analyzed by OEM software and reformed by Excel.

5.2.2.8. FTIR Studies

In order to explore any changes in the molecular level of 5-FU in formulations F to F3, FT-IR equipped with a Universal ATR (Perkin Elmer's Spectrum One, Waltham, MA, USA) was used. Preceding to analysis, methanol was used to clean the instrument to remove any residual chemicals left on the apparatus, after which a few milligrams of each of the formulations (solutions were dried completely to get powder forms) was used with a pressure of around 70 bar. Each of the samples was scanned three times over a range of 4000 cm^{-1} to 500 cm^{-1}.

5.2.2.9. Texture Analysis

The strength (ultimate compressive strength) of the coated and uncoated scaffolds was tested by a texture analyzer (Stable Micro Systems, Surrey, UK) with a 25 mm diameter cylinder probe. The test speed was set at 0.03 mm/Sec and the test method was set as "Return to Start" with compression mode. The data was analyzed by Exponent software.

5.2.2.10. Cancer Cell Culture with 3D Bio-Scaffolds

Scaffolds were transferred to a 12 well plate and UV sterilized. Cells were plated onto the scaffolds at a density of 0.4×10^5 in 10% DMEM and placed into a humidified incubator at 37 °C (5% CO2). 24, 96,120 h after plating, the scaffolds were transferred to a new well and washed three times with PBS (pH=7.4). Original wells were trypsinized and cell count was obtained. 0.4×10^5 cells were seeded onto transferred scaffolds. Images were taken prior to trypsinization at 4× magnification using a Floid Cell Imaging Station (ThermoFisher Scientific, Waltham, MA, USA).

5.2.2.11. Dissolution Studies and Drug Quantification

Dissolution in vitro test was carried out using USP dissolution apparatus II, paddle method (708-DS, Agilent Technologies, Santa Clara, CA, USA) to investigate the drug release pattern from various scaffolds (F1, F2 and F3). The dissolution medium was phosphate buffer (PBS pH 7.4, 900 mL) maintained at 37 °C with a rotation speed of 100 rpm. The coated scaffolds were placed in the dissolution medium and at different time intervals the medium was pumped into UV (Cary 60 UV-Vis, Agilent Technologies, Santa Clara, CAa, USA) and read the absorbance of 5-FU at a wavelength of 256 nm. The experiment was carried out in triplicate (n = 3) and the release profiles were plotted as a percentage of cumulative drug release versus time.

In order to quantify the amount of drug deposited on each scaffold during the coating process, each scaffold was placed in 50 mL phosphate buffer and sonicated for 20 min. The preliminary results showed that 20 min was enough to

dissolve all the drug deposited on scaffolds[119]. The final solution was diluted to be readable in the UV/Vis spectrophotometer at a wavelength of 256 nm.

5.3. Results and Discussion

5.3.1. 3D Printed Scaffolds and Its Surface Morphology

It has been reported that 3D printing can be an ideal approach to fabricate various micro/macroscale intricate structures owing to its outstanding repeatability and reproducibility which is assisted by a computer-aided method. This emerging technology has started a new era of designing and manufacturing tissue engineering cell-laden substitutes and biological constructs[111-112]. In this study, CPC scaffolds with interconnected pores (diameter 5 mm, thickness 2 mm) were printed using calcium phosphate semi-solid paste (α-tricalcium phosphate and calcium-deficient hydroxyapatite) exhibited rough surface morphology which could be attributed to the microcrystalline morphology of the CPC. An optimized 3D printing process involved the utilization of a commercially available semi-solid extrusion-based 3D printer with a maximum print resolution (layer height) of 100 microns. All obtained scaffolds exhibited excellent shape fidelity with interconnected homogenous pores, acceptable process parameters such as syringability, ease of extrusion and bio-ink malleability.

The blank/uncoated CPC scaffold and the other three scaffolds which were coated with formulations F1, F2, and F3 respectively were illustrated in Figure 5.2. Compared to those coated ones and the blank/uncoated one, these scaffolds show no obvious difference from their physical appearance. The surface morphology of the coated scaffolds (diameter 0.5 cm) via SEM are shown in Figure 5.3. The top view images (four images above) illustrates that the scaffolds

coated with F1 and F2 formulations have a relatively smooth surface. This could be due to the deposition of a homogenous layer of polymeric solution all over the scaffolds. The images of the cross-section were obtained by cutting the CPC scaffold across. Compared to the uncoated CPC scaffold, the presence of a thin polymeric coating layer on each coated scaffold exhibited some adsorbed particles like morphology on the surface which is not visible on the uncoated scaffold.

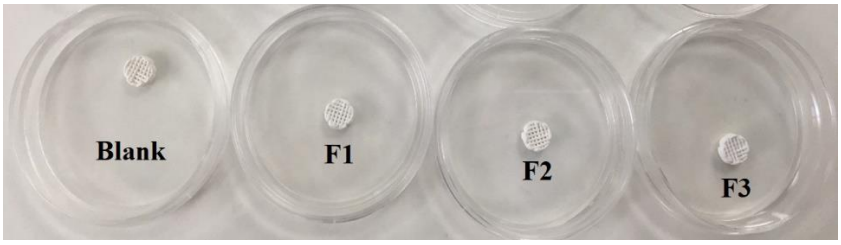

Figure 5.2. Uncoated/blank and F1-F3 coated scaffolds.

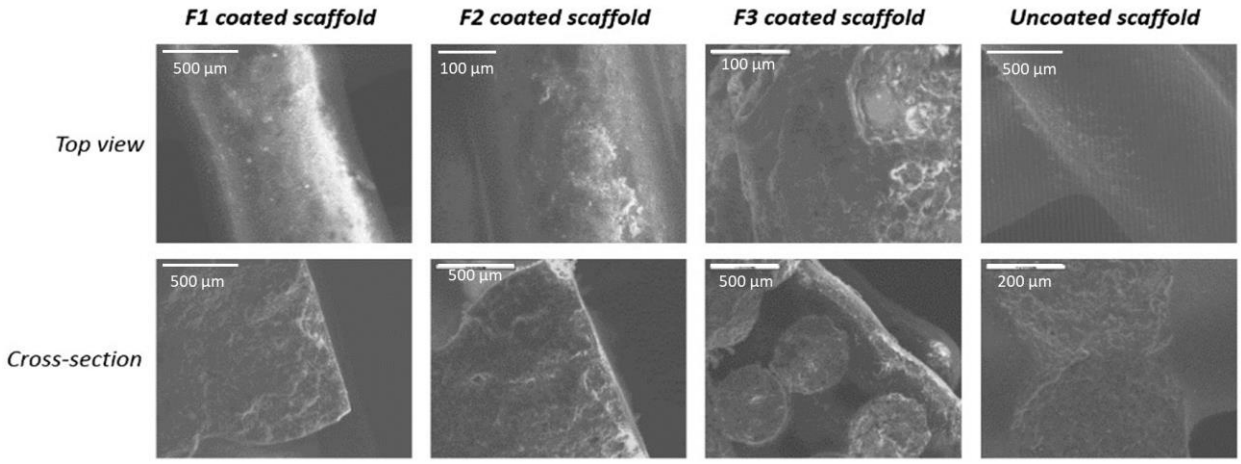

Figure 5.3. SEM images of coated and uncoated calcium phosphate cement (CPC) scaffolds.

5.3.2. Confocal Microscopy for 3D Bio-Scaffolds

An advanced surface analysis conducted via confocal microscopy revealed a homogenous distribution of the drug throughout the surface of the scaffolds, represented by the dark green pattern (only the drug is fluorescent in the formulations) (Figure 5.4). Comparing the three scaffolds coated with different 5-FU formulations showed that F3 coated scaffold (Figure 5.4c) gives the brightest signal. While the scaffolds coated with F1 and F2 solutions (Figure 5.4a, b) give more homogenous results. This is due to the fact that PEG contained in F3 has the highest elongational viscosity which leads to the high viscoelasticity[120-121]. The higher solution viscosity results in larger thickness deviations. Therefore, a larger amount of the polymer from F3 deposits on the surface of the scaffolds after the coating process. Due to the higher viscosity of PEG solution, it led to the higher coating thickness in F3 but with slightly less homogeneity compared to that of scaffolds coated with i.e., F2 solution. Histograms (Figure 5.4 mid and lower panel) show the distribution of fluorescence over the selected area for F1, F2, and F3 (results interpreted by commercial ImageJ). However, the higher

standard deviation values are due to the fact that the software also counts backgrounds signal. Nonetheless, this provides sufficient insights into the intensity profile of the homogenous fluorescent 5-FU coating on the surface of all CPC scaffolds.

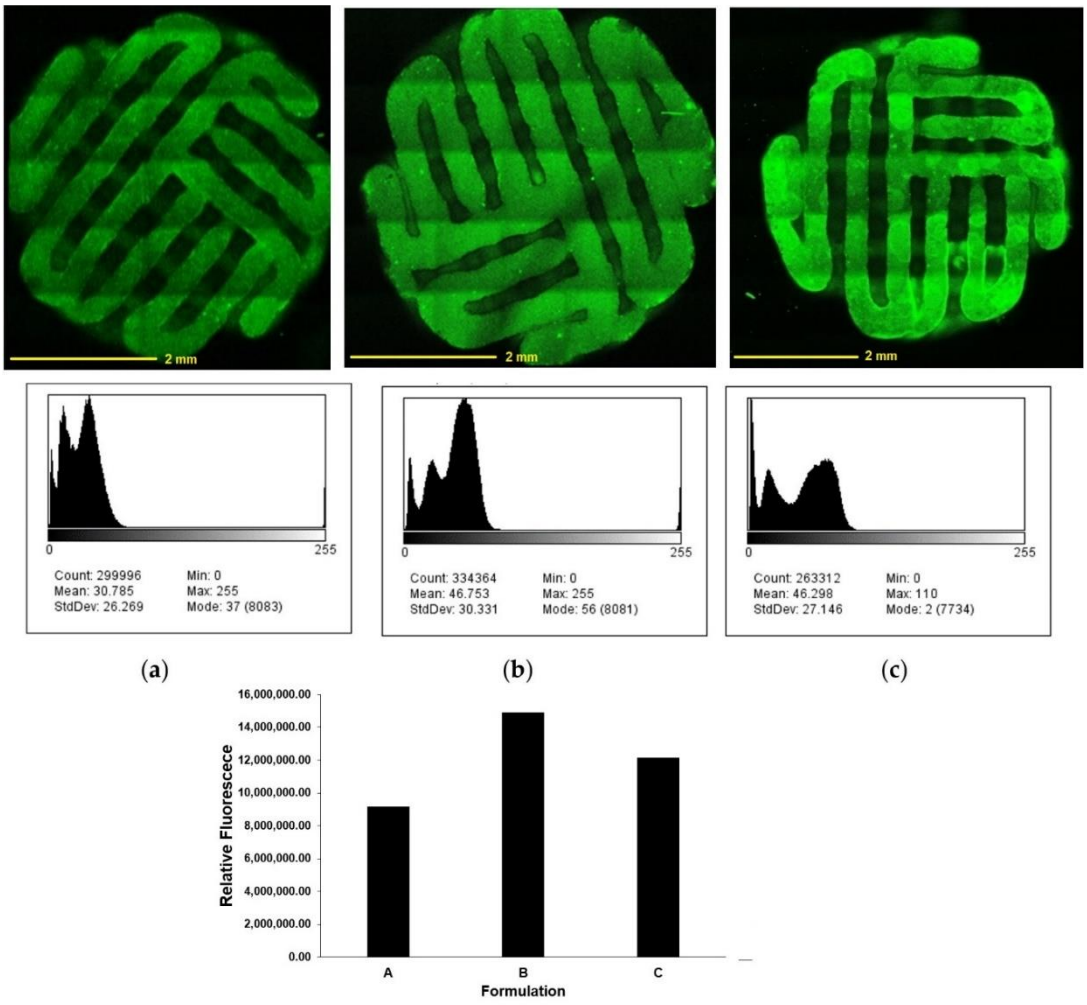

Figure 5.4. Confocal microscopic images of drug solution coated scaffolds with (**a**) F1, (**b**) F2, and (**c**) F3 (top panel), histograms showing intensity profiles as a function of fluorescence distribution (mid and lower panel).

5.3.3. DSC Analysis for Coating Ingredients

DSC traces for coating ingredients, API and formulations are shown in Figure 5.5. 5-FU DSC traces show a sharp peak at around 286 °C which corresponds to its

melting peak. The second broad peak around 350 °C could be attributed to the thermal degradation of 5-FU. Similarly, PEG 6000 exhibits a sharp endotherm at 68 °C correspondings to its melting point. As it can be seen from DSC traces of all formulations in Figure 5.5b, it is clear that the melting peak of 5-FU around 280 degrees is present in all the formulations (F1–F3). Comparing the thermal events of the bulk 5-FU and formulation F1 indicates that the peak around slightly higher than 100 °C is due to the evaporation of deionized water left in the coating formulation. The other two formulations (F2 and F3) show a similar thermal event because they were made by a similar evaporation technique to those coating solutions. Formulation F2 containing 5-FU and Soluplus shows a combined peak corresponding to the degradation of 5-FU and Soluplus around 350 °C. In addition, data from formulation F3 show a sharp peak around 65 °C, which may be due to the melting of PEG 6000. Figure 5.5a shows special peaks which can identify specific materials respectively. Whose peaks all show at the original temperature in the mixture formulations F1 to F3 (Figure 5.5b), which indicates there is no interaction between the components and 5-FU. This indicates that the selected polymers could be suitable polymers to be used along with 5-FU in the scaffold formulation.

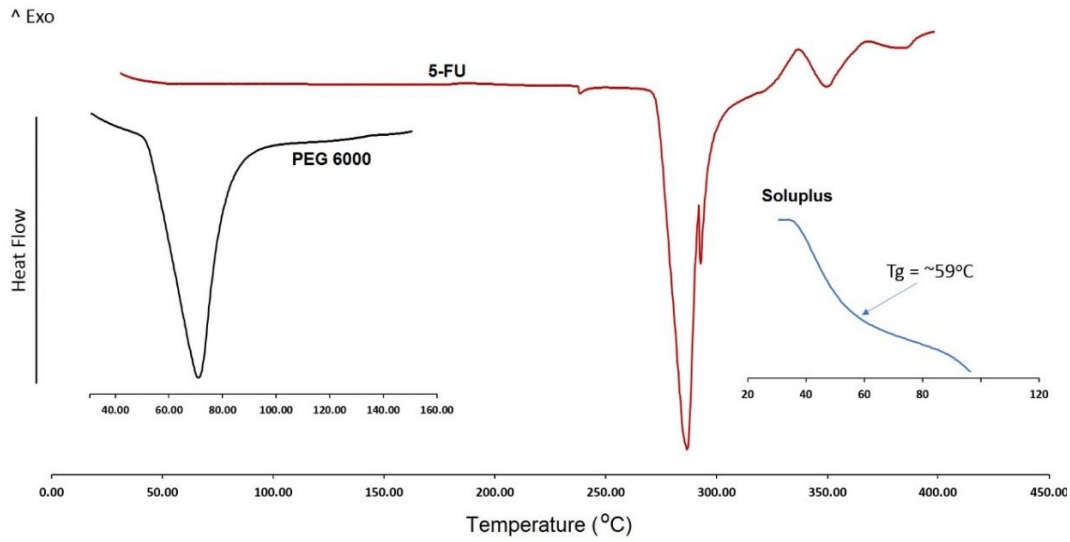

(**a**)

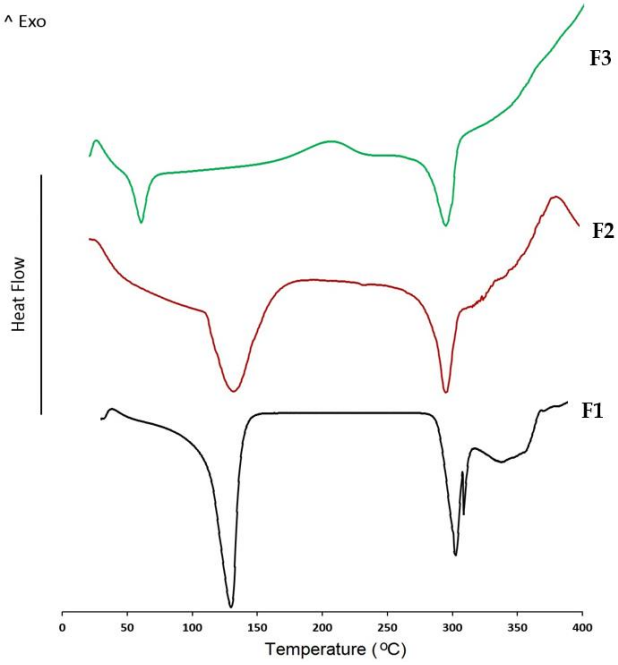

(**b**)

Figure 5.5. Differential scanning calorimetry (DSC) data of (**a**) bulk drug, Soluplus, and PEG 6000, (**b**) scaffold formulations (F1-F3).

5.3.4. XRD Analysis of the Coated Scaffolds

All CPC scaffolds are synthetic, porous, biocompatible as well as bioresorbable bone substitute materials consisting of α-tricalcium phosphate and microcrystalline hydroxyapatite phases as confirmed via XRD analysis. Shape peaks in XRD data illustrate crystalline molecules in the samples. The XRD data in Figure 5.6 illustrates that there was semi-crystalline structure (or partially amorphous) on the surface of the CPC scaffolds before the coating process with those three 5-FU drug solutions. The XRD data in Figure 5.6 illustrates that both blank scaffolds and scaffolds coated with solutions F2 to F3 show semi-crystalline structure (or partially amorphous) which is an indication of no major changes in the crystallinity of the scaffold before and after the coating process.

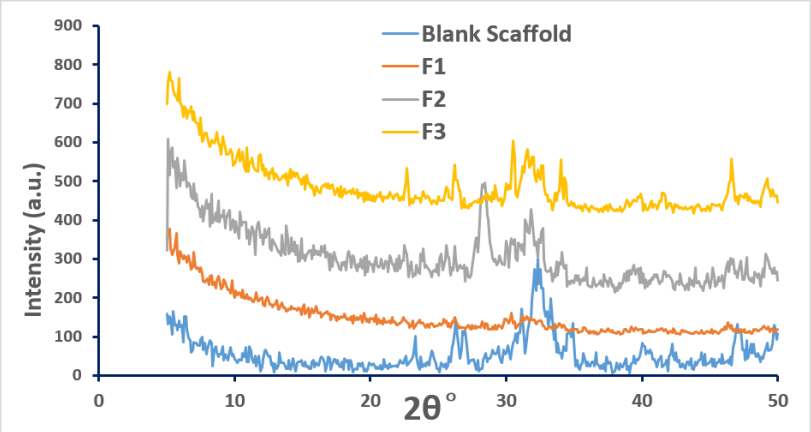

Figure 5.6. XRD data of blank scaffold (uncoated) and coated scaffolds: F1 (coated with 5-FU), F2 (coated with 5-FU and Soluplus, F3 (coated with 5-FU, Soluplus and PEG 6000).

5.3.5. FTIR Analysis

An FTIR analysis was conducted to analyze any potential interactions between the various components used for coating the CPC scaffolds. When molecules

absorb radiation at specific wavelengths under infrared radiation, the energy gap between ground state and excited state can be detected at the specific wavelength during FTIR analysis to obtain structure information of a molecule[122]. It is expected that any potential interaction between the drug and polymer will be reflected by the appearance of any additional bands, alterations in wavenumber position or potential broadening of functional groups when compared with the bulk materials. From the FTIR analysis (Figure 5.7), it can be seen that there are no major interactions between 5-FU and the polymer solutions used for coating. The absorption band of the bulk compounds are retained in the formulations and helps confirm the absence of chemical interactions between the components. However, a weak intermolecular interaction can be seen between 5-FU and Soluplus® in formulation F2 which is represented by the reduction in the intensity of the 5-FU carbonyl band at 1650 cm^{-1} region. This reduction in the intensity of the band only occurs at higher concentrations of Soluplus® i.e., when the ratio between 5-FU and Soluplus is 1:1 in formulation F2 but cannot be seen when the concentration of Soluplus® is lowered in formulation F3.

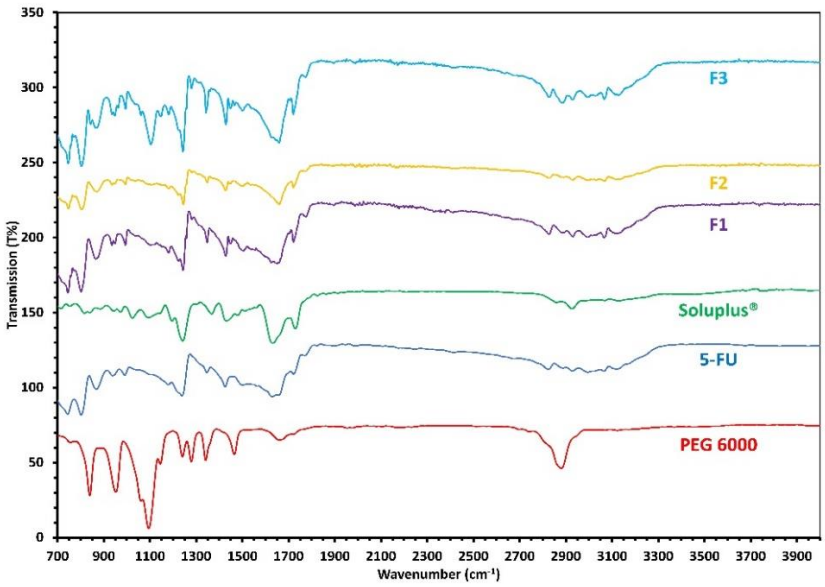

Figure 5.7. FTIR spectra of bulk materials and formulations F1, F2, and F3.

This could possibly be due to the presence of both amine and the carboxyl group in the coating formulations. It has been reported that during the FTIR process within carbonyl (COO-) groups two CO bands resonate. As a result, the characteristic CO absorption band can sometimes be replaced by an auto-symmetrical vibration of the COO- group from the polymer[123]. Nonetheless, this suggests that the reduction in the intensity of the 5-FU band at 1650 cm^{-1} in F2 is due to the presence of the excessive amount of Soluplus in the formulation (F2) which may form a weak interaction with the drug but when the amount is lower such as in F3, this interaction disappears[124].

5.3.6. Texture Analysis

Texture analysis was conducted to see the effect of coating on the strength of the scaffolds. The data from Figure 5.8 shows the stress/strain profile of the CPC scaffolds. Mechanical properties such as ultimate tensile strength—the maximum stress that a material can survive under increasing strain before breaking, can be determined from the results presented in Figure 5.8. The ultimate tensile strength of the blank scaffold is 274.43 kPa with a maximum strain of 84%. Interestingly none of the coating formulations have changed the stress-strain profiles of the 3D printed CPC scaffolds significantly ($p>0.05$). However, a slight increase in the strain value was observed for F2 (85.5%) which could be due to the presence of excessive viscous Soluplus polymer in the coating formulation. In F3 with the decrease of Soluplus content the strain value decreases while the tensile strength

is unaffected. In all cases, there is no significant ($p>0.05$) change observed in the mechanical properties of the scaffolds after coating.

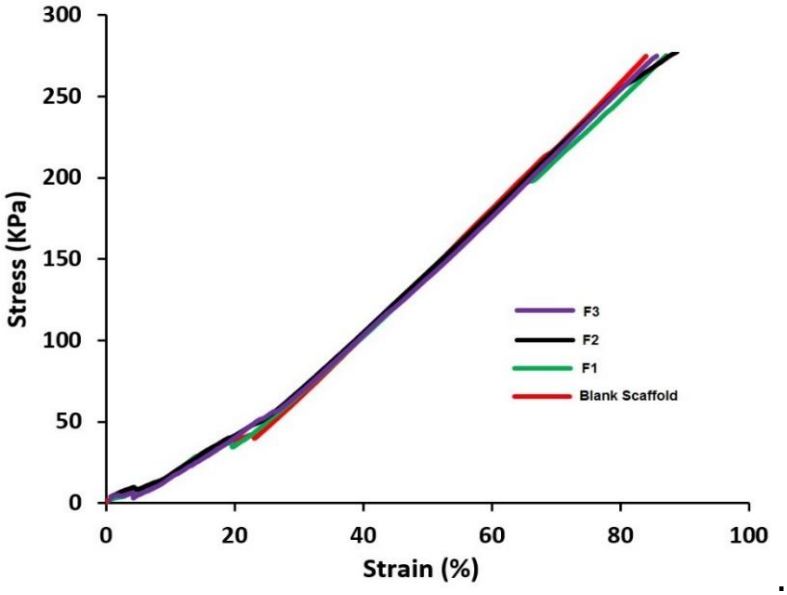

Figure 5.8. Stress–strain curve of blank scaffold (uncoated) and coated scaffolds: F1 (coated with 5-FU), F2 (coated with 5-FU and Soluplus, F3 (coated with 5-FU, Soluplus and PEG 6000).

5.3.7. In Vitro Dissolution Studies

Dissolution profiles of scaffolds coated with various formulations are shown in Figure 5.9. The results showed that all three coated scaffolds are able to release the entire drug within 2 h. The drug release rate is faster in F1 compared to that of F2 and F3. This was expected as formulation F1 has no polymer, whereas formulations F2 and F3 contained polymers which can potentially act as a barrier to affect the drug release. This slight delay in drug release from F2 and F3 could be attributed to the chemistry of the amphiphilic polymer, Soluplus® which tends to retard the release of the sparingly water-soluble drug i.e., 5-FU upon swelling in the dissolution media[125].

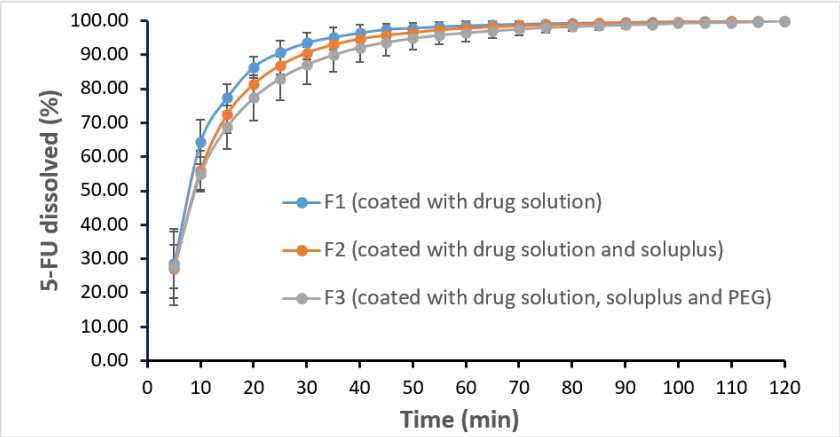

Figure 5.9. In vitro dissolution profiles of 5-FU from the coated scaffolds with different formulations.

As the polymers used in the coating of the scaffolds are hydrophilic polymers, therefore, these polymers cannot slow down the drug release for a longer time. It is obvious if a longer drug release is needed, it is suggested to use water-insoluble polymers such as ethyl cellulose. Nonetheless, efficient drug release profiles from the coated scaffolds indicate that the deposition of the drug from the coating solutions on each scaffold was achieved successfully.

When the amount of drug deposited on each scaffold was determined, the results showed that the scaffold coated with F1 formulation contained more drug (40.69 ± 1.93 mg) compared to scaffolds coated with formulations F2 (38.49 ± 1.06 mg) and formulations F3 (32.00 ± 2.02 mg), although the initial concentration of drug was kept constant in all coating solutions. This could be due to the change of solid content percentage in the formulations i.e., F1 contains 2.5% *w/w* solid whereas both F2 and F3 coating double the amount. Moreover, the viscosity of the coating formulations may play a key role in the deposition layer thickness, amount of the coating solution and thus the actual amount of drug on the scaffolds.

Nevertheless, in all cases, a sufficient amount of 5-FU (>30 mg/scaffold) was successfully deposited.

Drug release kinetics analysis was performed and 4 main kinetics of drug release namely zero-order release, first-order release, Higuchi and Peppas models were considered[117]. The results showed that all formulations followed first-order release kinetics with r^2 values of 0.980, 0.989, and 0.988 for F1, F2, and F3, respectively.

5.3.8. Cell Culture with 3D Bio-Scaffolds

In vitro cell culture studies in two different cell lines (HEK293T and HeLa) were conducted and the results showed a significant ($p<0.05$) reduction of the growth in the number of the cells (Figures 5.10 and 5.11). According to the images of the three 5-FU coated scaffolds in Figure 5.10, there are no visible cells that can be found around the surface of the scaffold. While the blank scaffold (uncoated) was surrounded by living cells. Figure 5.11 illustrates that the uncoated scaffold did not show any inhibition in the growth of either cell line reflected by an increase in the number of cells by 4–6 fold (after 5 days). In contrast, all formulations showed significant ($p<0.05$) cell growth inhibition. F2 and F3 coated scaffolds are seen to have similar inhibition abilities in terms of reduction in the growth of cells as represented by Figures 5.11. Although the scaffold coated with F1 shows a relatively weaker effect, the cell counts still went down to near 0 after 4 or 5 days. Nonetheless, it can be claimed that the developed 5-FU coated 3D printed scaffolds can successfully be used as bone graft materials to treat bone cancer and to deliver immediate potential effects for personalized medical solutions.

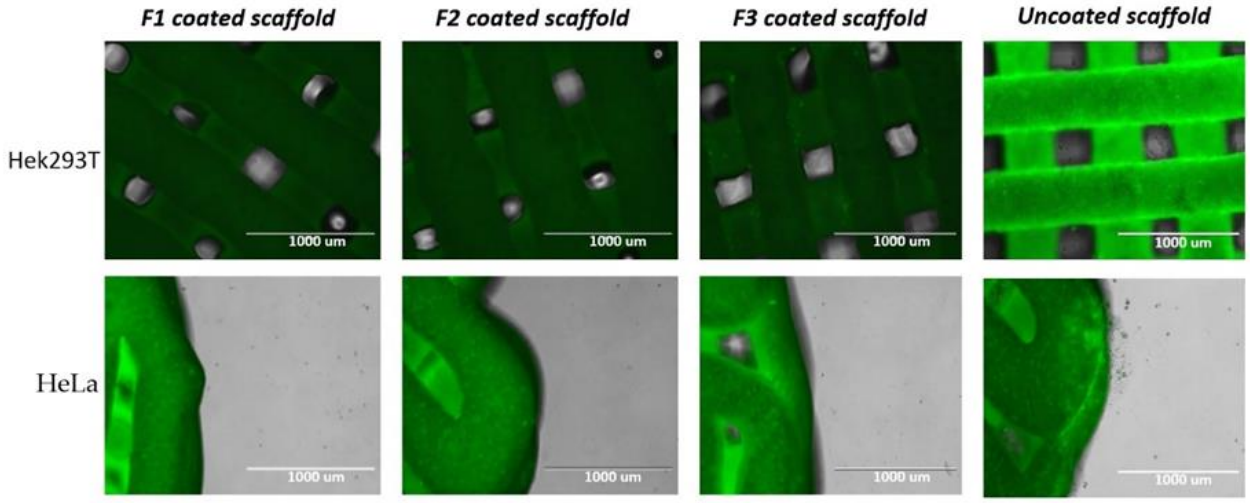

Figure 5.10. Microscopic images of cell cultured coated and uncoated CPC scaffolds.

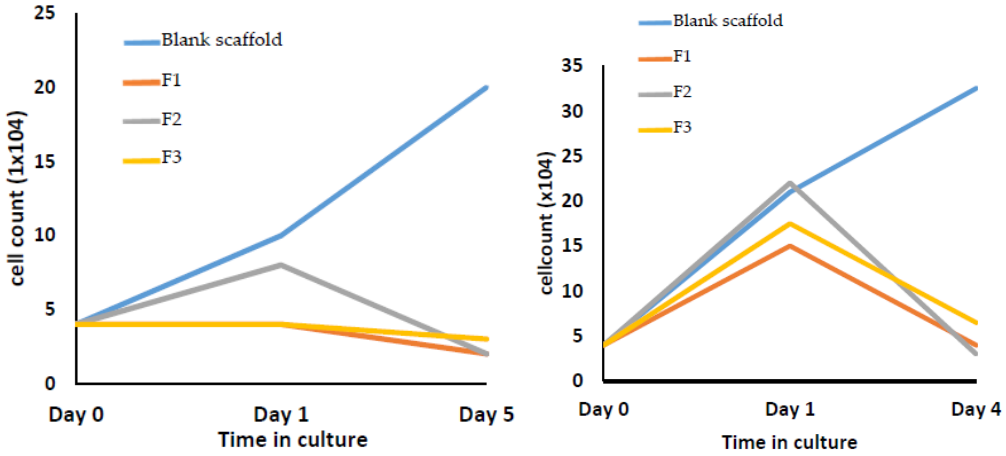

Figure 5.11. In vitro cell culture assessment of CPC blank scaffold and uncoated scaffold: F1 (coated with 5-FU), F2 (coated with 5-FU and Soluplus), F3 (coated with 5-FU, Soluplus and PEG 6000), with GFP labelled HEK293T(left) and HeLa(right) cells.

5.4. Conclusions

CPC scaffolds coated with different 5-FU formulations were created and evaluated in this research. The surface analysis conducted by SEM, confocal microscopy, and XRD illustrate the homogeneous drug-coated outcomes and the amorphous surface of the coated scaffolds. DSC analysis of the coating ingredients shows that there are no chemical reactions occurring between the coating ingredients during bone graft before or after the coating process. Similarly, FT-IR analysis indicated no significant interaction between drug and polymers ($p>0.05$), though a nominal interaction was observed in F2 due to the higher concentration of Soluplus presents in the formulations which disappeared in F3. Dissolution studies showed that all the coated scaffolds released all the drug within 2 h, and the drug release pattern followed first-order release kinetics. In addition, the anti-cancer cell studies confirmed the effective cell killing ability of these 5-FU coated CPC scaffolds. In other words, 5-FU coated 3D printed CPC scaffolds can be successfully used as a novel bone graft material and as a personalized drug delivery system in the treatment of bone cancer.

Chapter 6 Cell behaviour studies with alginate and calcium phosphate cement (CPC) scaffolds

6.1 Introduction

Bio-scaffold is a 2D or 3D structure which provides a suitable environment and supports the growth of cells into certain shapes or structures[127]. 3D bioprinting, which forms 3D shape layer by layer using bio-inks, is a widely-used technology in the bio-fabrication of bio-scaffolds[128]. The cell-free method of bio-printing, which stands for seeding and culturing cells with pre-printed bio-scaffolds, is one of the essential steps of tissue regeneration. Cells from individual patients can be used in culturing as personalised tissue, which is promising to reduce or avoid immune repulsion response after tissue implant surgery[129]. In addition, the bio-printed scaffolds can be loaded with anti-cancer drugs as a drug delivery system, which can be helpful to prevent the recurrence of cancer after tissue removal surgery[130].

In order to meet the requirement of tissue engineering and provide a suitable environment for the growth of cells, there are high demands for the material of bio-scaffolds to be bio-degradable, non-toxic and bio-compatible[131]. Natural alginate-based polymers (which are not expensive), and calcium phosphate cement (CPC) are widely used and promising materials for bio-scaffolds currently[132].

Human cancer cells and normal cells are two types of cells used in cell culture studies. Normal cells grow slowly compared to cancer cells, and the production

ability of cancer cells will not be reduced after cultivation due to their uncontrollable growing property[133]. 1BR is a cell line that was originally transformed from healthy Human skin fibroblast, which plays an important role in the process of wound healing[134]. While U2OS-GFP cell line was obtained from the bone tissue of a patient who suffered from osteosarcoma[135]. HEK293T-GFP, which is derived from the human embryonic kidney, is a classic sample cancer cell line applied in cell culture studies[136]. Those two cancer cell lines were purchased as green fluorescent protein (GFP) labelled for ensuring bioactivity and tracing the number of cells during the study.

There have been plenty of in-vitro studies on the effect of bio-scaffolds on cell behaviour in the last decades. Studies show that appropriate stiffness of bio-scaffolds may support efficient bone cell growth[137]. The behaviour of cells which was cultured with scaffolds in the same structure but with different stiffness was also explored as well[138]. However, it is still not clear how the morphology and behaviour of cancer and the normal cells can be affected and changed when cultured with bio-scaffolds in different materials and structures. In this study, 1BR, HEK293T-GFP, U2OS are used as three sample cell lines to culture with alginate-based and CPC scaffolds, aiming to provide more quantitively and qualitative information on the process of the interaction with bio-scaffolds. It can be useful as guidance of long-term scaffolds implant and tissue culture in the future for more effective and predictable tissue engineering results.

6.2 Materials and methods

6.2.1 Materials

1BR cell line, u2os-GFP cell line, HEK293T-GFP cell line and HeLa-GFP cell line (ATCC, Virginia, USA) were obtained from Genome Damage and Stability Centre, Sussex, UK. Commercial CPC scaffolds 3D size L (diameter ~20.0mm) and size S (diameter ~9.4mm); 2D size L (diameter ~20.4mm) and S (diameter ~9.6mm) were purchased from INNOTERE, Germany which is shown in Figure 6.1. Dulbecco's Modified Eagle Medium (DMEM), Minimum Essential Media (MEM), Phosphate-buffered saline (PBS, pH=7.4) were used during cell culture and wash (purchased from Fisher scientific, USA). Trypsin-EDTA solution (Sigma Aldrich, Missouri, USA) was applied to trip the cells before cell counting.

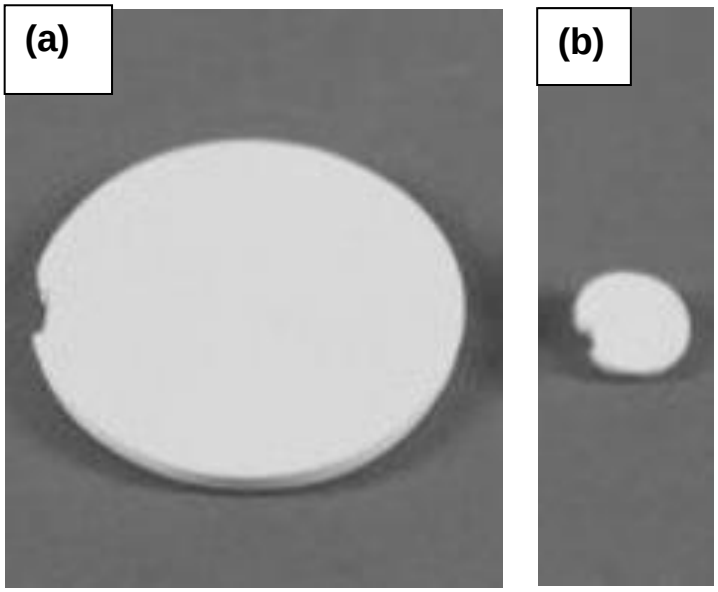

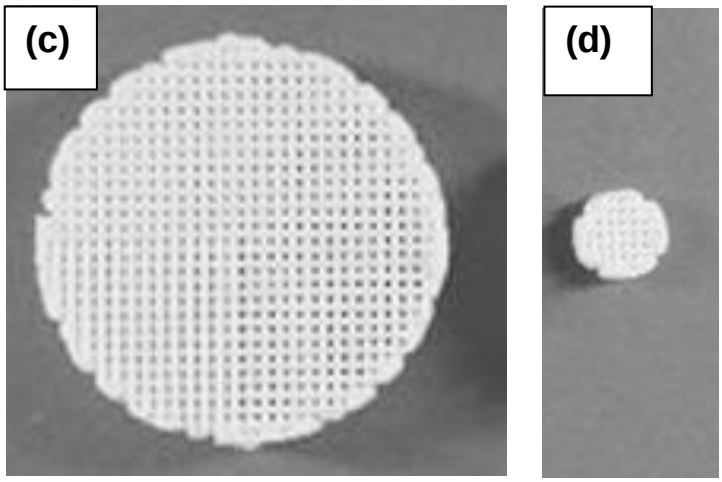

Figure 6.1. 2D size L (a), size S (b)and 3D size L (c), size S (d) CPC scaffolds.

6.2.2 Methods

6.2.2.1 The preparation of cell lines

All cell lines were defrosted at 37°C before culturing. 1BR Cell line was cultured in 10% MEM. u2os-GFP cell line, HEK293T-GFP cell line, HeLa-GFP cell line were cultured within 10% DMEM. They were both placed in a humidified incubator at 37 °C (5% CO2) for 1 week until the biological activity of the cells was recovered completely.

6.2.2.2 The study set up with/without CPC scaffolds

The scaffolds were transferred to a 6 well plate and UV sterilized. 0.4×10^5 cells were seeded onto transferred scaffolds. In 10, 21, and 28 days after plating, the scaffolds were transferred to a new well and washed three times with PBS (pH=7.4). Original wells and scaffolds were both trypsinized and cell count was obtained.

6.2.2.3 Microscopy investigation of cell behaviour

Images were taken prior to trypsinization at 4× magnification using Floid® Cell Imaging Station (Thermo Fisher Scientific, Waltham, MA, USA). The green fluorescent light channel was chosen for all the GFP-labelled cell lines and the white light was for 1BR cell line. The light intensity was set around 35%.

6.2.2.4 cell counting and data analysis

The cells were calculated under light microscopy (Celestron, California, United States) and data were analysed using Excel software.

6.3 Results and discussion

6.3.1 Cell only study

6.3.1.1 Microscopy study

The microscopy picture of three cell lines, 1BR, HEK293T and U2OS with GFP tag is shown in Figure 6.2. GFP tag labelled HEK293T and U2OS cells illustrate green under microscopy due to their fluorescent emission[139], while 1BR cells show no colour under white light. In terms of the different shapes of those cell lines, 1BR cells are long elegant shapes while the other two are round. In addition, HEK293T and U2OS cells tend to grow into several groups when 1BR cells grow separately. Those bio-differences of 1BR as primary cells and HEK293T and U2OS as cancer cells making them easy to be distinguished under microscopy.

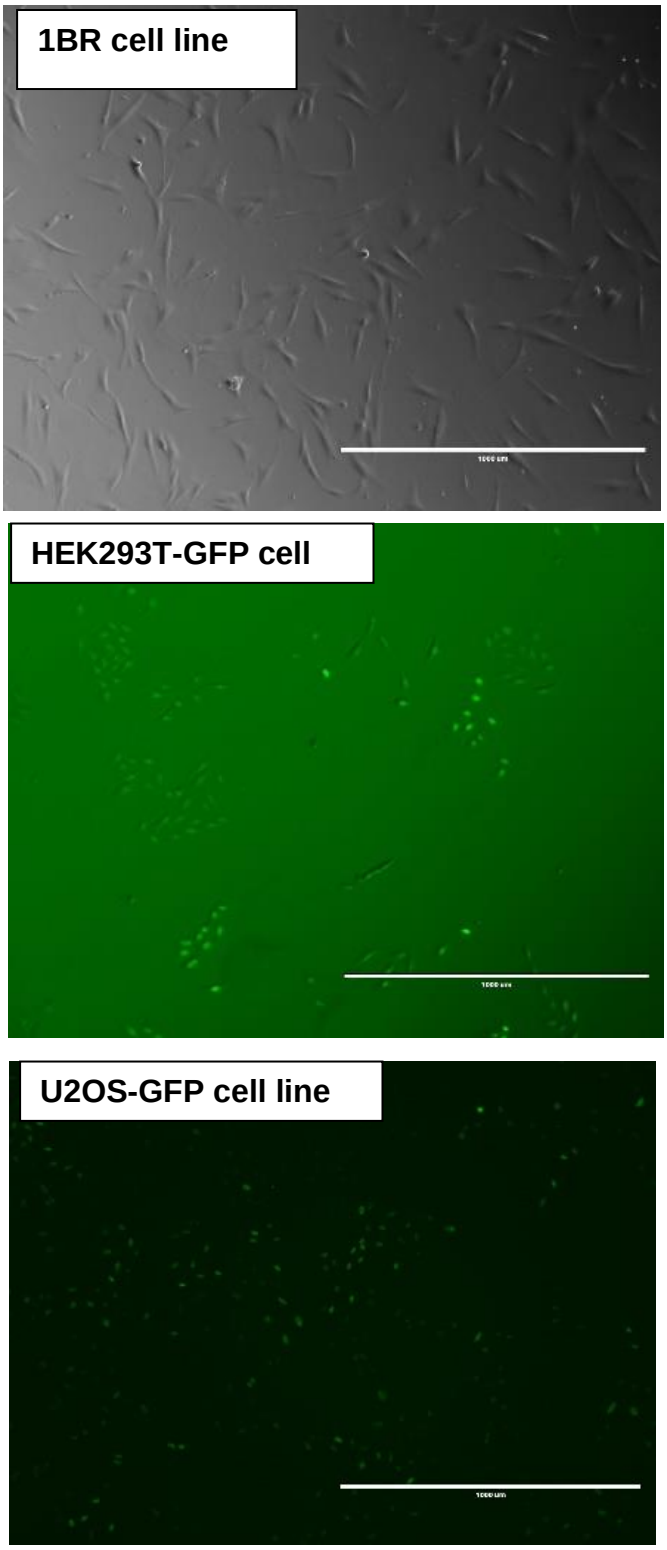

Figure 6.2. The cell morphology of 1BR, HEK293T-GFP and U2OS cell lines under microscopy.

6.3.1.2 Cell counting and analysis

Table 6.1 cell count of 3 cell lines during 6-day culture (X10^4)

Cell lines	Day 0	Day 1	Day 2	Day 3	Day 4	Day 6
1BR	4	3.876	----	5.4	---	6.332
HEK293T-GFP	1	1	----	---	11.9	---
U2OS-GFP	1	---	2	---	4.8	---
	2	2	---	3.6	---	8.63
	4	---	5.875	---	8.25	---

Three cells lines were cultured for a maximum of 6 days to analyse their growing parameter and speed and the results are illustrated in Table 6.1. It can be seen that the primary cell line 1BR grows much slower than those two cancer cell lines, HEK293T and U2OS. 1BR cell line has not even doubled its number after 6 days of the culture.

When U2OS was seeded as 1x10^4 on day 0, it quickly doubled the number in 2 days and finally increased 5 times on day 4 compared to day 0. While U2OS was seeded as 4 x10^4, it only doubled its number on day 4. This might be because the fast-growing cells become too crowded and their growth was limited. So, the seeding number should be limited to below 4 x10^4 in future culture studies due to its bio-properties[140].

What's more, the HEK293T cell line grew even faster than the U2OS cell line. Its total number on day 4 increased nearly 12 times compared to day 0, which shows

its higher breed ability compared to 1BR and U2OS cells. The results indicate that the HEK293T cell line is more suitable for short-period cell culture studies than the U2OS cell line.

6.3.2 Cell culture with alginate scaffold

6.3.2.1 Microscopy study (day 4)

Figure 6.3 illustrates the HEK293T-GFP cell line cultured with alginate-based scaffolds for 4 days. 5-FU loaded alginate and alginate-MC scaffolds showed much less HEK293T-GFP green signals compared with pure alginate scaffolds. And the HEK293T-GFP grew more separately with 5-FU loaded scaffolds.

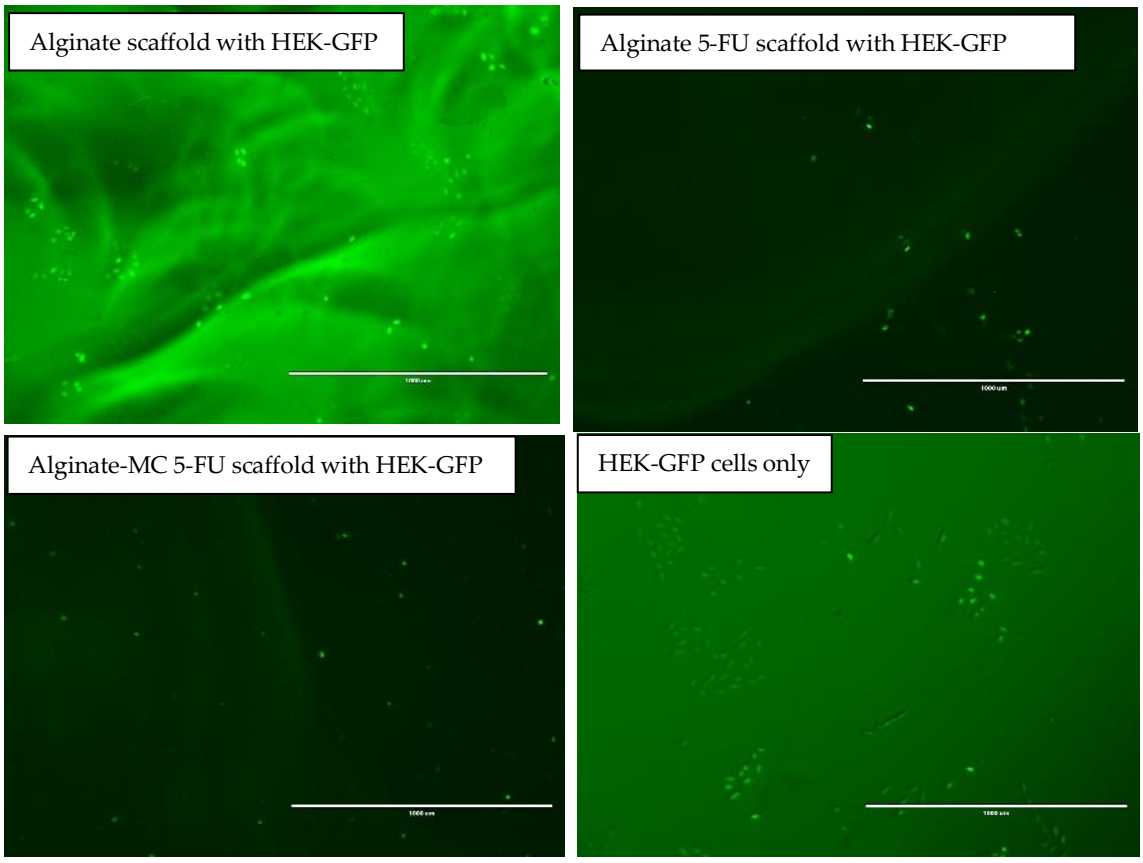

Figure 6.3 The morphology of HEK293T-GFP cells with alginate-based scaffolds.

Figure 6.4 illustrates the way 1BR cells grows with pure alginate scaffolds. Cells grow closely and even attach to scaffolds with no shape or function change, which indicates alginate scaffolds can cause no bio-toxic effects on 1BR as sample primary cell line.

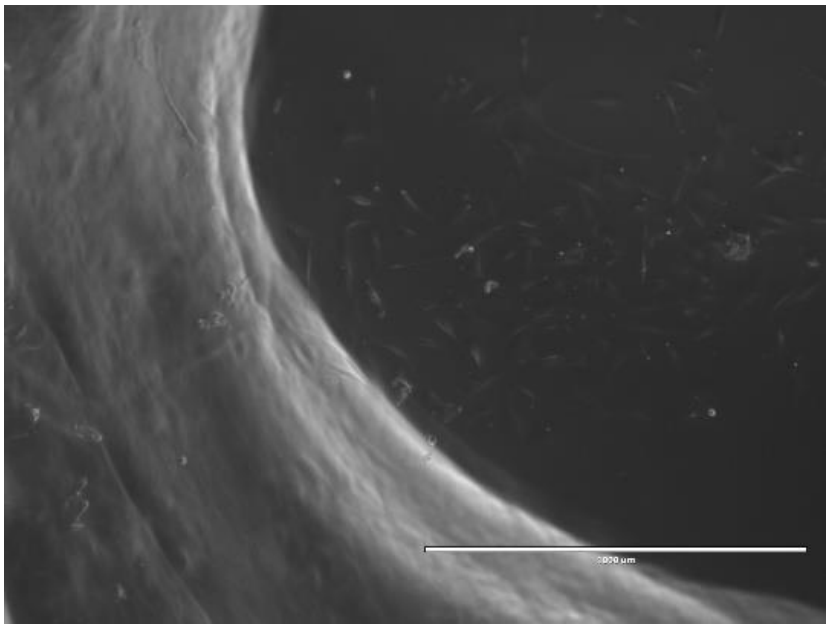

Figure 6.4 The morphology of 1BR cells grows with pure alginate scaffolds.

6.3.2.2 Cell counting and analysis

Figure 6.5 shows the cell count of HEK293T-GFP culture with alginate-based scaffolds. Pure alginate barely had any influence on cell growth and illustrate similar cell counts as the cells with no scaffolds or 5-FU. While those two 5-FU loaded scaffolds have a similar anti-cancer function. They both killed cancer cells to around $0.2x10^4$ density on day 4, even though the alginate-MC scaffolds show a higher cell count on day 2. This is due to that the MC polymer can reduce the drug release rate from the scaffold compared to pure alginate one. In other words,

the 5-FU loaded alginate and alginate-MC scaffold are both effective in killing cancer cells and can be employed as anti-cancer drug delivery systems.

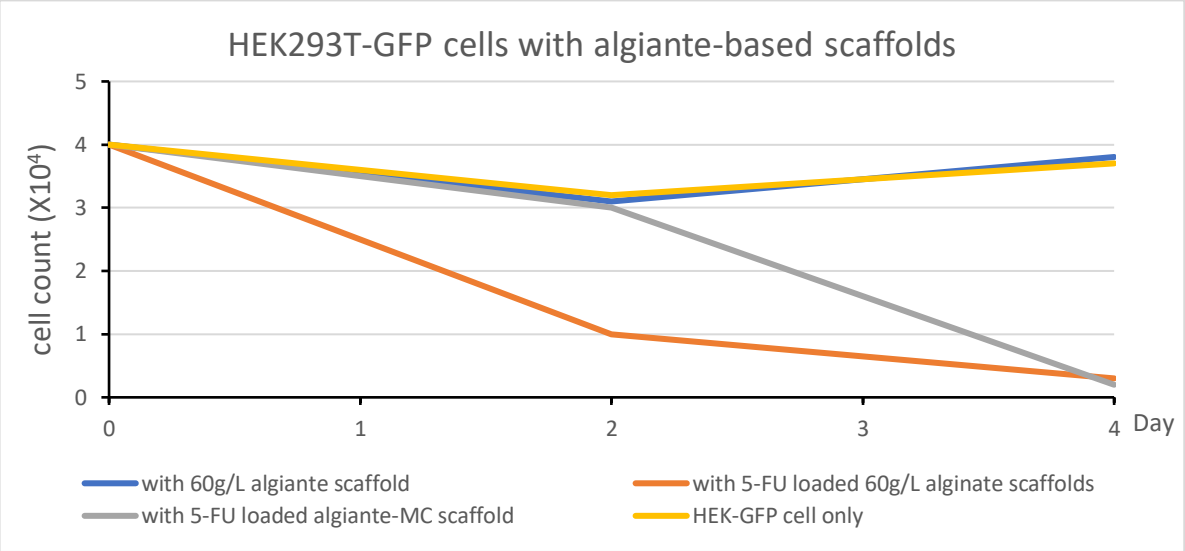

Figure 6.5 HEK293T-GFP cells count with alginate-based scaffolds.

6.3.3 1BR cell culture with CPC scaffolds

6.3.3.1 Microscopy studies

The behaviour differences of 1BR cells under microscopy are illustrated in Figure 6.6. 1BR cells attach with the edge of all CPC scaffolds after seeding for 21 days. The 2D size S scaffold illustrates a similar result as the cell well without any scaffold and drug, which indicates it is causing no apparent effect on cell behaviour. The figure shows that 3D scaffolds, both size L and S, attached less cells on the edge compared to 2D scaffolds. This may be due to that a part of 1BR cells grow into the porous structure of 3D scaffolds instead, while 2D scaffold has no porous structure.

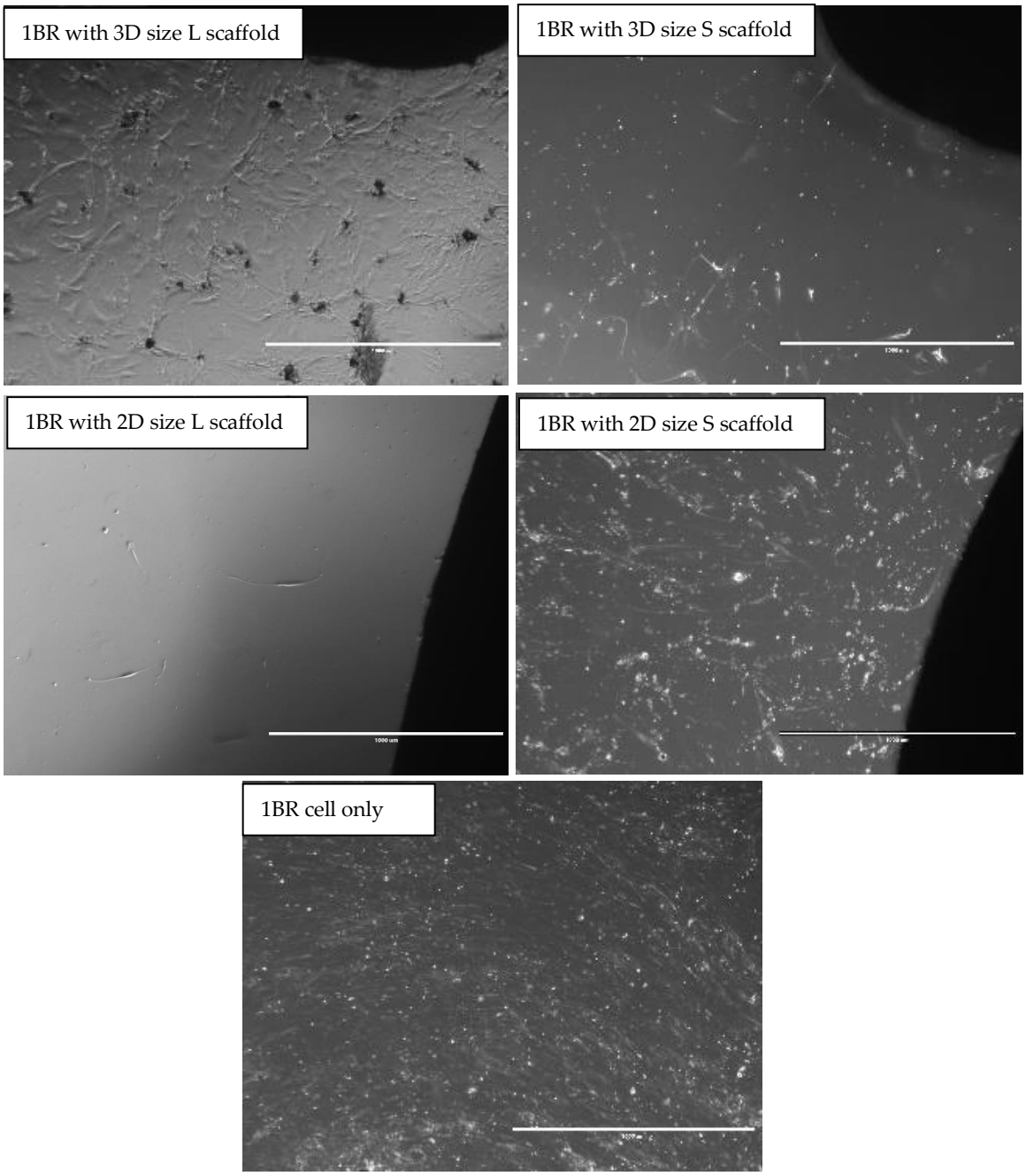

Figure 6.6 Microscopy analysis of 1BR cells with CPC 2D and 3D scaffolds on day 21.

6.3.3.2 Cell counting analysis

Figure 6.7 shows the total 1BR cell count over 28 days cultured with different CPC scaffolds. Only 2D size S scaffold has no effect on the growing speed of 1BR cells, the other three scaffolds all cause a decrease in the total cell number

during the first 10 days after seeding. Surprisingly, 1BR cells count went up at high speed between day 10 and day 21 when cultured with a 3D size S scaffold. The number of cells even went slightly higher than the cell-only group on day 21 (Figure 6.7). However, the 2D and 3D size L scaffolds were both caused a huge decrease in 1BR cell count, which may because the large size of the scaffold took up too much space in the cell culture well and inhibited the growth of cells. In conclusion, 3D size S CPC scaffolds are the most suitable size and structure for 1BR (as a sample primary cell line) to grow with for tissue regeneration over a long period of time.

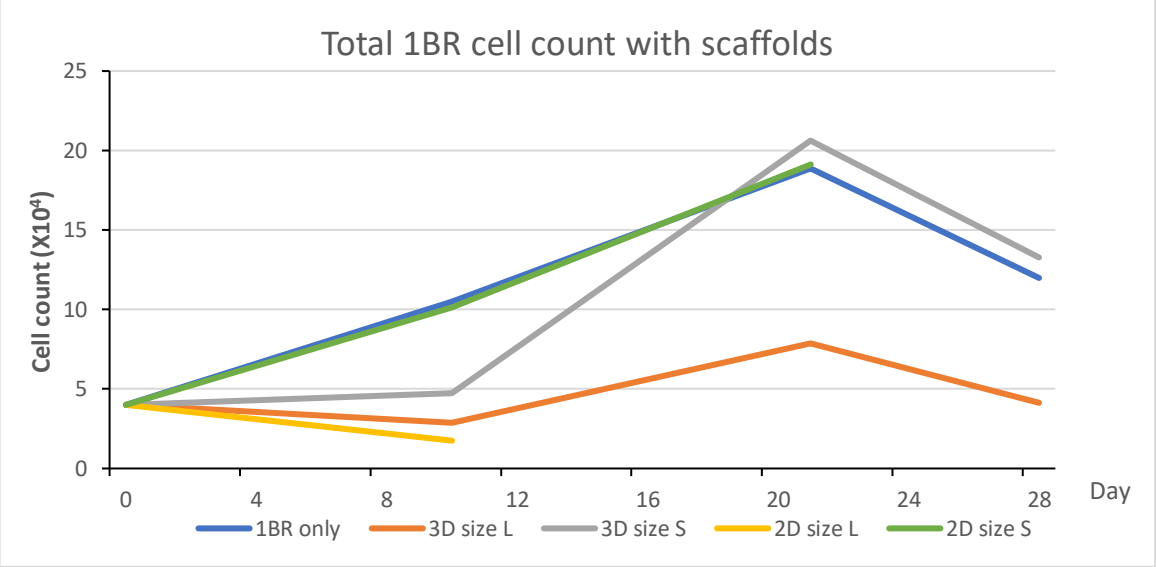

Figure 6.7. The effect of different scaffolds on 1BR cells' total cell count over 28 days.

In addition, the percentages of cells grown on the scaffolds were calculated and shown in Figure 6.8. 3D size L scaffold indicated the highest number of 1BR cells on day 21 while the 3D size S scaffold was the second highest one. This is due to the large surface area that the size L has and also 3D scaffolds turned out to

be more preferable for 1BR to grow compared to 2D structure ones. 2D size S scaffold showed the lowest percentage of cell attachment on day 10 and interestingly the cell attachment percentage stayed relatively the same on day 21. While around 42% of cells grow on the 2D size L scaffold on day 10, which could be an indication of another optimistic outcome as well.

Considering the data presented in Figure 6.7 and Figure 6.8 showed that the 3D size S scaffold indicated the highest total cell number as well as the highest percentage of cell attachment. It indicates that 3D size S is the most suitable and cell-preferable size and structure for 1BR, the sample primary cell line. It will give better and more promising results in primary cell culture for tissue regeneration.

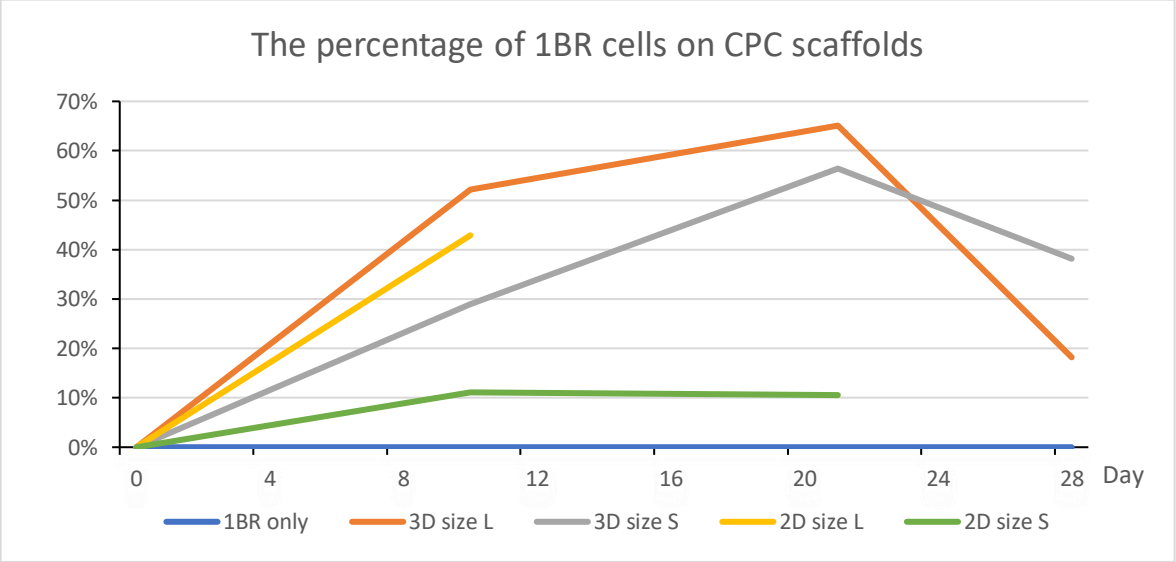

Figure 6.8. The percentage of 1BR cells grown on scaffolds at various days.

6.4 Conclusion

Cell behaviour with and without scaffolds was investigated in this study. Different growing behaviour was compared between primary cell line 1BR and cancer cell lines, HEK-GFP and U2OS-GFP. Also, the 5-FU loaded alginate-based scaffolds have affected cell behaviour quantitatively and qualitatively depending on the formulations of scaffolds. The results concluded that the size and structure of the CPC are two main factors that impacted the behaviour of 1BR cells during 28 days of culture. 3D scaffolds are preferable by 1BR cells compared to 2D ones to grow on due to their porous structure. In other words, this study provides a reference for future cell culture for tissue regeneration in terms of the choice of scaffold materials, size and structure for better drug delivery and tissue regenerating outcomes.

Chapter 7 General Conclusion and future work

7.1 General conclusion

Cancer, such as breast cancer, lung cancer and bone cancer, is a common disease worldwide, but its treatment is very challenging. The commonly used anti-cancer treatment methods in the UK include surgery, chemotherapy, radiotherapy, stem cell and bone marrow transplants and using targeted cancer drugs [141]. Forty-five percent of patients choose to remove the tumour as a part of the primary cancer treatment by surgery[142]. However, the survival rate of cancer patients for 10 or more years is only 50% in England and Wales[143]. The recurrence of cancer after cancer tissue removal surgery is still one of the biggest challenges for patients. In addition, the effectiveness of anti-cancer drugs and their serious side effects limited the safe usage of anti-cancer drugs. Thus, overcoming these two issues (lack of effectiveness and side effects) is essential in advanced anti-cancer treatment. 3D bioprinting using suitable bio-inks not only can create novel drug delivery, but also can fill in the wound gap after tissue removing surgery for every individual patient. However, the current level of bioprinting technology is not advanced enough to achieve this high-demand goal. Lacking suitable bio-ink and *in vitro* data for verifying the efficiency of the treatment are the major and urgent research gaps nowadays for the usage of 3D bioprinting in creating drug delivery systems and tissue regeneration. At the same time, it is always demanding to deliver anti-cancer drugs effectively using a novel drug delivery system and reduce the possible side effects. Upgrading 3D bioprinting and applying it for fabricating novel anti-cancer drug delivery systems is promising to fill the research gap.

This project covers the research on three areas of the applications of 3D bioprinting for the pharmaceutical industry and bioengineering: the creation and analysis of novel bio-inks, the bio-printing and analysis of scaffolds, and the *in vitro* cell culture study with scaffolds. Those three aspects of 3D bio-printing are essential for the development of new bio-printed scaffolds for advanced drug delivery and tissue regeneration. The novel 3D printed bio-scaffolds have excellent anti-cancer drug release properties as a promising new drug delivery system. At the same time, *in vitro* cell culture studies show satisfactory results in cancer cell killing rate.

Chapter 2 looks into the physical-chemical properties of pure alginate bio-inks which have a concentration between 10g/L to 40g/L. The viscosity, dipping and syringability of 7 alginate bio-inks were analyzed and compared in pH=1.2, 6.6 and 7.2. The relationship between the concentration of alginate and viscosity in different pH environments was explored, which is $V=0.0019C^{4.9061}$ at pH=1.2, $V=73.097e^{0.1788C}$ at pH=6.6 and $V=0.4059C^{2.7997}$ at pH=7.2. The properties of alginate bio-inks become predictable using the mathematical model in three pH environments. It provided useful insight for the future development of alginate or alginate-based bio-inks.

In chapter 3, an attempt was made to prepare 9 bio-inks formulations containing alginate, methylcellulose (MC) and nano-clay, followed by physicochemical properties analysis such as viscosity, dipping and syringability. Bio-ink formulations (alginate: MC 1:1 and alginate: MC 2:1) were chose to be loaded

with 1%, 2%, 5%, 10% v/v 5-FU solutions and to be printed as 3D bio-scaffolds in the same shape designed by computer. The printing outcome proved that controlling the volume of 5-FU solution under 10% can make sure the fidelity of 3D scaffolds. Also, cell culture study was conducted with those 5-FU loaded alginate-based scaffolds. Positive anti-cancer cell culture results illustrated that 3D scaffolds printed with alginate-based bio-inks are suitable and can be potentially used as a novel delivery systems for anticancer drugs such as 5-FU.

Chapters 2 and 3 focus on the exploration of the physicochemical properties of bio-inks to give insight for the development of bio-inks for 3D bioprinting in general, which makes the selection of formulation more effectively and accelerate the pre-printing process for future 3D bio-printing.

Chapter 4 aimed to bio-print novel scaffolds for the application of endothelial cell repair. Various compositions of polylactic acid (PLA), polyethylene glycol (PEG) and pluronic F127 formulations were prepared and optimized to create biodegradable and biocompatible bio-inks. In this study model drugs (erythropoietin (EPO) or dimethyloxalylglycine (DMOG)) with a concentration of 30% w/w was loaded into formulations before the 3D porous bio-scaffolds were fabricated by the bio-printer. The results from the bioassay showed that DMOG was released sustainedly and led to the increase of HIF-1α levels throughout 48 days. a HIF-1α target gene (VEGF) was transcriptionally activated after culturing scaffolds with rat aortic endothelial cells (RAECs) for 2 h. This research provided an insight into polymer-based biodegradable scaffolds that can potentially be used for clinical applications, such as endothelial cell repair.

Chapter 5 explored the properties of anti-cancer drug-coated 3D CPC scaffolds as a novel drug delivery system. Scaffolds were coated with three different 5-FU solutions and the properties, such as surface uniformity and texture were analyzed and compared. The test results illustrated that all solutions with 5-FU were successfully coated on the whole surface of the scaffolds homogeneousl. and the coating process had not caused any significant effects on the texture of 3D CPC scaffolds ($p>0.05$). What's more, dissolution test and cell culture studies using two different cell lines (Hek293T and HeLa) were conducted to compare the drug release profile and anti-cancer functions of three coated scaffolds *in vitro*. It turned out that the drug release pattern followed first-order release kinetics and CPC scaffold coated with formulation 3 (5-FU, Soluplus and PEG 6000) has the better inhibition abilities in terms of reduction in the growth of cells within 4 days.

Chapters 4 and 5 give insights into studying the therapeutic effect of novel 3D bio-printed scaffolds. The efficient drug release profile and positive *in vitro* cell culture result from chapters 4 and 5 proved that 3D bio-printed polymer-based and CPC scaffolds are both promising for cell repair and anti-cancer treatment as novel drug delivery systems.

Chapter 6 explored how cell behaviour changes when cancer cells were cultured with different alginate bio-scaffolds and CPC scaffolds. Primary cell line 1BR and cancer cell lines, HEK-GFP and U2OS-GFP were used as model cell lines for comparing cell viability and their attaching behaviour. In addition, 1BR cells were cultured with 4 kinds of CPC scaffolds for 28 days to analyze the effect of post-

printing environment on the healthy cell behaviour both qualitatively and quantitatively and indicated that CPC scaffolds in 3D size S are the most suitable and cell-preferable for 1BR. The quantitative research illustrated that the size and the structure of CPC scaffolds were two important factors affecting the behaviour of model cells. The study provided information on the changing process of model cell behaviour during 28 days in terms of the total cell counts and the percentage of cells growing on/off scaffolds, which can be a valuable reference for future tissue regeneration in the long term.

7.2 Future work

Although 3D bio-printing has unimaginable potential, it is still a young technology[144]. There are still some further studies which are worthy to be carried out in the future in this area.

First, more bio-ink formulations need to be tested and analyzed with different anticancer drugs with different solubilities. Due to the limitation of time and experimental equipment, bio-ink formulations can only be tested and analyzed in certain parameters using certain tools. There are still more aspects of the physical-chemical properties yet to be explored, such as the rheology and thermal properties in detail. The more properties we know about the bio-inks, the more flexibly we can handle and adjust their behaviour during and after the 3D bioprinting process.

Second, there are still more novel applications of 3D bio-printing in drug delivery systems and tissue regeneration waiting to be created, such as new control-

released DDS and printing different tissue of the human body even organs. The future application of 3D bio-printing in those two areas is unlimited.

Last but not the least, the author believes that applying data science tools in analysis and predicting the properties of different bio-ink formulations will be a new and promising method in the creation of novel bio-inks. Though the analysis and predicting model will need to be upgraded and trained constantly with more and more known bio-ink properties in the future to make it increasingly accurate. The model or algorithm can provide guidance and save plenty of time for the process of bio-ink seeking and formulation creation, which will be more efficient for 3D bioprinting as well to get better and more controllable final printing results. What's more, machine learning can also help with choosing suitable cells for printing and predicting the cell behaviour within the different bio-printing environments. In a word, combining data science/machine learning and 3D bio-printing can be a new promising research area for future DDS and tissue regeneration development.

References

1. R.J. Klebe, Cytoscribing: a method for micropositioning cells and the construction of two-and three-dimensional synthetic tissues. Exp Cell Res, 179 (2) (1988), pp. 362-373

2. Lepowsky, Eric, and Savas Tasoglu. "3D printing for drug manufacturing: A perspective on the future of pharmaceuticals." International Journal of Bioprinting 4, no. 1 (2018).

3. Murphy, Sean V., and Anthony Atala. "3D bioprinting of tissues and organs." Nature biotechnology 32, no. 8 (2014): 773-785.

4. Moroni, Lorenzo, Thomas Boland, Jason A. Burdick, Carmelo De Maria, Brian Derby, Gabor Forgacs, Jürgen Groll et al. "Biofabrication: a guide to technology and terminology." Trends in biotechnology 36, no. 4 (2018): 384-402.

5. Gu, Zeming, Jianzhong Fu, Hui Lin, and Yong He. "Development of 3D bioprinting: From printing methods to biomedical applications." Asian Journal of Pharmaceutical Sciences 15, no. 5 (2020): 529-557.

6. Kačarević, Željka P., Patrick M. Rider, Said Alkildani, Sujith Retnasingh, Ralf Smeets, Ole Jung, Zrinka Ivanišević, and Mike Barbeck. "An introduction to 3D bioprinting: possibilities, challenges and future aspects." Materials 11, no. 11 (2018): 2199.

7. Park, Jae H., Isabelle Rivière, Mithat Gonen, Xiuyan Wang, Brigitte Sénéchal, Kevin J. Curran, Craig Sauter et al. "Long-term follow-up of

CD19 CAR therapy in acute lymphoblastic leukemia." New England Journal of Medicine 378, no. 5 (2018): 449-459.

8. Ma, Jennifer, Matea Pender, and Meredith Welch. "Education Pays 2016: The Benefits of Higher Education for Individuals and Society. Trends in Higher Education Series." College Board (2016).

9. Matsusaki, Michiya, Kayo Sakaue, Koji Kadowaki, and Mitsuru Akashi. "Three-dimensional human tissue chips fabricated by rapid and automatic inkjet cell printing." Advanced healthcare materials 2, no. 4 (2013): 534-539.

10. Kang, Hyun-Wook, Sang Jin Lee, In Kap Ko, Carlos Kengla, James J. Yoo, and Anthony Atala. "A 3D bioprinting system to produce human-scale tissue constructs with structural integrity." Nature biotechnology 34, no. 3 (2016): 312-319.

11. Choi, Tsan-Ming, Chun-Hung Chiu, and Hing-Kai Chan. "Risk management of logistics systems." Transportation Research Part E: Logistics and Transportation Review 90 (2016): 1-6.

12. Kim, Hyun, Jong-Hyeok Lee, and Seung-Hoon Na. "Predictor-estimator using multilevel task learning with stack propagation for neural quality estimation." In Proceedings of the Second Conference on Machine Translation, pp. 562-568. 2017.

13. Xiao, Ying, Seon Hwa Lee, and Yang-Kook Sun. "The application of metal sulfides in sodium ion batteries." Advanced energy materials 7, no. 3 (2017): 1601329.

14. Ashammakhi, Nureddin, Samad Ahadian, Fan Zengjie, Kasinan Suthiwanich, Farnaz Lorestani, Gorka Orive, Serge Ostrovidov, and Ali Khademhosseini. "Advances and future perspectives in 4D bioprinting." Biotechnology journal 13, no. 12 (2018): 1800148.

15. Grand View Research, “3D Bioprinting Market Size, Share & Trends Analysis Report By Technology (Magnetic Levitation, Inkjet-based), By Application (Medical, Dental, Biosensors, Bioinks), By Region, And Segment Forecasts, 2021 - 2028”, Jan, 2021, https://www.grandviewresearch.com/industry-analysis/3d-bioprinting-market.

16. Yang, Xingchen, Zhenhui Lu, Huayu Wu, Wei Li, Li Zheng, and Jinmin Zhao. "Collagen-alginate as bioink for three-dimensional (3D) cell printing based cartilage tissue engineering." Materials Science and Engineering: C 83 (2018): 195-201.

17. Hölzl, Katja, Shengmao Lin, Liesbeth Tytgat, Sandra Van Vlierberghe, Linxia Gu, and Aleksandr Ovsianikov. "Bioink properties before, during and after 3D bioprinting." Biofabrication 8, no. 3 (2016): 032002.

18. Murdock, Mark H., and Stephen F. Badylak. "Biomaterials-based in situ tissue engineering." Current opinion in biomedical engineering 1 (2017): 4.

19. Zhang, Yi, Dezhi Zhou, Jianwei Chen, Xiuxiu Zhang, Xinda Li, Wenxiang Zhao, and Tao Xu. "Biomaterials based on marine resources for 3D bioprinting applications." Marine drugs 17, no. 10 (2019): 555.

20. Gupta, Deepak, Arnav Julka, Sanchit Jain, Tushar Aggarwal, Ashish Khanna, N. Arunkumar, and Victor Hugo C. de Albuquerque. "Optimized

cuttlefish algorithm for diagnosis of Parkinson's disease." Cognitive systems research 52 (2018): 36-48.

21. Alginic acid, sodium salt, Pubchem, URL: https://pubchem.ncbi.nlm.nih.gov/compound/45357541

22. Ahlfeld, Tilman, Falko Doberenz, David Kilian, Corina Vater, Paula Korn, Günter Lauer, Anja Lode, and Michael Gelinsky. "Bioprinting of mineralized constructs utilizing multichannel plotting of a self-setting calcium phosphate cement and a cell-laden bioink." Biofabrication 10, no. 4 (2018): 045002.

23. Lode, Anja, Katrin Meissner, Yongxiang Luo, Frank Sonntag, Stefan Glorius, Berthold Nies, Corina Vater, Florian Despang, Thomas Hanke, and Michael Gelinsky. "Fabrication of porous scaffolds by three - dimensional plotting of a pasty calcium phosphate bone cement under mild conditions." Journal of tissue engineering and regenerative medicine 8, no. 9 (2014): 682-693.

24. Tasoglu, Savas, and Utkan Demirci. "Bioprinting for stem cell research." Trends in biotechnology 31, no. 1 (2013): 10-19.

25. Gudapati, Hemanth, Madhuri Dey, and Ibrahim Ozbolat. "A comprehensive review on droplet-based bioprinting: Past, present and future." Biomaterials 102 (2016): 20-42.

26. Calvert, Paul D., Skander Limem, Soumya Iyengar, and Prabir K. Patra. "Inkjet printing of insoluble biopolymer and polymer complexes." (2007).

27. Knowlton, Stephanie, Shivesh Anand, Twisha Shah, and Savas Tasoglu. "Bioprinting for neural tissue engineering." Trends in neurosciences 41, no. 1 (2018): 31-46.

28. Zeng, Xiangbin, Zijie Meng, Jiankang He, Mao Mao, Xiao Li, Pengyu Chen, Jinhai Fan, and Dichen Li. "Embedded bioprinting for designer 3D tissue constructs with complex structural organization." Acta biomaterialia (2021).

29. Rider, Patrick, Željka Perić Kačarević, Said Alkildani, Sujith Retnasingh, and Mike Barbeck. "Bioprinting of tissue engineering scaffolds." Journal of tissue engineering 9 (2018).

30. Hölzl, Katja, Shengmao Lin, Liesbeth Tytgat, Sandra Van Vlierberghe, Linxia Gu, and Aleksandr Ovsianikov. "Bioink properties before, during and after 3D bioprinting." Biofabrication 8, no. 3 (2016): 032002.

31. Wang, Wei, Rita Vignani, Monica Scali, and Mauro Cresti. "A universal and rapid protocol for protein extraction from recalcitrant plant tissues for proteomic analysis." Electrophoresis 27, no. 13 (2006): 2782-2786.

32. Martin, Ivan, David Wendt, and Michael Heberer. "The role of bioreactors in tissue engineering." TRENDS in Biotechnology 22, no. 2 (2004): 80-86.

33. Schubert, Thomas, Sébastien Lafont, Gwen Beaurin, Guillaume Grisay, Catherine Behets, Pierre Gianello, and Denis Dufrane. "Critical size bone defect reconstruction by an autologous 3D osteogenic-like tissue derived from differentiated adipose MSCs." Biomaterials 34, no. 18 (2013): 4428-4438.

34. Ahlfeld, Tilman, Falko Doberenz, David Kilian, Corina Vater, Paula Korn, Günter Lauer, Anja Lode, and Michael Gelinsky. "Bioprinting of mineralized constructs utilizing multichannel plotting of a self-setting calcium phosphate cement and a cell-laden bioink." Biofabrication 10, no. 4 (2018): 045002.

35. Sachlos, Eu, and J. T. Czernuszka. "Making tissue engineering scaffolds work. Review: the application of solid freeform fabrication technology to the production of tissue engineering scaffolds." Eur Cell Mater 5, no. 29 (2003): 39-40.

36. Cheah, C. M., C. K. Chua, K. F. Leong, and S. W. Chua. "Development of a tissue engineering scaffold structure library for rapid prototyping. Part 1: investigation and classification." The International Journal of Advanced Manufacturing Technology 21, no. 4 (2003): 291-301.

37. Lee, Mi-Jeong, Yuanyuan Wu, and Susan K. Fried. "Adipose tissue remodeling in pathophysiology of obesity." Current opinion in clinical nutrition and metabolic care 13, no. 4 (2010): 371.

38. Jang, Jinah, Hee-Gyeong Yi, and Dong-Woo Cho. "3D printed tissue models: present and future." ACS Biomaterials Science & Engineering 2, no. 10 (2016): 1722-1731.

39. Yanagawa, Fumiki, Shinji Sugiura, and Toshiyuki Kanamori. "Hydrogel microfabrication technology toward three dimensional tissue engineering." Regenerative Therapy 3 (2016): 45-57.

40. Osaki, Tatsuya, Vivek Sivathanu, and Roger D. Kamm. "Vascularized microfluidic organ-chips for drug screening, disease models and tissue engineering." Current opinion in biotechnology 52 (2018): 116-123.

41. Rafii, Shahin, Jason M. Butler, and Bi-Sen Ding. "Angiocrine functions of organ-specific endothelial cells." Nature 529, no. 7586 (2016): 316-325.

42. Turnbull, Gareth, Jon Clarke, Frédéric Picard, Philip Riches, Luanluan Jia, Fengxuan Han, Bin Li, and Wenmiao Shu. "3D bioactive composite scaffolds for bone tissue engineering." Bioactive materials 3, no. 3 (2018): 278-314.

43. Vermeulen, Niki, Gill Haddow, Tirion Seymour, Alan Faulkner-Jones, and Wenmiao Shu. "3D bioprint me: a socioethical view of bioprinting human organs and tissues." Journal of Medical Ethics 43, no. 9 (2017): 618-624.

44. Li, Xiaoming, Rongrong Cui, Lianwen Sun, Katerina E. Aifantis, Yubo Fan, Qingling Feng, Fuzhai Cui, and Fumio Watari. "3D-printed biopolymers for tissue engineering application." International Journal of Polymer Science 2014 (2014).

45. Wang, Li-Shan, Joo Eun Chung, Peggy Pui-Yik Chan, and Motoichi Kurisawa. "Injectable biodegradable hydrogels with tunable mechanical properties for the stimulation of neurogenesic differentiation of human mesenchymal stem cells in 3D culture." Biomaterials 31, no. 6 (2010): 1148-1157.

46. Lee, Kuen Yong, and David J. Mooney. "Alginate: properties and biomedical applications." Progress in polymer science 37, no. 1 (2012): 106-126.

47. Ashammakhi, Nureddin, Samad Ahadian, Chun Xu, Hossein Montazerian, Hyojin Ko, Rohollah Nasiri, Natan Barros, and Ali Khademhosseini. "Bioinks and bioprinting technologies to make heterogeneous and biomimetic tissue constructs." Materials Today Bio 1 (2019): 100008.

48. Symon, Keith R. Mechanics (3rd ed.). Addison-Wesley. Boston, USA, 1971.

49. Abasalizadeh, Farhad, Sevil Vaghefi Moghaddam, Effat Alizadeh, Elmira Kashani, Seyyed Mohammad Bagher Fazljou, Mohammadali Torbati, and Abolfazl Akbarzadeh. "Alginate-based hydrogels as drug delivery vehicles in cancer treatment and their applications in wound dressing and 3D bioprinting." Journal of biological engineering 14, no. 1 (2020): 1-22.

50. EO Lab, “KM0051 – Phosphate Buffered Saline (PBS)”. (2018).UAL: https://www.eolabs.com/product/km0051-phosphate-buffered-saline/

51. Garth, Andrew. “Analysing data using SPSS” (2008). UAL: https://students.shu.ac.uk/lits/it/documents/pdf/analysing_data_using_spss.pdf

52. Tasoglu, Savas, and Utkan Demirci. "Bioprinting for stem cell research." Trends in biotechnology 31, no. 1 (2013): 10-19.

53. Lepowsky, Eric, Metin Muradoglu, and Savas Tasoglu. "Towards preserving post-printing cell viability and improving the resolution: Past, present, and future of 3D bioprinting theory." Bioprinting 11 (2018): e00034.

54. Kačarević, Željka P., Patrick M. Rider, Said Alkildani, Sujith Retnasingh, Ralf Smeets, Ole Jung, Zrinka Ivanišević, and Mike Barbeck. "An

introduction to 3D bioprinting: possibilities, challenges and future aspects." Materials 11, no. 11 (2018): 2199.

55. Park, Ju Young, Jinah Jang, and Hyun-Wook Kang. "3D Bioprinting and its application to organ-on-a-chip." Microelectronic Engineering 200 (2018): 1-11.

56. Ma, Xuanyi, Xin Qu, Wei Zhu, Yi-Shuan Li, Suli Yuan, Hong Zhang, Justin Liu et al. "Deterministically patterned biomimetic human iPSC-derived hepatic model via rapid 3D bioprinting." Proceedings of the National Academy of Sciences 113, no. 8 (2016): 2206-2211.

57. Matsusaki, Michiya, Kayo Sakaue, Koji Kadowaki, and Mitsuru Akashi. "Three‐dimensional human tissue chips fabricated by rapid and automatic inkjet cell printing." Advanced healthcare materials 2, no. 4 (2013): 534-539.

58. Kang, H.W., Lee, S.J., Ko, I.K., Kengla, C., Yoo, J.J. and Atala, A., 2016. A 3D bioprinting system to produce human-scale tissue constructs with structural integrity. Nature biotechnology, 34(3), p.312.

59. Choi, Yeong‐Jin, Taek Gyoung Kim, Jonghyeon Jeong, Hee‐Gyeong Yi, Ji Won Park, Woonbong Hwang, and Dong‐Woo Cho. "3D cell printing of functional skeletal muscle constructs using skeletal muscle‐derived bioink." Advanced healthcare materials 5, no. 20 (2016): 2636-2645.

60. Kim, Byoung Soo, Jung-Seob Lee, Ge Gao, and Dong-Woo Cho. "Direct 3D cell-printing of human skin with functional transwell system." Biofabrication 9, no. 2 (2017): 025034.

61. Mandić, M., T. Galeta, P. Raos, and V. Jugović. "Dimensional accuracy of camera casing models 3D printed on Mcor IRIS: A case study." Advances in Production Engineering & Management 11, no. 4 (2016).

62. Li, Huijun, Yu Jun Tan, Kah Fai Leong, and Lin Li. "3D bioprinting of highly thixotropic alginate/methylcellulose hydrogel with strong interface bonding." ACS applied materials & interfaces 9, no. 23 (2017): 20086-20097.

63. Fedorovich, Natalja E., Wouter Schuurman, Hans M. Wijnberg, Henk-Jan Prins, P. René Van Weeren, Jos Malda, Jacqueline Alblas, and Wouter JA Dhert. "Biofabrication of osteochondral tissue equivalents by printing topologically defined, cell-laden hydrogel scaffolds." Tissue Engineering Part C: Methods 18, no. 1 (2012): 33-44.

64. KGaA, Merck. "Darmstadt, Germany and/or its affiliates." Recuperat de https://www. sigmaaldrich. com/catalog/product/sial/77036 (2019).

65. Maniruzzaman, M. 3D and 4D Printing Technology in Biomedical Applications: Process Engineering and Additive Manufacturing; Wiley and Sons: Chichester, West Sussex, UK, 2019; ISBN 978-3-527-34443-7.

66. Khong, T.D.; Maniruzzaman, M.; Nokhodchi, A. Advanced pharmaceutical applications of Hot-Melt Extrusion coupled with Fused Deposition Modelling (FDM) 3D printing for personalised drug delivery. Pharmaceutics 2018, 10, 1–23.

67. Ahmed, J.; Mulla, M.; Maniruzzaman, M. Rheological and Dielectric Behavior of 3D-Printable Chitosan/Graphene Oxide Hydrogels. ACS Biomater. Sci. Eng. 2019.

68. Shieh, S.J.; Terada, S.; Vacanti, J.P. Tissue engineering auricular reconstruction: In vitro and in vivo studies. Biomaterials 2004, 25, 545–1557.

69. Zhou, L.; Pomerantseva, I.; Bassett, E.K.; Bowley, C.M.; Zhao, X.; Bichara, D.A.; Kulig, K.M.; Vacanti, J.P.; Randolph, M.A.; Sundback, C.A. Engineering ear constructs with a composite scaffold to maintain dimensions. Tissue Eng. Part A 2011, 17, 1573–1581.

70. Boland, T.; Mironov, V.; Gutowska, A.; Roth, E.A.; Markwald, R.R. Cell and organ printing 2: Fusion of cell aggregates in three-dimensional gels. Anat. Rec. Part A Discov. Mol. Cell. Evol. Biol. 2003, 272, 497–502.

71. Mironov, V.; Boland, T.; Trusk, T.; Forgacs, G.; Markwald, R.R. Organ printing: Computer-aided jet-based 3D tissue engineering. Trends Biotechnol. 2003, 21, 157–161.

72. Ilkhanizadeh, S.; Teixeira, A.I.; Hermanson, O. Inkjet printing of macromolecules on hydrogels to steer neural stem cell differentiation. Biomaterials 2007, 28, 3936–3943.

73. Lee, Y.B.; Polio, S.; Lee, W.; Dai, G.; Menon, L.; Carroll, R.S.; Yoo, S.S. Bio-printing of collagen and VEGF-releasing fibrin gel scaffolds for neural stem cell culture. Exp. Neurol. 2010, 223, 645–652.

74. Amit, P.; Tan, L.P. Current status of bioinks for micro-extrusion-based 3D bioprinting. Molecules 2016, 21, 685.

75. Hospodiuk, M.; Dey, M.; Sosnoski, D.; Ozbolat, I. The bioink: A comprehensive review on bioprintable materials. Biotechnol. Adv. 2017, 35, 217–239.

76. Collino, M.; Thiemermann, C.; Cerami, A.; Brines, M. Flipping the molecular switch for innate protection and repair of tissues: Long-lasting effects of a non-erythropoietic small peptide engineered from erythropoietin. Pharmacol. Ther. 2015, 151, 32–40.

77. Brines, M.; Anthony, C. The receptor that tames the innate immune response. Mol. Med. 2012, 18, 486–496.

78. Dragun, D. The detection of antibodies to the Angiotensin II-type 1 receptor in transplantation. Methods Mol. Biol. 2013, 1034, 331–333

79. Ghezzi, P.; Brines, M. Erythropoietin as an antiapoptotic, tissue-protective cytokine. Cell Death Differ. 2004, 11, 37.

80. Leist, M.; Ghezzi, P.; Grasso, G.; Bianchi, R.; Villa, P.; Fratelli, M.; Savino, S.; Bianchi, M.; Nielsen, J.; Gerwien, J.; et al. Derivatives of erythropoietin that are tissue protective but not erythropoietic. Science 2004, 305, 239–242.

81. Heikal, L.; Ghezzi, P.; Mengozzi, M.; Stelmaszczuk, B.; Feelisch, M.; Ferns, G.A. Erythropoietin and a nonerythropoietic peptide analog promote aortic endothelial cell repair under hypoxic conditions: Role of nitric oxide. Hypoxia 2016, 4, 121.

82. Heikal, L.; Ghezzi, P.; Mengozzi, M.; Ferns, G.A. Low Oxygen Tension Primes Aortic Endothelial Cells to the Reparative Effect of Tissue-Protective Cytokines. Mol. Med. 2015, 21, 709–716.

83. Paul, A.; Elias, C.B.; Shum-Tim, D.; Prakash, S. Bioactive baculovirus nanohybrids for stent based rapid vascular re-endothelialization. Sci. Rep. 2013, 3, 2366.

84. Shand, J.A.; Kodoth, V.; Menown, I.B. Novel stent and drug elution technologies. Interv. Cardiol. 2011, 3, 473–481.

85. Müller, M.; Becher, J.; Schnabelrauch, M.; Zenobi-Wong, M. Nanostructured Pluronic hydrogels as bioinks for 3D bioprinting. Biofabrication 2015, 7, 035006.

86. Mengozzi, M.; Cervellini, I.; Villa, P.; Erbayraktar, Z.; Gökmen, N.; Yilmaz, O.; Erbayraktar, S.; Manohasandra, M.; Van Hummelen, P.; Vandenabeele, P.; et al. Erythropoietin-induced changes in brain gene expression reveal induction of synaptic plasticity genes in experimental stroke. Proc. Natl. Acad. Sci. USA 2013, 109, 9617–9622.

87. Cervellini, I.; Annenkov, A.; Brenton, T.; Chernajovsky, Y.; Ghezzi, P.; Mengozzi, M. Erythropoietin (EPO) increases myelin gene expression in CG4 oligodendrocyte cell through the classical EPO receptor. Mol. Med. 2013, 19, 223–229.

88. Heikal, L.; Ghezzi, P.; Mengozzi, M.; Ferns, G. Assessment of HIF-1α expression and release following endothelial injury in-vitro and in-vivo. Mol. Med. 2018, 24, 22.

89. Lepowsky, E.; Muradoglu, M.; Tasoglu, S. Towards preserving post-printing cell viability and improving the resolution: Past, present, and future of 3D bioprinting theory. Bioprinting 2018, 11,

90. Eeckman F, Amighi K, Moës AJ. Effect of some physiological and non-physiological compounds on the phase transition temperature of thermoresponsive polymers intended for oral controlled-drug delivery. International Journal of Pharmaceutics. 2001 Jul 17;222(2):259-70.

91. Webinar Fundamentals of DSC Analysis, URL: https://www.mt.com/gb/en/home/library/on-demand-webinars/lab-analytical-instruments/DSC_TA.html

92. Kapourani A, Palamidi A, Kontogiannopoulos KN, Bikiaris ND, Barmpalexis P. Drug Amorphous Solid Dispersions Based on Poly (vinyl Alcohol): Evaluating the Effect of Poly (propylene Succinate) as Plasticizer. Polymers. 2021 Aug 30;13(17):2922.

93. Murphy, S.V.; Atala, A. 3D bioprinting of tissues and organs. Nat. Biotechnol. 2014, 32, 773–785.

94. Moroni, L.; Boland, T.; Burdick, J.A.; De Maria, C.; Derby, B.; Forgacs, G.; Groll, J.; Li, Q.; Malda, J.; Mironov, V.A.; et al. Biofabrication: A Guide to Technology and Terminology. Trends Biotechnol. 2018, 36, 384–402.

95. Park, J.Y.; Jang, J.; Kang, H.-W. 3D Bioprinting and its application to organ-on-a-chip. Microelectron. Eng. 2018, 200, 1–11.

96. Kang, H.-W.; Lee, S.J.; Ko, I.K.; Kengla, C.; Yoo, J.J.; Atala, A. A 3D bioprinting system to produce human-scale tissue constructs with structural integrity. Nat. Biotechnol. 2016, 34, 312–319.

97. Choi, Y.-J.; Kim, T.G.; Jeong, J.; Yi, H.-G.; Park, J.W.; Hwang, W.; Cho, D.-W. 3D Cell Printing of Functional Skeletal Muscle Constructs Using Skeletal Muscle-Derived Bioink. Adv. Healthc. Mater. 2016, 5, 2636–2645.

98. Kim, B.S.; Lee, J.-S.; Gao, G.; Kim, Y.K. Direct 3D cell-printing of human skin with functional transwell system. Biofabrication 2017, 9, 025034.

99. Gudapati, H.; Dey, M.; Ozbolat, I.T. A comprehensive review on droplet-based bioprinting: Past, present and future. Biomaterials 2016, 102, 20–42.

100. Lepowsky, E.; Tasoglu, S. 3D Printing for Drug Manufacturing: A Perspective on the Future of Pharmaceuticals. Int. J. Bioprinting 2018, 4, 119.

101. Kenny, S.M.; Buggy, M. Bone cements and fillers: A review. J. Mater. Sci. Mater. Med. 2003, 14, 923–938.

102. Xu, H.H.; Wang, P.; Wang, L.; Bao, C.; Chen, Q.; Weir, M.D.; Chow, L.C.; Zhao, L.; Zhou, X.; Reynolds, M.A. Calcium phosphate cements for bone engineering and their biological properties. Bone Res. 2017, 5, 17056.

103. Kilian, D.; Ahlfeld, T.; Akkineni, A.R.; Bernhardt, A.; Gelinsky, M.; Lode, A. 3D Bioprinting of osteochondral tissue substitutes – in vitro-

chondrogenesis in multi-layered mineralized constructs. Sci. Rep. 2020, 10, 1–17.

104. Ahlfeld, T.; Cubo-Mateo, N.; Cometta, S.; Guduric, V.; Vater, C.; Bernhardt, A.; Akkineni, A.R.; Lode, A.; Gelinsky, M. A Novel Plasma-Based Bioink Stimulates Cell Proliferation and Differentiation in Bioprinted, Mineralized Constructs. ACS Appl. Mater. Interfaces 2020, 12, 12557–12572.

105. Trombetta, R.P.; Ninomiya, M.J.; El-Atawneh, I.M.; Knapp, E.K.; Bentley, K.L.D.M.; Dunman, P.M.; Schwarz, E.M.; Kates, S.L.; Awad, H. Calcium Phosphate Spacers for the Local Delivery of Sitafloxacin and Rifampin to Treat Orthopedic Infections: Efficacy and Proof of Concept in a Mouse Model of Single-Stage Revision of Device-Associated Osteomyelitis. Pharmaceutics 2019, 11, 94.

106. Diasio, R.B.; Harris, B.E. Clinical Pharmacology of 5-Fluorouracil. Clin. Pharmacokinet. 1989, 16, 215–237.

107. CAMEO Chemical Datasheet, Flurouracil. Available online: https://cameochemicals.noaa.gov/chemical/5005 (accessed on 19 October 2020).

108. BASF, The Chemical Company, Soluplus, Technical Information, 2010. Available online: http://www.rumapel.com.ar/pharma_excipientes/ficha_tecnica/Soluplus.pdf (Accessed on 10 November 2020).

109. BASF SE 2020. Soluplus—For Better Solubility and Bioavailability. Available online: https://pharmaceutical.basf.com/en/Drug-Formulation/Soluplus.html (accessed on 19 September 2020).

110. Kanmani, P.; Lim, S.T. Synthesis and characterization of pullulan-mediated silver nanoparticles and its antimicrobial activities. Carbohydr. Polym. 2013, 97, 421–428.

111. Maniruzzaman, M. 3D and 4D Printing in Biomedical Applications: Process Engineering and Additive Manufacturing; John Wiley & Sons: Hoboken, NJ, USA, 2019.

112. Malda, J.; Visser, J.; Melchels, F.P.; Jüngst, T.; Hennink, W.E.; Dhert, W.J.A.; Groll, J.; Hutmacher, D.W. 25th Anniversary Article: Engineering Hydrogels for Biofabrication. Adv. Mater. 2013, 25, 5011–5028.

113. Sakai, S.; Yoshii, A.; Sakurai, S.; Horii, K.; Nagasuna, O. Silk fibroin nanofibers: A promising ink additive for extrusion 3D bioprinting. Mater. Today Bio 2020, 8, 100078,.

114. Lee, J.; Hong, J.; Kim, W.; Kim, G.H. Bone-derived dECM/alginate bioink for fabricating a 3D cell-laden mesh structure for bone tissue engineering. Carbohydr. Polym. 2020, 250, 116914.

115. Wu, Y.; Heikal, L.; Ferns, G.; Ghezzi, P.; Nokhodchi, A.; Maniruzzaman, M. 3D Bioprinting of Novel Biocompatible Scaffolds for Endothelial Cell Repair. Polymers 2019, 11, 1924.

116. Pina, S.; Ribeiro, V.P.; Marques, C.F.; Maia, F.R.; Silva, T.H.; Reis, R.L.; Oliveira, J. Scaffolding Strategies for Tissue Engineering and Regenerative Medicine Applications. Materials 2019, 12, 1824.

117. Van Belleghem, S.; Torres, L.; Santoro, M.; Mahadik, B.; Wolfand, A.; Kofinas, P.; Fisher, J. Hybrid 3D Printing of Synthetic and Cell‐Laden Bioinks for Shape Retaining Soft Tissue Grafts. Adv. Funct. Mater. 2020, 30, 1907145.

118. Kistler, S.F.; Schweizer, P.M. Liquid Film Coating: Scientific Principles and Their Technological Implications; Chapman & Hall: New York, NY, USA, 1997; pp. 401–536.

119. Shi K, Tan DK, Nokhodchi A, Maniruzzaman M. Drop-on-powder 3D printing of tablets with an anti-cancer drug, 5-fluorouracil. Pharmaceutics. 2019 Apr 1;11(4):150.

120. Hong, Y. Electrospun Fibrous Polyurethane Scaffolds in Tissue Engineering. In Advances in Polyurethane Biomaterials; Woodhead Publishing: Sawston/Cambridge, UK, 2016; pp. 543–559.

121. Maniruzzaman, M.; Douroumis, D. An in-vitro-in-vivo taste assessment of bitter drug: Comparative electronic tongues study. J. Pharm. Pharmacol. 2014, 67, 43–55.

122. Skoog DA, Holler FJ, Crouch SR. Principles of instrumental analysis. Cengage learning; 2017 Jan 27.

123. Shi, K.; Tan, D.K.; Nokhodchi, A.; Maniruzzaman, M. Drop-On-Powder 3D Printing of Tablets with an Anti-Cancer Drug, 5-Fluorouracil. Pharmaceutics 2019, 11, 150.

124. Madan JR, Dere SG, Awasthi R, Dua K. Efavirenz loaded mixed polymeric micelles: Formulation, optimization, and in vitro characterization. Assay and drug development technologies. 2021 Jul 1;19(5):322-34.

125. Akbari, J.; Adrangui, M.; Farid, D.; Siahi-Shadbad,M.R.; Saeedi, M.; Nokhodchi, A. The effects of various factors on the release rate of a poorly solubledrug (carbamazepine) from hydroxypropyl methylcellulose matrices. S.T.P. J. Pharma. Sci. 2000, 10, 473–478.

126. Martin, Ivan, David Wendt, and Michael Heberer. "The role of bioreactors in tissue engineering." TRENDS in Biotechnology 22, no. 2 (2004): 80-86.

127. Roche, Christopher D., Russell JL Brereton, Anthony W. Ashton, Christopher Jackson, and Carmine Gentile. "Current challenges in three-dimensional bioprinting heart tissues for cardiac surgery." European Journal of Cardio-Thoracic Surgery 58, no. 3 (2020): 500-510.

128. Rider, Patrick, Željka Perić Kačarević, Said Alkildani, Sujith Retnasingh, and Mike Barbeck. "Bioprinting of tissue engineering scaffolds." Journal of tissue engineering 9 (2018).

129. Wu, Yan, Lisa Woodbine, Antony M. Carr, Amit R. Pillai, Ali Nokhodchi, and Mohammed Maniruzzaman. "3D printed calcium phosphate cement (CPC) scaffolds for anti-cancer drug delivery." Pharmaceutics 12, no. 11 (2020): 1077.

130. O'brien, Fergal J. "Biomaterials & scaffolds for tissue engineering." Materials today 14, no. 3 (2011): 88-95.

131. Wang, Chong, Wei Huang, Yu Zhou, Libing He, Zhi He, Ziling Chen, Xiao He et al. "3D printing of bone tissue engineering scaffolds." Bioactive materials 5, no. 1 (2020): 82-91.

132. O'Connor, Clare M., Jill U. Adams, and Jennifer Fairman. "Essentials of cell biology." Cambridge, MA: NPG Education 1 (2010): 54.

133. European Collection of Authenticated Cell Cultures (ECACC), ECACC General Cell Collection: 1BR.3.G,URL< https://www.phe-culturecollections.org.uk/products/celllines/generalcell/detail.jsp?refId=90020507&collection=ecacc_gc>

134. ATCC, U-2 OS, URL <https://www.atcc.org/products/htb-96>

135. van der Eb A. "USA FDA CTR For Biologics Evaluation and Research Vaccines and Related Biological Products Advisory Committee Meeting"(PDF). Lines 14–22: USFDA. p. 81. Archived from the original (PDF) on 2017-05-16. Retrieved August 11,2012.

136. Maggi, Alessandro, Hanqing Li, and Julia R. Greer. "Three-dimensional nano-architected scaffolds with tunable stiffness for efficient bone tissue growth." Acta biomaterialia 63 (2017): 294-305.

137. Chen, Guobao, Chanjuan Dong, Li Yang, and Yonggang Lv. "3D scaffolds with different stiffness but the same microstructure for bone tissue engineering." ACS applied materials & interfaces 7, no. 29 (2015): 15790-15802.

138. Tsien, Roger Y. "The green fluorescent protein." Annual review of biochemistry 67, no. 1 (1998): 509-544.

139. Cancer Research UK, https://www.cancerresearchuk.org/about-cancer/cancer-in-general/treatment, Accessed [01] [2022].

140. Todaro GJ, Green H. Quantitative studies of the growth of mouse embryo cells in culture and their development into established lines. The Journal of cell biology. 1963 May 1;17(2):299-313.

141. National Cancer Registration & Analysis Service and Cancer Research UK: "Chemotherapy, Radiotherapy and Tumour Resections in England: 2013-2014" workbook(link is external). London: NCRAS; 2017.

142. Cancer Research UK, https://www.cancerresearchuk.org/health-professional/cancer-statistics/survival/all-cancers-combined#heading-Zero, Accessed [01] [2022].

143. Ghilan, Alina, Aurica P. Chiriac, Loredana E. Nita, Alina G. Rusu, Iordana Neamtu, and Vlad Mihai Chiriac. "Trends in 3D printing processes for biomedical field: opportunities and challenges." Journal of Polymers and the Environment 28, no. 5 (2020): 1345-1367.

144. Pakhomova, Catherine, Dmitry Popov, Eugenii Maltsev, Iskander Akhatov, and Alexander Pasko. "Software for bioprinting." International Journal of Bioprinting 6, no. 3 (2020).